The University Of Sheffield.

The Synthesis and Oxygen Binding Properties of Self-assembled Fluorinated Copolymers and Their Possible Application as Blood Substitutes

Meng Fan

A thesis submitted for the degree of Doctor of Philosophy

Department of Chemistry
The University of Sheffield
Sheffield
S3 7HF

April 2020

Acknowledgment

Firstly, I would like to express my sincere thanks and utmost gratitude to my supervisor, Dr. Lance Twyman for his invaluable guidance and support throughout the project. His guidance helped me in all the time of research and writing of this thesis. I could not have imagined having a better supervisor and mentor for my PhD study.

I am also grateful to work with the entire Twyman research group who created a wonderful and friendly atmosphere, especially Dr. Devanshi Singh, Dr. Alaa Kadhim, Dr. Jawad K Abaies, Dr. Hamza Qasem, Dr. Samira Hussein, Dr. Bunian Shareef, Dr. Azrah Abdul Aziz and Mr. Yuliang Zhang. I would also like to thank Ms Heather Grievson and Mr. Robert Hanson for the help with technique issues. My thanks also extend to my friends who has helped me directly or indirectly towards completing this research project, especially Dr. Erik Jan Cornel and Dr. Ning Yin from Armes group.

I thank the chemistry department for providing a such safe and innovative place for study and research.

Last but not the least, I would like to thank my parents, without their endless love and support, this work would not be accomplished.

Abstract

One of the most important functions of blood is to solubilise and distribute oxygen within the body. As such, it is vital that this property is replicated (safely) by any artificial blood product. This thesis focuses on developing a series of fluorinated polymers to be used for oxygen carriers as improved oxygen transporting volume expanders for the emergencies and as potential artificial blood materials.

The first area of study concerned the synthesis of a series of fluorinated diblock copolymers that were capable of self-assembling into micellar structures at concentrations between 0.003 and 0.01 mg/mL. The aqueous solutions of these aggregated structures could retain oxygen and release it (into the aqueous bulk phase), as was demonstrated by a dissolved oxygen meter. The increased oxygen solubility was measured indirectly based on the rate and half-life of oxygen release. These experiments indicated that oxygen retention/dissolution was dependent on the fluorine concentration. ^{19}F NMR and DLS carried out on oxygen loaded/oxygen free samples, confirmed that oxygen dissolution occurred within the fluorine region(core) of the polymer aggregates. A modified enzyme/glucose oxidation assay was applied to measure oxygen concentrations directly, and these were found to be 33% higher in the polymer solutions, compared to water alone. To improve circulation times and in an effort to generate more stable and larger systems, this work was extended towards the development of much larger and irreversible self-assembled nano structures. Specifically, we modified our polymer design so that they could assemble into a water soluble polyion complex. This was also able to solubilize and carry

oxygen efficiently. The process involved the synthesis of two amphiphilic fluoro-containing block copolymers, with positive or negative ions respectively. Both polymers could self-assemble into homo micelles in aqueous media, with CMCs around 0.002 to 0.006 mg/mL. However, when mixing these two polymers at a 1:1 stoichiometric ratio of ions, a neutral solution was observed and a PIC with a size of around 300 nm were obtained. Dissolved oxygen and DLS measurements confirmed that the PIC could dissolve oxygen inside, leading to an overall increase in the aqueous solubility of oxygen.

Abbreviations

ATRP	atom transfer radical polymerisation
$CDCl_3$	deuterated chloroform
CMC	critical micelle concentration
^{13}C NMR	carbon-13 nuclear magnetic resonance
DCM	dichloromethane
DLS	dynamic light scattering
DMAEMA	2- (dimethyl amino)ethyl methacrylate
DO	dissolved oxygen
DP	degree of polymerisation
ES	electrospray
^{19}F NMR	fluorine-19 nuclear magnetic resonance
GPC	gel permeation chromatography
^{1}H NMR	proton nuclear magnetic resonance
LMW	low molecular weight
MAA	methacrylic acid
Mn	number average molecular weight
Mw	weight average molecular weight
mPEG	poly (ethylene glycol) methyl ether
mPEG-Br	poly (ethylene glycol) methyl ether -2-brom -oisobutyrate

mPEG-b-PTFEMA	poly (ethylene glycol) monomethyl ether-*block*-poly(2,2,2-trifluoroethyl methacrylate)
mPEG-b-PPFPMA	poly (ethylene glycol) monomethyl ether-*block*-poly(2,2,3,3,3- pentafloropropyl methacrylate)
mPEG-b-PMMA	poly (ethylene glycol) monomethyl ether-*block*-poly(methyl methacrylate)
mPEG-P(TFEMA-*ran*-DMAEMA)	poly (ethylene glycol) monomethyl ether-*block*-poly[(2,2,2-trifluoroethyl meth acrylate)-*ran*-(2-(dimethyl amino)ethyl m ethacrylate)]
mPEG-P(TFEMA-*ran*-tBMA)	poly (ethylene glycol) monomethyl ether-*block*-poly[(2,2,2-trifluoroethyl meth acrylate)-*ran*-(*tert*-butyl methacrylate)]
mPEG-P(TFEMA-*ran*-tBMA-*ran*-MAA)	poly (ethylene glycol) monomethyl ether-*block*-poly[(2,2,2-trifluoroethyl meth acrylate)-*ran*-(*tert*-butyl methacrylate)-*ran*-(methacrylic acid)]
MS	mass spectrometry
MWD	molecular weight distribution
NMP	nitroxide-mediated Polymerisation

PDI	polydispersity index
PFPMA	2,2,3,3,3-pentafluoropropyl methacrylate
PMAA	poly (methacrylic acid)
PMDETA	N, N, N′, N″, N″-pentamethyldiethylenetriamine
PMMA	poly (methyl methacrylate)
PtBMA	poly (*tert*-butyl methacrylate)
RAFT	reversible addition fragmentation chain transfer polymerisation
tBMA	*tert*-butyl methacrylate
TEM	transmission electron microscope
TFA	trifluoroacetic acid
TFEMA	2,2,2-trifuloroethyl methacrylate
THF	tetrahydrofuran

NMR Abbreviations

d	doublet
m	multiplet
q	quartet
s	singlet
t	triplet

Table of Contents

Chapter 1

Introduction

Introduction

Blood, which is a red body fluid in vertebrates, is responsible for delivering nutrients and oxygen, as well as removing metabolic waste. The average volume of blood in an adult human male is 5-6 litres, while it is 4-5 litres in an adult female. This difference is mainly due to the difference in the body size.[1] The composition of blood is complex. It consists of plasma (55%), while the remaining 45% is made up of red blood cells, white blood cells and platelets and so on. The percentage of water in plasma is 92%, while proteins, glucose, mineral ions and hormones, constitute the other 8%. The blood cells are suspended in the plasma, of these the most abundant are red blood cells, also known as erythrocytes, which are responsible for the transport of oxygen. The others are white blood cells for the immune system and platelet for clotting.[2]

To replace blood loss, scientists have historically focused attention on the development of a safe blood transfusion. The first successful blood transfusion can be traced back to the 17th century. A doctor transfused an animal's blood into a human. Although the patient underwent a horrible immunoreaction, they eventually recovered.[3] However, this practice was not universally accepted, and it was extremely unsafe. The contiguous blood transfusion practices were highly variable and outcomes were somewhat uncertain until Landsteiner discovered the ABO blood group system in 1900. This great discovery provided the scientific basis for compatible and safe blood transfusion. Since then, blood banks have been established,[4] and safe blood transfusions have been carried out for decades. Nevertheless, the public faith in the safety of blood transfusion was severely affected by

the AIDS epidemic. Approximately, 60% of the population is eligible to donate blood, but fewer than 5% are regular blood donors.[5] On the one hand, humanitarian considerations, social pressure and reward motivated people to donate blood.[6] However, there were still a number of people who tended to believe that the process of donating blood was not as safe as it ought to be. To a certain extent, the latter view made some sense. Allergic reactions, infectious risks and/or administrative errors could be made unexpectedly. Furthermore, the storage period of blood donation is 35 to 42 days; thus, it is impossible to stockpile blood.[7] All these challenges have driven scientists to try to develop a blood substitute in order to solve the shortage problem of blood donation in emergency situations. In theory, artificial blood products can provide a number of important advantages. First, compared to natural human blood, artificial blood can be prepared easily and rapidly, and the shelf life of artificial blood is much longer. Second, it demonstrates close to 100% functionality even after filtration and pasteurisation processes, avoiding virus contamination. Third, it does not have a blood type, so it can be used for patients immediately without the blood type determination step. Hence, people who have rare blood types can benefit from it. Lastly, an ideal artificial blood can also eliminate the immunosuppression in the recipient.[8]

However, because of the complex composition of blood, it has been impossible to replicate completely the full components and functions of human blood in a laboratory. However, one of the most important functions of blood is its ability to bind and transport oxygen around the body. Thus, major efforts have been exerted to develop artificial oxygen carriers to replace the erythrocytes of human blood.

Up to now, two major types of red cell substitutes have been studied: haemoglobin-based

oxygen carriers and perfluorocarbon (PFC) -based oxygen carriers. Other ideas have also attracted attention: For example, mimicking the chemical environment of the haem group using micelles as carriers. However, these are still very early and remain in the laboratory stage.

1.1 Human Blood

Human blood is a complex material, but there are two important proteins responsible for oxygen storage and transport and their properties are summarised below.

1.1.1 Haemoglobin

Inside erythrocytes, the protein that binds oxygen reversibly is haemoglobin. Haemoglobin is composed of two α and two β polypeptide chains (**Figure 1.1**).[9] Within each chain, there is a haem unit. Haem is an iron-porphyrin complex, which is also the primary red pigment of vertebrate blood.

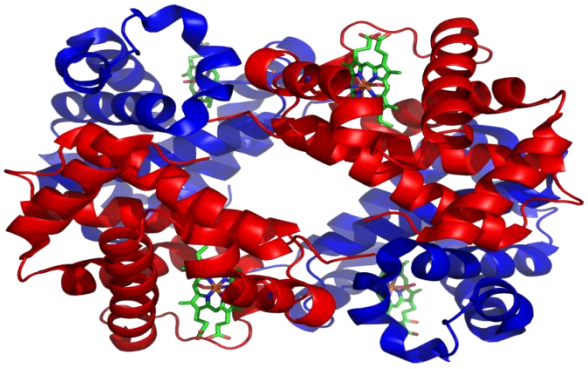

Figure 1.1: Haemoglobin structure

The haem unit is the active binding centre for an oxygen molecule. Therefore, a haemoglobin unit is able to load four oxygen molecules during one binding process. The

iron core of the haem molecule forms coordinate valent bonds with four pyrrole nitrogen and one axial nitrogen from a proximal histidine residue.[10] The latter bond stabilises the protein structure by slowing the haem dissociation; thus, affecting the reactivity of the haem iron on the opposite side.

1.1.2 Myoglobin

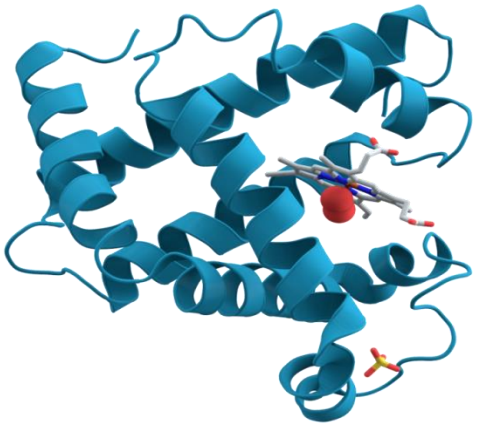

Figure 1.2: Myoglobin structure[11]

Another important protein is myoglobin (**Figure 1.2**), which can be found in muscle tissue of almost all mammals.[12] The function of myoglobin is similar to haemoglobin, in that it stores and delivers oxygen. It is a monomeric globin that has only one polypeptide chain, holding one haem group inside. Thus, compared with haemoglobin, it can only bind one oxygen molecule.

1.1.3 Mechanism of Oxygen Binding

Haem units are the essence of oxygen transportation. Once oxygen enters the blood stream, it binds with haem and then, as a part of haemoglobin, it is transported throughout the body.

The binding process is cooperative, and has been characterised by the two-state model, which is also called the MWC Model.[13] According to this model, there are two states in the binding equilibrium: the T (tense) state and the R (relaxed) state. In the T state, haemoglobin has a low affinity for oxygen; while in the R state, the affinity is much higher. The iron (II) core binds with the axial nitrogen of a proximal histidine, which pulls the iron atom out of the 'equatorial' plane of the porphyrin and towards the proximal histidine residue, forming a domed shape. In this conformation, the haem group is in the T state and is deoxygenated. Once an oxygen molecule is attached to the iron (II) core, the conformation returns to a planar configuration (**Scheme 1.1**).[10] As the proximal histidine shifts its position, there is movement of the other amino acids in the polypeptide chains. Therefore, the structure of the four subunits is altered, leading to the cooperative binding of more oxygen and elimination of any bound CO_2.

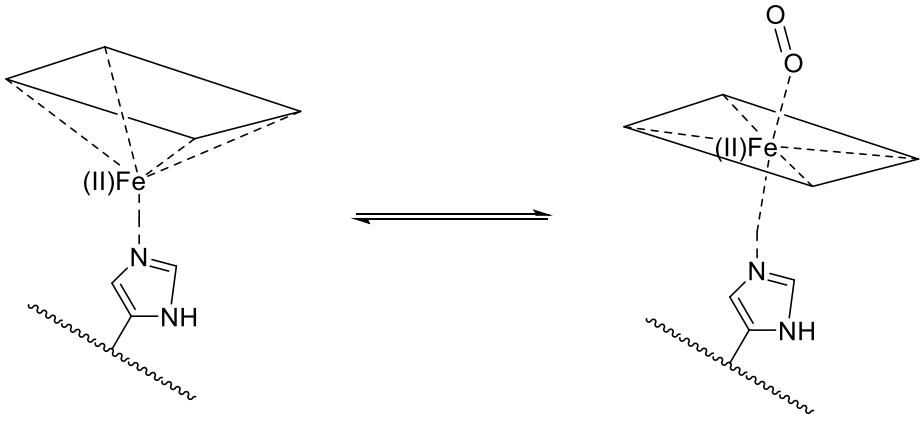

Scheme 1.1: Configuration changed from 'domed' shape (left) to a planar one (right).

Without the protein structure providing the axial and proximal histidine residue, the oxygen binding process is irreversible. In this case, the oxygenation of the central iron results in a reaction to form a peroxo-bridged intermediate (peroxo-Fe (III)). This then converts to the

ultimate product, which is μ-oxo dimer (**Scheme 1.2**).[14,15] At this point, the oxygen is fixed. As such, the oxygen binding and transport properties of blood cannot be replaced with a simple porphyrin unit.

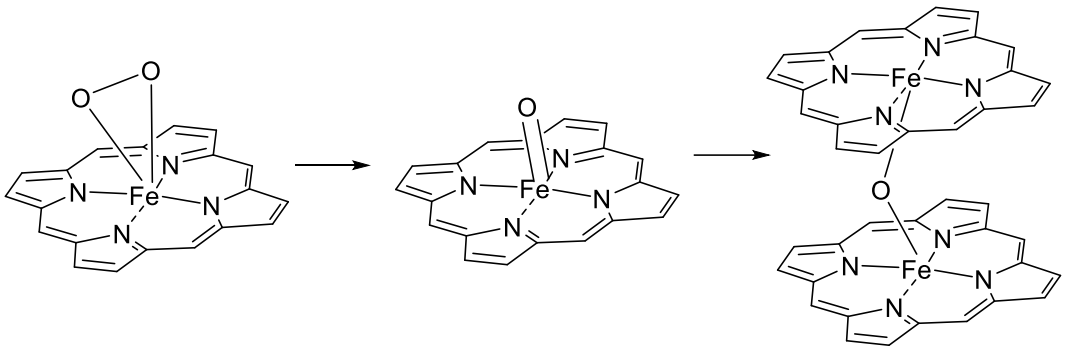

Scheme 1.2: Peroxo-Fe (III) is converted to μ-oxo dimer.

1.2 Haemoglobin-based Oxygen Carriers

Haemoglobin-based oxygen carriers use haemoglobin extracted from human, animal and recombinant sources.[16] Human haemoglobin usually comes from donated blood that has reached its expiration date. However, if the need for blood donors increases rapidly, this source can be limited. However, obtaining haemoglobin from animals, such as cows has problems.[17] For example, people are concerned about the safety of this source, since the cows can possess bovine spongiform encephalopathy or other pathogens.[8,17] In order to have safe products, large investment is required to ensure that the cows were born and raised in clean and healthy farms; a quarantine inspection would also be required.

Recombinant haemoglobin is synthesised using specific bacterial or yeast growth, such as *Escherichia coli* or *Saccharomyces cerevisiae*.[18] This method not only avoids infectious risks, but also allows the possibility for designing and constructing alternative haemoglobin products.[19]

Generally, haemoglobin exists as a tetramer within red blood cells. Since there is a cell membrane to provide a stable environment, haemoglobin is not easily decomposed. However, without this protective environment, stroma free haemoglobin (SFH) will rapidly breakdown into dimers and monomers during transfusion[20], which can be toxic and can cause renal damage. Once SFH is obtained, it needs be modified before application in order to decrease the toxicity of the solutions. There are mainly three approaches to modify and enhance SFH: environmental modifications, cross-linking and polymerisation.

1.2.1 Environmental Modification

2,3-Bisphosphoglyceric acid (2,3-DPG) could have an important role in haemoglobin deoxygenation/oxygenation, as its conformation fits in the deoxygenated haemoglobin conformation (**Scheme 1.1**). Thus, it helps with the oxygen releasing process by stabilising the deoxygenated haemoglobin. However, as stroma-free haemoglobin lacks 2,3-DPG, it possesses an excessive affinity for oxygen.[21, 22]

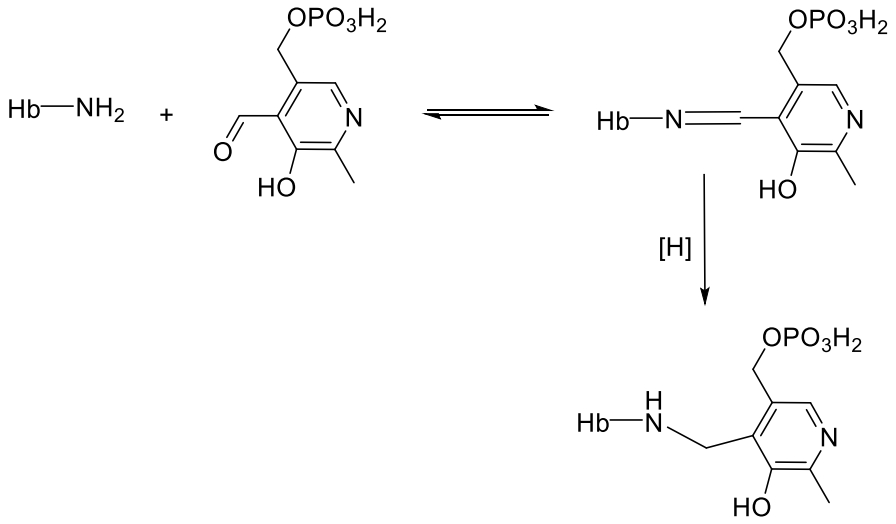

Scheme 1.3 Hb modification by pyridoxal phosphate[8]

Hence, one approach to control this affinity is to associate deoxy-Hb with 2,3-DPG

substitutes. This process is achieved by allowing deoxy-Hb to react with pyridoxal phosphate. During the modification, two negative charges on the phosphate group can help to position the reagent at the 2, 3-DPG binding site to substitute 2,3-DPG (**Scheme1.3**).[8,23] This modification successfully regulates the oxygen affinity for haemoglobin. Nevertheless, it still cannot maintain the haemoglobin tetramer structure without dissociating into dimers and monomers. As well as affinity control, efforts are also made to maintain the haemoglobin structure whilst in circulation. Liposomes, constructed from lipid bilayer membranes, have been investigated as drug carriers; these have the potential to mimic the erythrocyte environment. The incorporation of haemoglobin within liposomes has been investigated, but when large amounts are used, liposomes often aggregate in the blood stream.[24,25,26] For the purpose of preventing such aggregation, scientists have developed surface modified liposomes using hydrophilic polymers, such as polyethylene glycol (PEG).

1.2.2 Cross-linked Haemoglobin

Cross-linked haemoglobin can be classified into two types: intramolecular cross-linked haemoglobin, and intermolecular cross-linked haemoglobin.

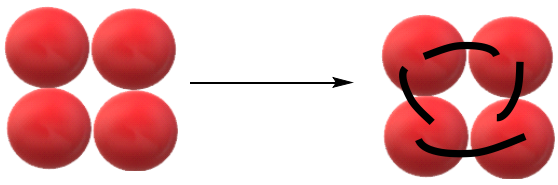

Scheme 1.4 Intramolecular cross-linked Hb

Intramolecular cross-linking haemoglobin aims to prevent tetramer dissociation and to reduce oxygen affinity. Small molecules have been used to create a bridge between the

amino acids of haemoglobin dimers. (**Scheme 1.4**) The bridging molecules can be NFPLP[27,28], DIBS[29] and DBBF[30], which generate negative charges to provide site specificity for the cross-link. Bifunctional and multifunctional cross-linkers, such as activated diesters, also reduce dissociation. However, intramolecular cross-linked haemoglobin faces a difficult situation when applied to medical treatments. For instance, HemAssist[31], which is a cross-linked haemoglobin product developed by the US Army, was withdrawn because of high mortality rates in phase III trials. This was due in part to the relatively small size of the intramolecular cross linked systems, allowing haemoglobin to leak out of from veins and build up in surrounding tissue, leading to a number of problems, including toxicity.

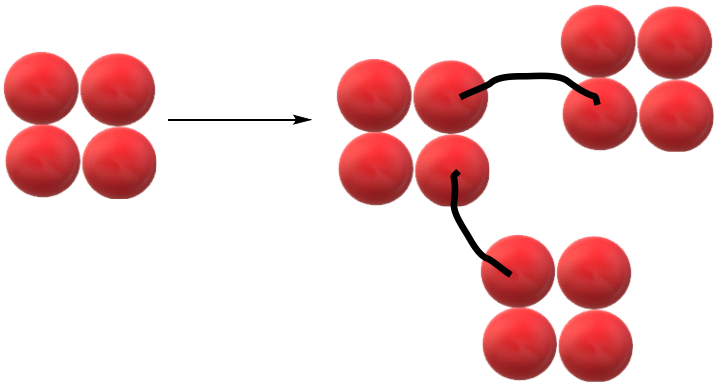

Scheme 1.5 Intermolecular cross-linked Hb

An intermolecular cross-linkage involves creating a cross-link between two or more haemoglobin units (**Scheme 1.5**), resulting in the 'oligomerisation' of haemoglobin. The purpose of making intermolecular cross-linkages is to reduce the protein's oncotic pressure and to increase the overall size so as to prevent rapid metabolism by the body. The most popular intermolecular cross-link reagent is glutaraldehyde[32]. It can give an unsaturated

polymer, which contains aldehyde groups that can react with the amino acids of haemoglobin. However, if the Schiff bases produced during the reaction have not been reduced completely, depolymerisation and glutaraldehyde will form, which is highly toxic.[33] This can be improved if the haemoglobin molecules are decorated by PEG strands, which increases the molecules' size and hydrophilicity.

1.2.3 Haemoglobin Mimicry

Since haemoglobin as a raw material is limited and the modification processes of haemoglobin are complicated, some scientists have focused on synthesising and mimicking the functions of the polypeptide chains surrounding the haem units.[34] Hyperbranched polymers and dendrimers have been used to achieve this objective. The globular structure, formed by a dendrimer, is able to offer a shape and size similar to that of the natural haem-containing proteins. Binding the oxygen reversibly was achieved, but the synthetic the challenge was difficult. Twyman et al.[35] proposed one-step synthesis using a functional porphyrin as an initiator core to generate a hyperbranched polymer that grows around the porphyrin. (**Scheme 1.6**). It was confirmed that this polymer could bind oxygen in the form of Fe (II)-O_2 reversibly in 5-6 cycles before the iron (II) core was fully oxidised.

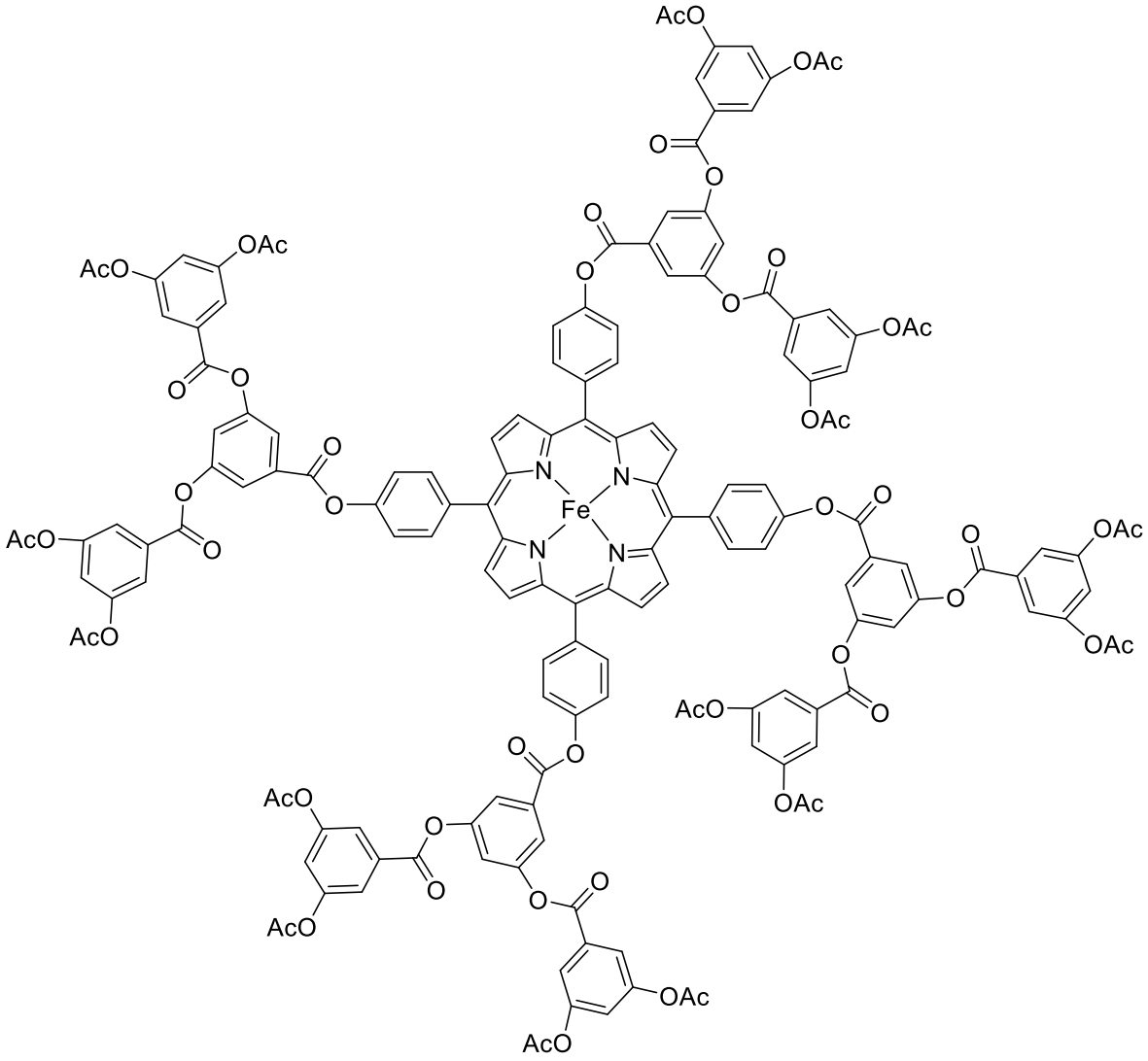

Scheme 1.6 Fe (II) cored hyper-branched polymer.[35]

The Shen group[36] developed a different type of micelle constructed from the hierarchical assembly of a diblock copolymer, poly(ethylene glycol)-block-poly(L-lysine), tetrakis(4-sulfonato-phenyl)porphinato cobalt(II). The cobalt coordinated to oxygen in a similar way to Fe in haemoglobin. Therefore, oxygen binding was a coordination reaction similar to that of haemoglobin.[35]

1.3 Perfluorocarbon-based Oxygen Carriers (PFCs)

1.3.1 Perfluorocarbon Liquid

Perfluorocarbons are organofluorine molecules that contain only carbon and fluorine. In the 1960s, Clark and Gollan discovered that mammals could survive submerged in oxygen-saturated perfluorocarbon liquids for several hours, which established the foundation for perfluorocarbon use as a potential blood substitute.[37] Previous experiments showed that perfluorocarbons have the capacity to dissolve 50 times more oxygen than water or plasma.[38] The oxygen transport mechanism of perfluorocarbon is totally different from that of haemoglobin and simply involves dissolution the oxygen; there is no specific binding or coordination process.

Due to their hydrophobicity, PFCs are usually emulsified before use. In addition, they are lipophobic, which explains the challenge in making PFCs into emulsions. As such they tend to be small (pre-gaseous) liquids. The selection of an appropriate fluorocarbon for both emulsion and medical use is crucial. To prevent pulmonary emboli, the vapour pressure (lower than 20 torr) needs to be considered.[22] Furthermore, the emulsion particle size is an important parameter; if too large, that may cause elimination to be unacceptably lengthy in duration. PFCs are inert and do not dissociate and metabolise during blood circulation. They are principally excreted by exhalation through the lungs, which can cause mild thrombocytopenia and flu-like symptoms.[39] The capacity of PFC emulsions to carry oxygen increases linearly with an increase in the oxygen partial pressure, which is different

from that of haemoglobin. Hence, in therapeutic applications, they are often used with high concentrations of oxygen, which may result in oxygen toxicity. [16] The first generation of perfluoro emulsions is Fluosol, developed by the Green Cross Corp.[22] This emulsion contained perfluorodecalin and perfluorotripropylamine. In 1989, it was licensed for use as a blood substitute for heart surgery. A second-generation material, that used phospholipids as the emulsifier, was easier to prepare and more stable than the previous emulsion.

1.3.2 Fluorinated Polymeric Micelles

The ability of perfluorocarbons to dissolve large volumes of gas is attributed to the strong intramolecular bond and the weak intermolecular interactions caused by the characteristics of fluorine, which generate 'holes' to hold gas molecules. On the other hand, extremely stable C-F bonds make the whole molecule inert.[8] One of the areas with a growing interest is the synthesis of polymeric micelles based on PEG containing diblock polymers. Since PEG is non-toxic, chemically inert and highly water-soluble, it has been widely used in the biomedical area to prepare delivery systems.[40,41] As such, fluorinated polymer micelles for oxygen dissolution are theoretically achievable. There has been previous research into the synthesis and application of fluorinated micelles that can dissolve oxygen. Pitarresi et al.[42] synthesised a fluorinated polymer based on polyaspartamide bearing polyethylene glycol chains. The polymers could dissolve in water to form micelles, and the solution had high oxygen solubility. In addition, the size of the fluorine-containing polymeric micelles changed depending on whether CO_2 or O_2 were bubbled through the aqueous micellar

solutions.[43,44]

1.4 Amphiphilic Diblock Copolymer

As a consequence of the different composition of a diblock copolymer, the solubility and surface energy of the two kinds of chain segments are also different. If the copolymer contains both hydrophobic and hydrophilic chains, it can self-assemble into micelles or other aggregates in an aqueous solution. Under certain conditions, the hydrophilic chains stretch out into the solvent to form a solvophilic shell, while hydrophobic chains concentrate together to form a poly solvophobic core **(Figure 1.3**). This behaviour can be characterised as the critical micelle concentration (CMC). If the concentration is below the

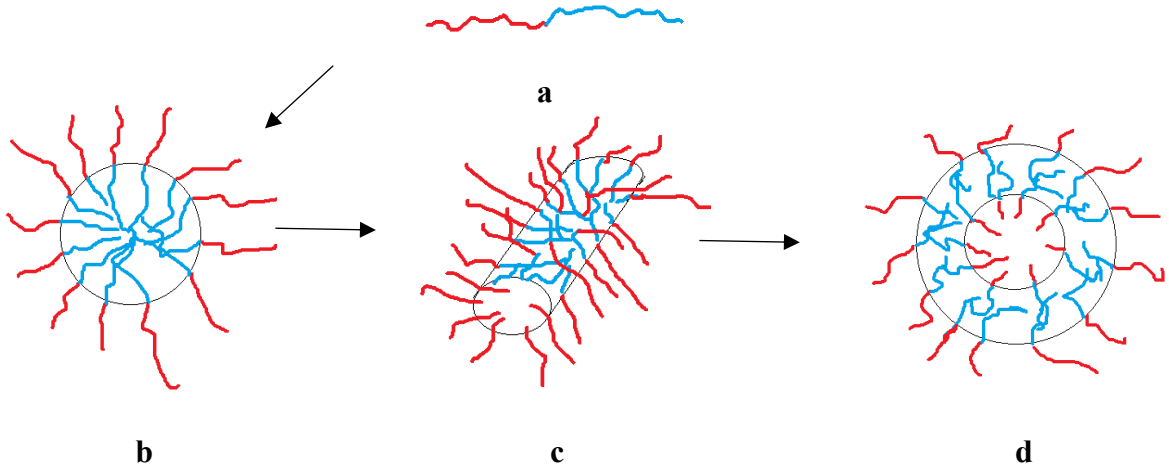

Figure 1.3 a) amphiphilic diblock copolymer (red block was hydrophilic and blue block was hydrophobic) **b)** micelle **c)** worm-like rod **d)** vesicle [45]

CMC, only unimers can be observed. If the concentration is above the CMC, the multimolecular micelles are in equilibrium with the unimers.[45]

The self-assembly morphologies can be various, for example, they can form micelles, worm-like rods and vesicles. Variation mainly depend upon the composition of the copolymer component blocks, their concentration and temperature. The composition of the copolymers can be changed by being mixed with other chemicals and by using different block lengths.[46] Eisenberg's group[47] made a series of polystyrene-b-poly (acrylic acid) diblock copolymers by adding different ions, which then self-assembled into different nanoparticle morphologies (spherical micelles, worm-like micelles, and vesicles). Karagoz et al.[48] used "polymerisation induced self-assembly" (PISA) for the synthesis of block copolymer nanoparticles. PISA is based on the poor solubility of the second chain segment of diblock copolymers. During the polymerisation process, co-monomers are added sequentially. Thus, the second block can grow on the first block. Due to the insolubility of the second block, the self-assembly of this copolymer was induced along with the polymerisation. With the increase of D_p, the morphology changed from the spherical micelle to the worm-like micelle before progressing to the vesicle. The influence of nanoparticle morphologies on cancer cell line uptake was also demonstrated.

On the other hand, temperature can also affect the morphologies of micelles. Two blocks of a diblock copolymer have different sensitivity to the temperature. If the temperature is changed, the hydrophobicity and the hydrophilicity of these two blocks will change unevenly, which will cause different morphologies.[49,50] Furthermore, solvent can also affect morphology. If the solvent becomes less conducive to the dissolution of the core block, the volume of the micelle core will increase, and the inner chain segments will extend. Hence, the morphology can change from spherical to rod-like then to the vesicle shape.[51] In some

cases, the micelle can break up and this has been used as “smart” mechanism for drug delivery and release. What’s more, the pH of the solution can also influence the hydrophilic-hydrophobic property of chain segments and micelle stability. The self-assembly morphology can be shifted by balancing the hydrogen-bonding and hydrophobic forces as well as by applying the steric and electrostatic forces.[52]

This thesis mainly focuses on the oxygen capacity of the diblock amphiphilic copolymers that contain perfluoro blocks. In order to achieve a controlled self-assembled structure, it is important that the copolymer components can be synthesised with a controlled and specifically designed molecular weight. It is also vital that each component has controlled and narrow polydispersity. As such, the target copolymers must be synthesised using a controlled living polymerisation.

1.5 Living Radical Polymerisation

The synthesis of diblock copolymers can be achieved by applying many approaches.[53] A controlled living radical polymerisation has proved, in many circumstances, to be the one of the best ways to make well-defined amphiphilic diblock copolymer.

Radical polymerisation is a robust technique that is not only applicable to a range of vinyl monomers, but can also operate in a wide range of conditions. However, as radicals are very reactive species, a radical polymerisation has poor selectivity and relatively poor control over polymer product. This is a problem when synthesising amphiphilic polymers for self-assembly, as poor control of polymer structure and degrees of polymerisation, result in poor control over self-assembly. Hence, controlled living radical polymerisations have

attracted increasing attention.[54] (**Figure 1.4**)

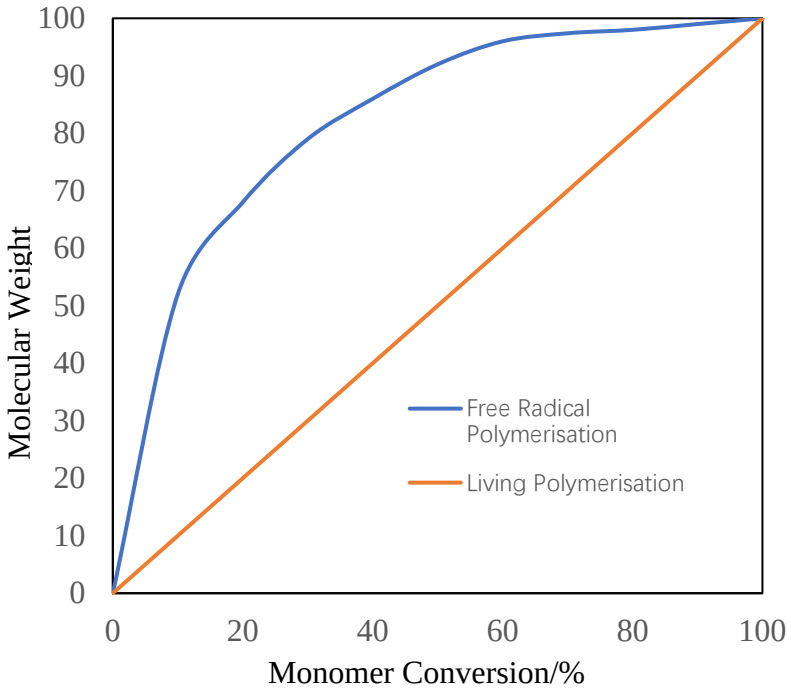

Figure 1.4 Comparison between free radical polymerisation and living polymerisation in terms of molecular weight and conversion(adapted from paper[55])

As shown in **Figure 1.4**, for a free radical polymerisation, the increase of the molecular weight is not linear with the monomer conversion, which is extremely hard, even impossible, to get the polymer with designed polymerisation degree and narrow weight distribution. However, a living polymerisation provide a linear increase on molecular weight against the conversion. Under the ideal situation, by controlling the monomers' feed, the molecular weight can be manipulated, as shown in **Equation 1** where $[M]_0$ is the initial monomer molar concentration, $[I]_0$ is the starting molar concentration of the initiator.

$$D_p = \frac{[M]_0}{[I]_0} \qquad \textbf{Equation 1}$$

The common strategy for controlled polymerisation has been to reduce the concentration

of the propagating polymer radical species. Thus, termination is depressed, and control of polymerisation can be achieved. There are a number of ways to achieve this and they are described below.

1.5.1 Nitroxide-mediated Polymerisation (NMP)

Typically, the main principle of NMP is based on reversible termination between the propagating polymer radical and nitroxide, which acts as a control agent. This kind of polymerisation produces a series of alkoxyamine continuously throughout the reaction. (**Scheme 1.7**)

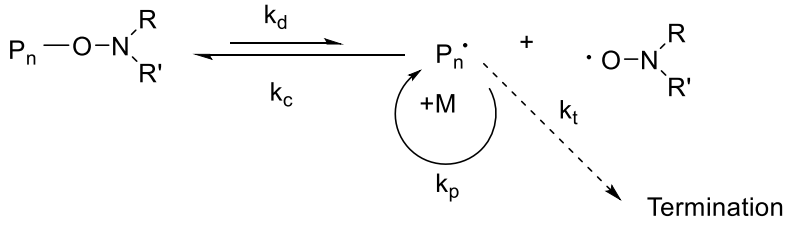

Scheme 1.7 'living' mechanism of propagation of NMP

As the temperature increases, these compounds can easily separate themselves from the propagating radical and the nitroxide through a homolytic cleavage. The combination and the cleavage collaborate to build the equilibrium of the polymerisation, which controls the reaction.[56,57]

1.5.2 Reversible Addition Fragmentation Chain Transfer (RAFT) Polymerisation

The principal distinction between RAFT and atom transfer radical polymerisation (ATRP) is that RAFT polymerisation involves a reversible chain transfer, whereas ATRP involves reversible chain termination. The radicals are provided by conventional free-radical initiators such as AIBN. [58] The key player in the RAFT process is the chain transfer agent (CTA), which is a dithioester. The structure of this kind of dithioester and the RAFT mechanism are presented in **Scheme 1.8**.

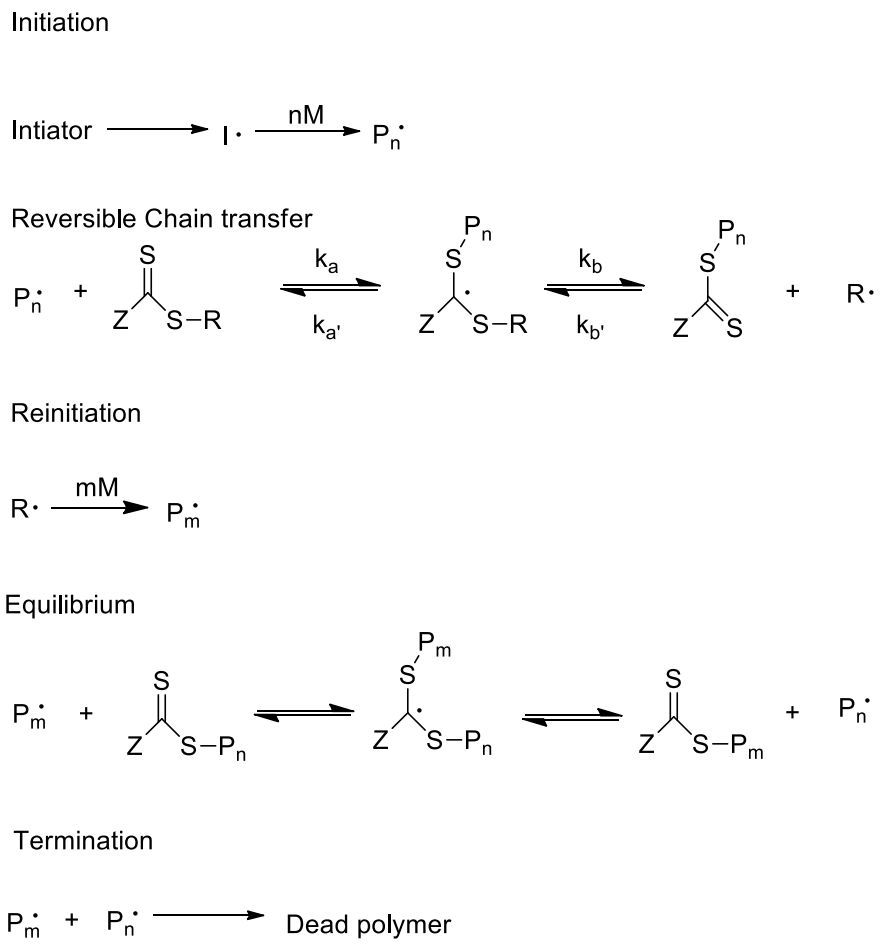

Scheme 1.8 The structure of CTA and the mechanism of RAFT[59]

The Z-group is used to stabilise the transition state and the intermediate radical formed by the addition of the propagating radical. The R-group must be a good (radical) leaving group, which is capable of re-initiating polymerisation. Because of this unusual structure, CTA can be used to synthesise a variety of copolymers.[60–61]

1.5.3 Atom Transfer Radical Polymerisation (ATRP)

ATRP was first introduced by Wang and Matyjaszewski in 1995.[62] The mechanism for this kind of polymerisation is shown in **Scheme 1.9**. This method uses simple alkyl halides as initiators and a variety of transition-metal complexes as catalysts. The whole process is based on a reversible oxidation-reduction reaction. A central metal atom, such as copper, is oxidised from Cu (I) to Cu (II). Meanwhile, the alkyl halide loses its halogen to become a free radical, which can initiate and then propagate the polymerisation by adding monomers. This process is reversible under certain conditions, and the rate of propagation is much faster than the rate of termination.[63] Additionally, the molecular weight of the product is linear with the conversion that provides the ability to make block copolymers by sequential monomer addition.

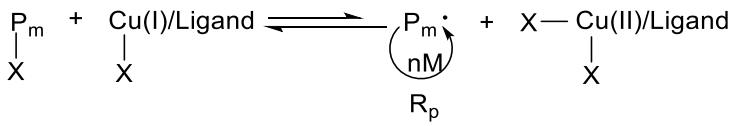

Scheme 1.9 Simple scheme of mechanism of ATRP

Normal ATRP is initiated by a redox reaction between an initiator with a radically

transferable atom or group and a catalyst complex comprising a transition metal compound. One problem it faces is that the transition metal can be easily oxidised to a higher oxidation state. Therefore, to prevent the oxidation, special handling operations are required, and the catalysts must be stored under an inner atmosphere. Oxygen or other oxidants should be removed before the reaction, which could be a big challenge to get a consistent synthesis result.

To minimise the influence of oxygen, an "activator generated by electron transfer" (AGET) for ATRP (AGET ATRP) was reported by the Matyjaszewski Group.[64] Fundamentally, AGET ATRP introduced a reducing agent into the system where the oxidised catalyst complex could be reduced prior to normal ATRP starting. (**Scheme 1.10**)

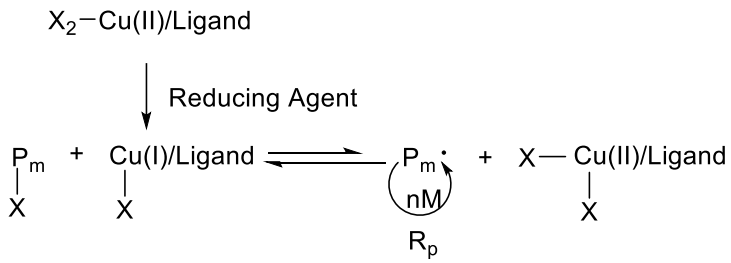

Scheme 1.10 Simple scheme of mechanism of AGET ATRP

This type of polymerisation involves the addition of the reducing agent, which could remove dissolved oxygen from the system, so that the tolerance of a small amount of oxygen is higher than normal ATRP. The experimental procedure was simplified by the addition of all reagents together before starting the reaction without taking any precautions regarding oxidation. In this thesis, normal ATRP worked as expected, but during development of the procedure, AGET ATRP was also tested. However, the reducing agent $Sn(EH)_2$, is a liquid with high viscosity, which made it hard to determine (and control) the

amount of the reducing agent added into the system.

1.6 Dissolved Oxygen (DO)

1.6.1 Partial Pressure and Dalton's law

In a mixture of gases, each constituent gas has a partial pressure, which is the notional pressure of that constituent gas. The 'notional pressure' here means the pressure of the constituent gas if it were the only gas occupying the entire volume of the original mixture at the same temperature.[65] The sum of the partial pressures of the gases in the mixture is the total pressure, is described as Dalton's law, which is shown in **Equation 2.**

$$P_{total} = P_{gas1}+P_{gas2}+P_{gas3}\ldots\ldots \qquad \textbf{Equation 2}$$

The partial pressure of a gas, which is different to the fraction of the gas, is a measure of the thermodynamic activity of the gas's molecules. Gases dissolve, diffuse and react according to their partial pressures. For example, breathing increased partial pressures of oxygen can result in hyperoxia, which is also called 'oxygen toxicity'. Hence, when researching oxygen concentrations in the areas of the blood and blood substitutes, dissolved oxygen concentrations are actually measurements of the partial pressure of oxygen.

1.6.2 Dissolved Oxygen Concentration Measurement

Determining the concentration of oxygen is essential when studying artificial oxygen carriers. Increasing the amount of dissolved oxygen in a polymer solution is a direct indication of the success of the oxygen carrier's efficiency. For humans, pulse oximetry is

a convenient non-invasive method of measuring blood oxygen saturation. The principle for pulse oximetry is measuring the fractional saturation of oxyhaemoglobin and deoxyhaemoglobin at separate resonant wavelengths. Thus, the signal could be affected by other parameters, such as pigments with significant absorbance near these two wavelengths and can give an inaccurate number.[66] It also needs to be applied to a narrow part of the body, like fingertips. Hence, it cannot be a substitute for laboratory-level measurements of blood gases or dissolved oxygen. It also requires the oxygen carrier to have suitable spectroscopic properties (when oxygenated and non-oxygenated).

A more accurate approach to measuring dissolved oxygen in blood is to use a blood gas analyser. In addition to measuring partial oxygen pressures (Po_2), this technique is able to measure pH and partial pressure of carbon dioxide (Pco_2). A traditional blood gas analyser has electrodes with a permeable membrane. The electrodes are in a solution where the H^+, CO_2 and O_2 can pass through the membrane and react with the electrodes in the solution, causing a current or voltage change, which is then converted to pH, Pco_2 and Po_2.[67] Generally, blood gas analysers are expensive pieces of equipment and only available for use in clinical situations. Such a machine was not available for our project as it is expensive and not suitable for measuring Po_2 in synthetic polymer solutions. Therefore, it was necessary to find an alternative and convenient method for measuring DO/ Po_2.

In environmental sciences, optical technologies for measuring DO in water has quickly become a well-accepted method, since it is fast, accurate and has a low operating cost. An optical DO sensor relies on luminescent lifetime technology.[68] During the measurement, a lumiphore for the oxygen is excited by a blue light, and the lumiphore then emit red light.

Oxygen molecules can quench the excited lumiphore and prevent/reduce the emission of red light.[69] The luminescence-quenching signal, which has a linear response towards oxygen concentrations. This method is shown in **Figure 1.5** and is a very simple method for measuring DO concentrations. For these reasons, it was applied for the determination of oxygen concentrations in this thesis.

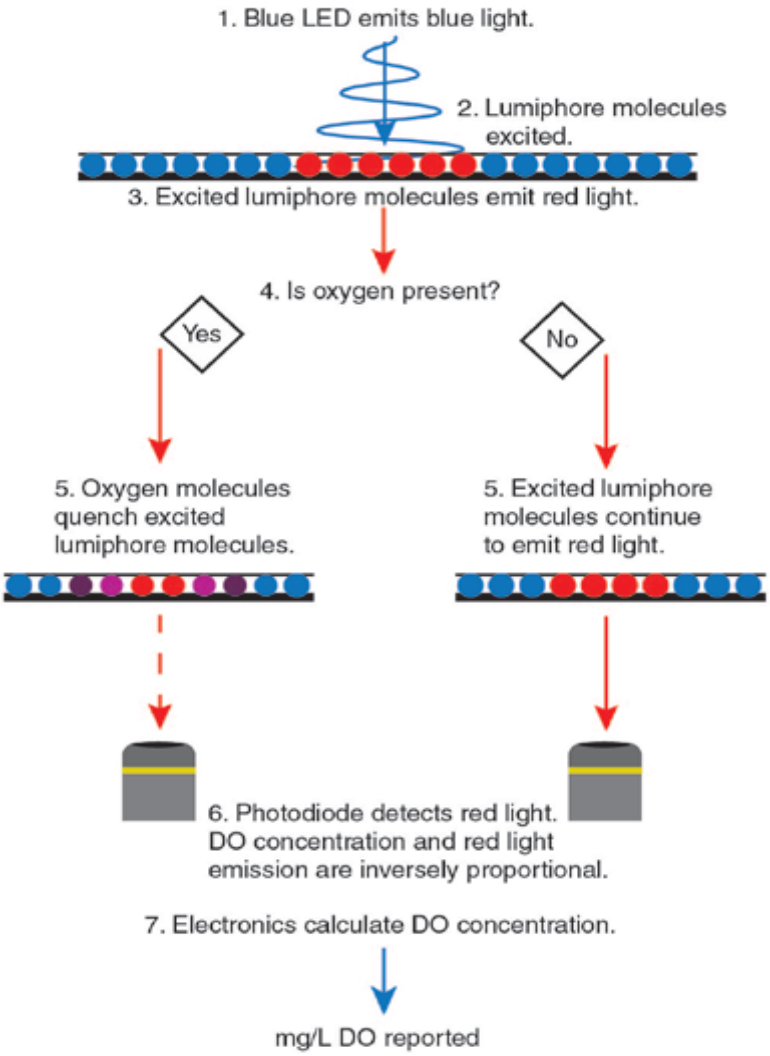

Figure 1.5 Lumiphore excitation process (Brand et al., 2002)[69]

However, it is important to distinguish between oxygen in bulk solution and any oxygen bound within a polymer or self-assembled system. The technology can only measure free

oxygen in solution. That is, the technique can only measure oxygen that can cross a membrane and cannot detect the oxygen trapped or bound within the polymer systems. Nevertheless, the technology can be used to indirectly measure oxygen concentrations by bubbling pure oxygen through the test solutions. Specifically, 100% oxygen is used to saturate the test solutions. We then measure the rate that oxygen inside the polymers re-equilibrates with oxygen in solution and then air (where it only makes up around 20% of the composition), be used as an indirect measure of oxygen concentration. This experiment is described in more detail within the research and development chapters.

Chapter 2
Fluorinated diblock copolymer micelles as oxygen carriers

This Chapter is taken from our previous publication[70]

2.1 Aims and Hypothesis

The aim of the work was to develop a system that could efficiently carry oxygen and overcome the problems of using small perfluoro compounds that necessitated the use of emulsions. To achieve this, we decided to synthesis a series of mPEG-polyfluoro amphiphilic diblock copolymers that could form micelles in aqueous media. As such, the self-assembled micellar structures would possess a fluorine rich core that could dissolve oxygen, leading to an increased concentration of oxygen in water (**Figure 2.1**). A number of fluorine containing polymers and diblock polymers have been reported. [42,43,44] However, no work has been directed at quantifying their oxygen dissolution and release properties or their potential application for use as an artificial blood system.

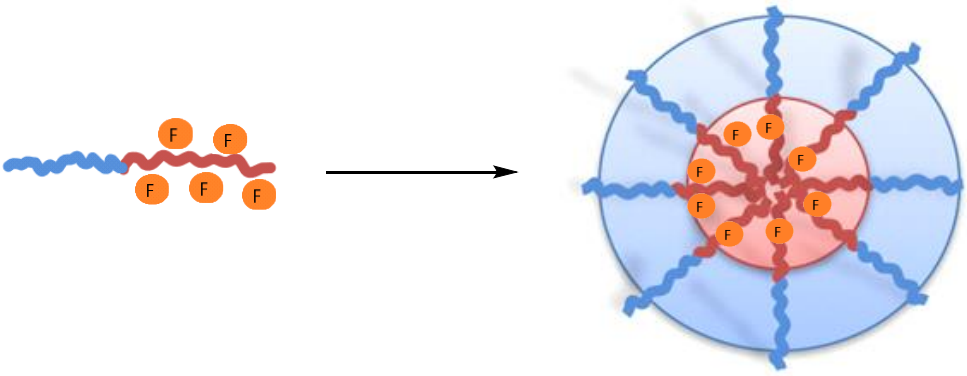

Figure 2.1 Amphiphilic diblock copolymer with fluoroblock forms micelles with fluorine rich core. (Blue chain is the hydrophilic block; red chain is the hydrophobic block, which covalently binds with fluorine atoms)

For the proposed mPEG-polyfluoro amphiphilic diblock copolymers, the amount of fluorine in the core could be controlled by increasing the fluoroblock chain length (the

degree of polymerisation) or using a monomer with more fluorine atoms. 2,2,2-Trifluoroethyl methacrylate was chosen for the initial synthesis of the diblock copolymer and 2,2,3,3,3-pentafluoropropyl methacrylate was chosen for the second diblock copolymer. Theoretically, both copolymers could form micelles in aqueous media and this would be investigated using DLS and CMC measurements.

Assuming the polymers formed micelles the oxygen dissolving ability would be tested and their ability to increase the solubility of oxygen in water assessed indirectly using a DO meter. In addition, direct oxygen concentrations will also be measured using a modified enzymatic assay that was originally designed to measure glucose concentrations in the presence of excess oxygen. Both measurements will be used to measure oxygen concentrations and to see if the oxygen capacity of these fluorinated micelles solutions is superior to that of water alone.

2.2 Results and Discussion

To achieve our aims, we required a diblock polymer that was biocompatible and contained a core block that was rich in fluorine. Our prototype design was relatively simple and would include a solubilising PEG block as a macroinitiator for an ATRP synthesis. ATRP was chosen as the main polymerisation method due to its efficiency in carrying out diblock copolymer synthesis and its ability to control polymer weight and weight distribution. In addition, the copper could be removed easily by a neutral/basic aluminium oxide column,

resulting in a pure nontoxic polymer for any potential biological test.

2.2.1 Synthesis of 2, 2, 2-trifluoroethyl methacrylate (4)

To begin with, 2, 2, 2-trifluoroethyl methacrylate was used for the fluorinated block, as it contains methacrylate double bonds which were required for radical polymerisation via ATRP. 2, 2, 2-trifluoroethyl methacrylate was synthesised by mixing methacryloyl chloride with trifluoroethanol to give 2, 2, 2-trifluoroethyl methacrylate by esterification. (**Scheme 2.1**). The structure was confirmed by ^{1}H NMR (**Figure 2.2**).

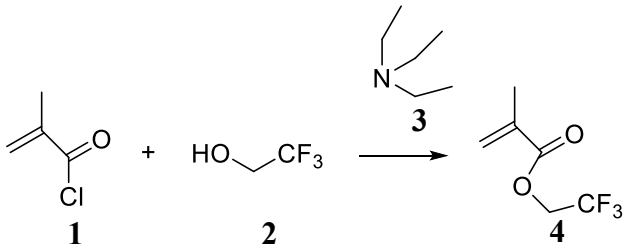

Scheme 2.1 Synthesis of 2, 2, 2-trifluoroethyl methacrylate

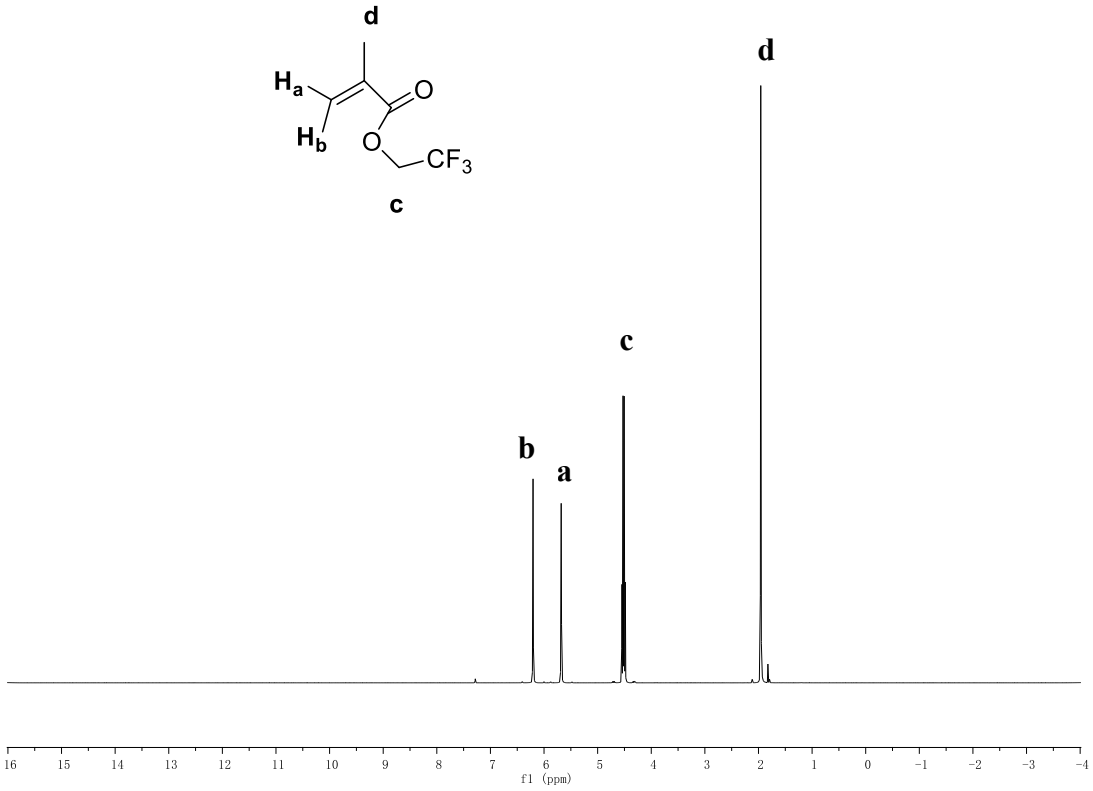

Figure 2.2 ^{1}H NMR result of 2, 2, 2-trifluoroethyl methacrylate

The chemical shift of the two singlets at 6.21 ppm and 5.68 ppm corresponded to the double bond of the methacrylate. Each peak had an integration value of 1. The -CH_2- on the side chain was found at 4.53 ppm, as a quartet with integration of 2. The singlet of methyl group was found at 1.96 ppm. ^{19}F was also used to confirm the structure and a peak at -72.81 ppm, corresponding to the CF_3 was also observed. For both steps, vacuum distillation was used to purify each compound. The yield of monomer was low (around 10%-20% for the monomer).

2.2.2 Synthesis of macroinitiator mPEG-Br (7)

mPEG was chosen as the hydrophilic block of the copolymer, since it is highly soluble in water and biocompatible. The polymer's solubility is not only determined by its structure, but also by its molecular weight. It is important that the PEG component is soluble, as this controls the solubility of any fluoro-diblock. mPEG2000 and mPEG5000 were initially tested as macroinitiators and we found that mPEG5000 failed to achieve full conversion and the resulting polymers were poorly soluble. However, full conversions could be achieved with mPEG2000, and the resulting polymers soluble in aqueous solution. Therefore, mPEG2000 was subsequently chosen as the macroinitiator for all future diblock polymers.

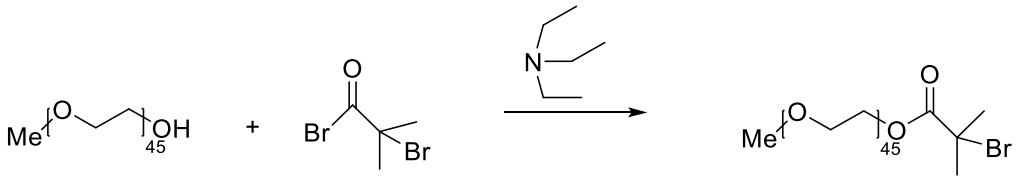

5 **6** **7**

Scheme 2.2 Synthesis of mPEG-Br

Poly (ethylene glycol) methyl ether 2-bromoisobutyrate macroinitiator was synthesised by esterification with 2-bromoisobutyl bromide. The reaction mixture was dried by azeotropic distillation and dry triethylamine was added as an acid binding reagent to prevent the reverse process taking part. The salt that formed was insoluble in toluene, thus a filtration could efficiently purify the product.

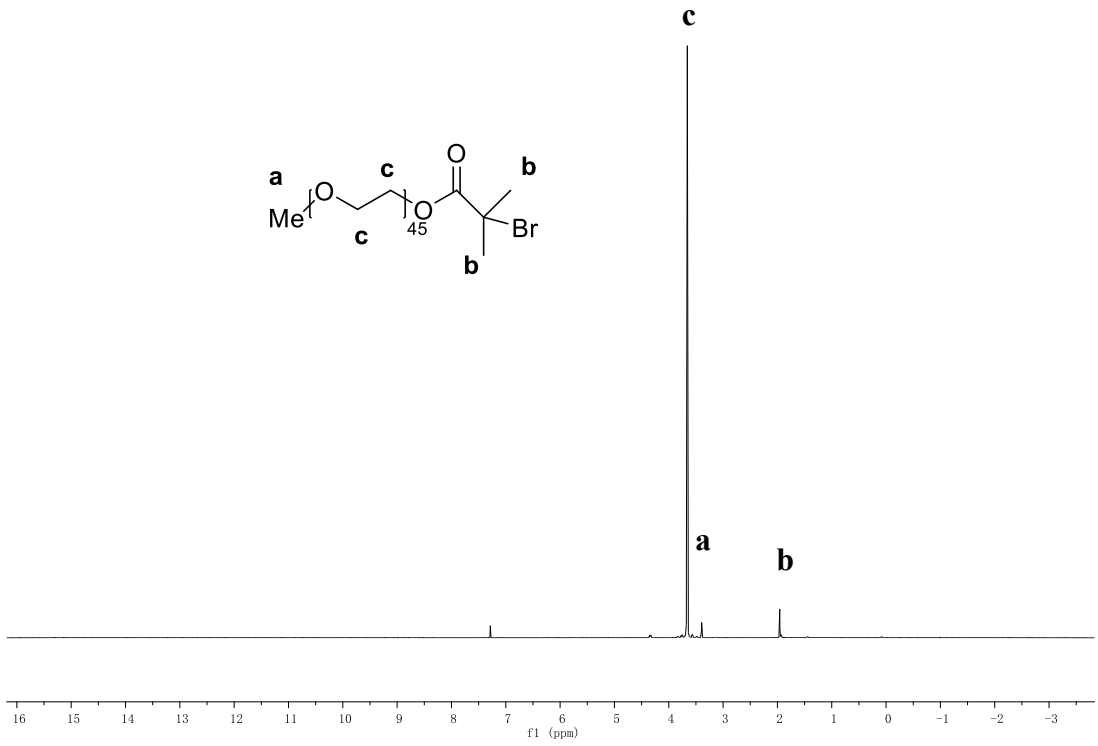

Figure 2.3 ^{1}H NMR spectrum for mPEG-Br

The ^{1}H NMR spectrum **(Figure 2.3)** shows a small singlet at 1.96 ppm, which was assigned to the protons of -$(CH_3)_2$Br. The protons from the CH_3O- backbone were observed at 3.40 ppm as a large singlet. The integration ratio of these two peaks was 6:3, which indicated that the synthesis was successful. A new peak at 4.34 ppm appeared on the spectrum of mPEG-Br due to the -CH_2-OCO- protons at the ester end of the chain. Furthermore, integration of this peak against the terminal methyl peak of CH_3O- was 2:3 and provides good evidence for the full conversion of the mPEG hydroxyl chain end. In addition, the GPC trace was unimodal with a low molecular weight distribution, which confirms that the macro-initiator was pure and had not been degraded during the synthesis.

2.2.3 Synthesis of mPEG-Poly(methyl metharylate) (9)

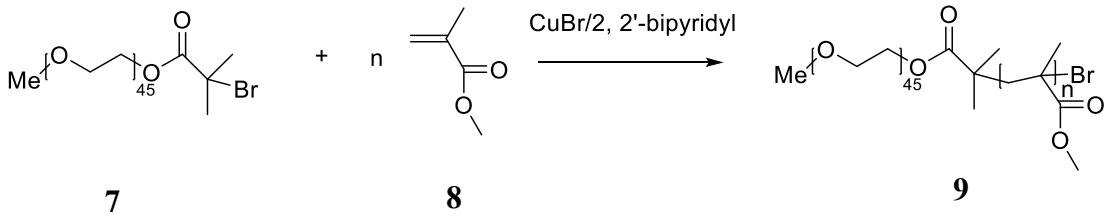

7 **8** **9**

Scheme 2.3 Synthesis of mPEG-b-PMMA

The first diblock synthesised was the control polymer mPEG-b-PMMA (**9**), as this has a similar structure to mPEG-b-PTFEMA (**10 –** described later), except it lacks the CF_3 group. Hence, in order to make sure the differences in the level of oxygen solubility were due to the fluorine environment, it was synthesised for use as a reference. The synthesis was carried out by an ATRP procedure using 2,2-bipyridine as the ligand. The synthesis was successful, but the conversion (60%-70%) was lower than expected. This was probably caused by oxygen leaking into the Schlenk flask when the ligand was added. A ligand is required to bind CuBr and move it from the solid phase into the liquid phase. The ligand was 2,2-bipyridine, which is added as a solid during the last step. To prevent oxygen entering the flask, the liquid N,N-PMDETA ligand was tested, as it can be degassed in advance, and added by syring, reducing the possibility of introducing oxygen. The reaction was successful and the ^{1}H NMR spectrum proved that the structure of the copolymer was correct. (**Figure 2.4**)

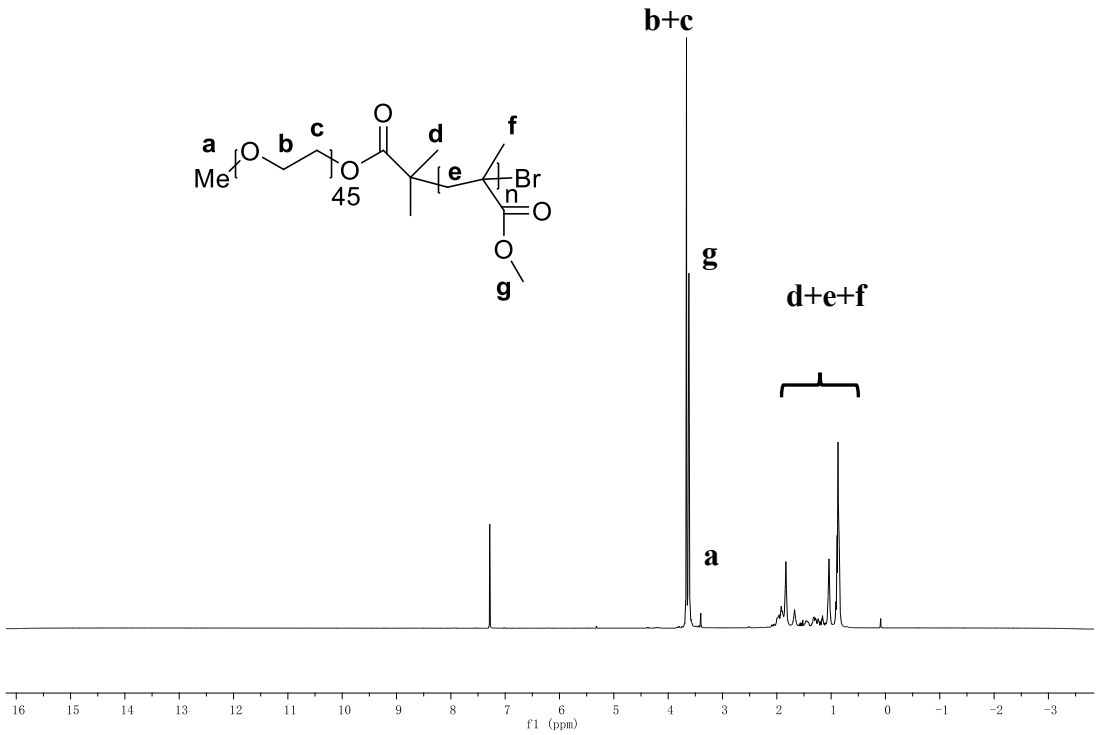

Figure 2.4 ^{1}H NMR for mPEG-b-PMMA

The backbone protons of the mPEG block were observed at 3.66 ppm. The resonances at 3.40 and 3.62 ppm were assigned to the methyl (-OCH_3) protons of the mPEG block and the pendant chain of the PMMA block respectively. The peaks from 0.8 ppm to 2.0 ppm were due to the PMMA backbones. Specifically, the two peaks that appeared between 0.8 and 1.04 were due to the methyl (-CH_3) protons caused by different tacticity.

The GPC trace was unimodal with a narrow molecular weight distribution for both polymers synthesised using the liquid 2,2-bipyridine or PMDETA ligand. Whilst the molecular weight of the polymer synthesised using the solid 2,2-bipyridine ligand was not controlled, with a higher D_p than expected and high PDI.

Table 1 Results of mPEG-b-PMMA synthesised by two ligands.

Copolymers		Copolymers theoretical n[a]	Actual n[b]	Mn (NMR)	Mn(GPC)	PDI	Ligand
mPEG-b-PMMA	**9a**	20	45	6581	8800	1.18	2,2-bipyridine
	9b	20	21	4181	5100	1.15	PMDETA
	9c	10	9	2981	4200	1.16	PMDETA

Note: n in subscripts represents the number of repeat MMA monomer in copolymer chain. All the copolymers have contained fixed $mPEG_{45}$

a. A series composition of PMMA designed before the experiment

b. As determined by integration of ^1H NMR in CDCl3

2.2.4 Synthesis of mPEG-Poly (2, 2, 2-trifluoroethyl methacrylate) (10)

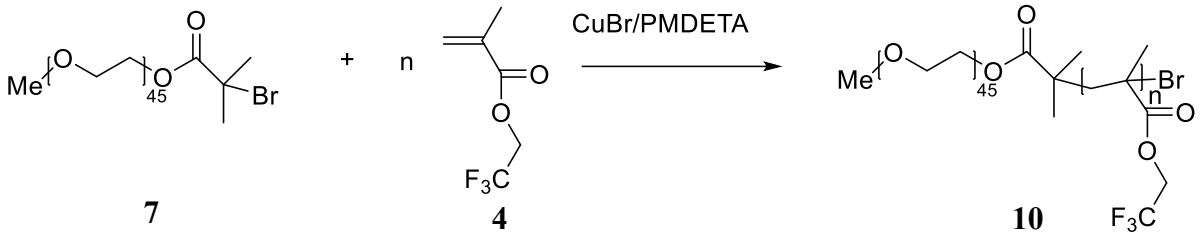

Scheme 2.4 Synthesis of mPEG-Poly(2, 2, 2-trifluoroethyl methacrylate)

Our initial attempt to synthesise the a fluoro diblock polymer was attempted using the monomer 2, 2, 2-trifluoroethyl acrylate (**1**), but this was unsuccessful. After passing through a neutral aluminium oxide and final filtration, there was no product collected. The failure might be due to the fact that 2, 2, 2-trifluoroethyl acrylate cannot form stable radicals under ATRP conditions. As such, we switched to the methacrylate monomer (2, 2, 2-

trifluoroethyl methacrylate) in the hope that the methyl group that could stabilise the radical. It was also satisfying to note, that this monomer was much cheaper to be synthesised. The reaction was repeated using the liquid ligand PMDETA, which gave a deep green colour at the beginning of the reaction, confirming formation of a Cu(I) complex. When the mixture was exposed to the air, the Cu(I) was oxidised to Cu(II) and the colour changed from green to blue. As a result of the improved procedure, the molecular weight was well controlled. (**Table 2**)

Table 2 Synthesis results of mPEG-b-PTFEMA

Copolymers		Copolymers theoretical n^a	Actual n^b	Mn（NMR）	Mn(GPC)	PDI
mPEG-b-PTFEMA	**10a**	15	17	4856	5200	1.42
	10b	25	25	6200	6630	1.55
	10c	35	33	7544	8540	1.53
	10d	45	50	10400	11400	1.60

Note: n in subscripts represents the number of repeat TFEMA monomer in copolymer chain. All the copolymers have contained fixed $mPEG_{45}$

a. A series composition of PTFEMA designed before the experiment

b. As determined by integration of ^1H NMR in CDCl3

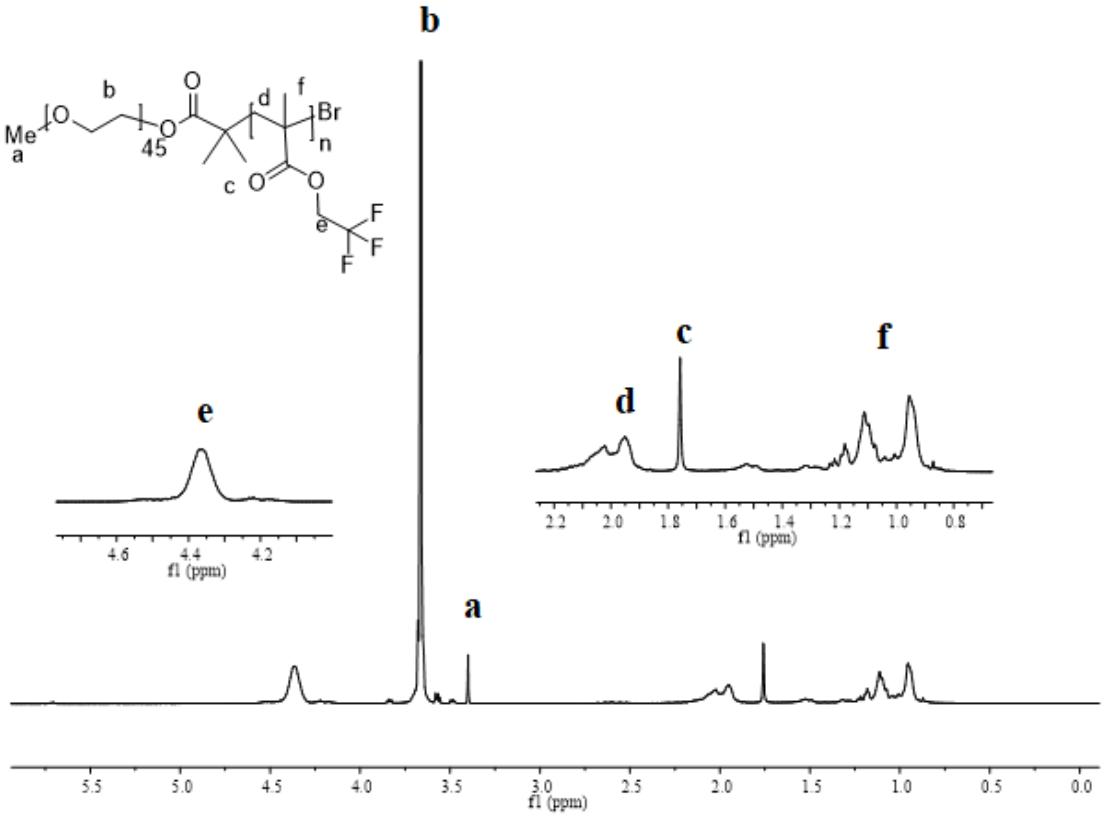

Figure 2.5 mPEG-b-PTFEMA ^{1}H NMR spectrum

Figure 2.5 shows the ^{1}H NMR spectrum of mPEG-b-PTFEMA (**10**) with the backbone protons of the mPEG block located at 3.66 ppm. The resonances at 3.40 ppm correspond to the terminal methyl protons of the mPEG block. The peaks between 1.46 ppm and 2.24 ppm were due to the protons on the PTFEMA backbone. Specifically, two peaks appeared between 0.80 and 1.19 ppm, which were due to the number of methyl environments along the backbone, caused by different tacticity. The D_p was calculated by comparing the integration value of the peaks at 3.66 ppm with the CH_2 and CH_3 peaks at 4.36 ppm and 3.40 ppm respectively.

When the ^{1}H NMR spectrum of the polymers was obtained using deuterated water, a very

different series of spectra was obtained. In these aqueous solutions and at the concentrations studied (1×10^{-3} M), the only peaks observed in the spectrum were the peaks corresponding to the PEG protons. This is typical behaviour for PEG-based micellar structures and indicates aggregation of the diblock polymer and congestion within the core. This congestion restricts and slows down any free-motion/rotation of the fluoro monomers, resulting in coalescence (with respect to the NMR timescale).[71,72]

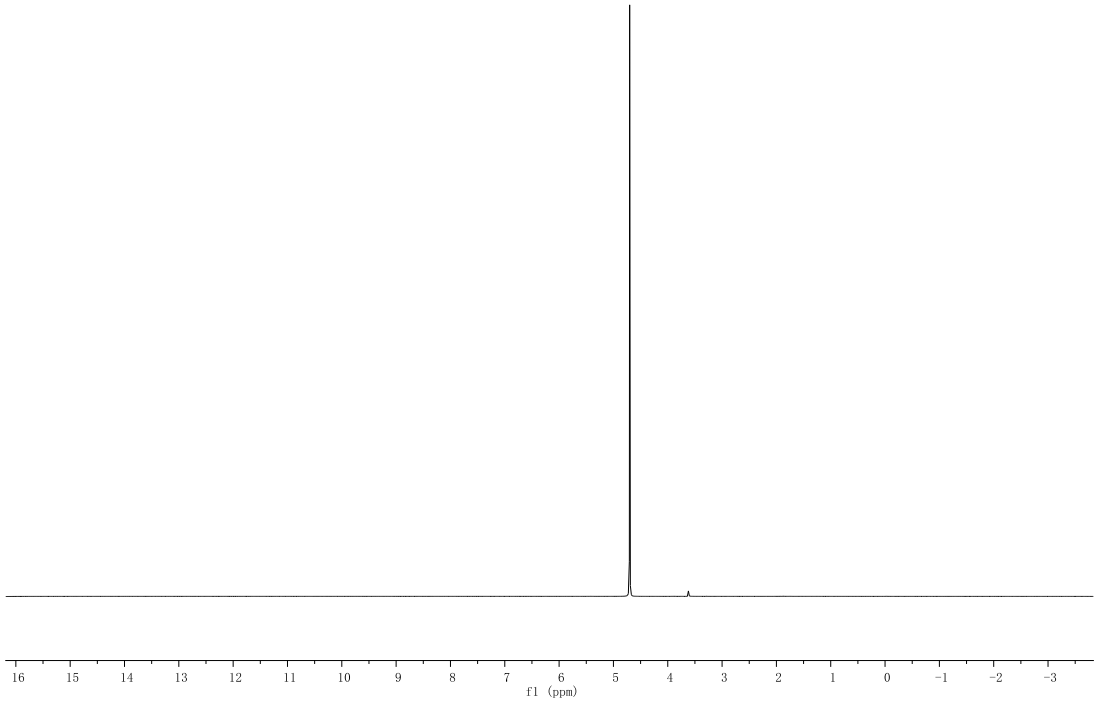

Figure 2.6 mPEG-b-PTFEMA ^{1}H NMR in D_2O.

The ^{19}F NMR spectra showed a similar result that a strong peak at -73.3 ppm could be observed in $CDCl_3$, but only a very weak signal was visible in the D_2O spectrum at -73.1 ppm (1×10^{-3} M in both solvents). (**Figure 2.7**)

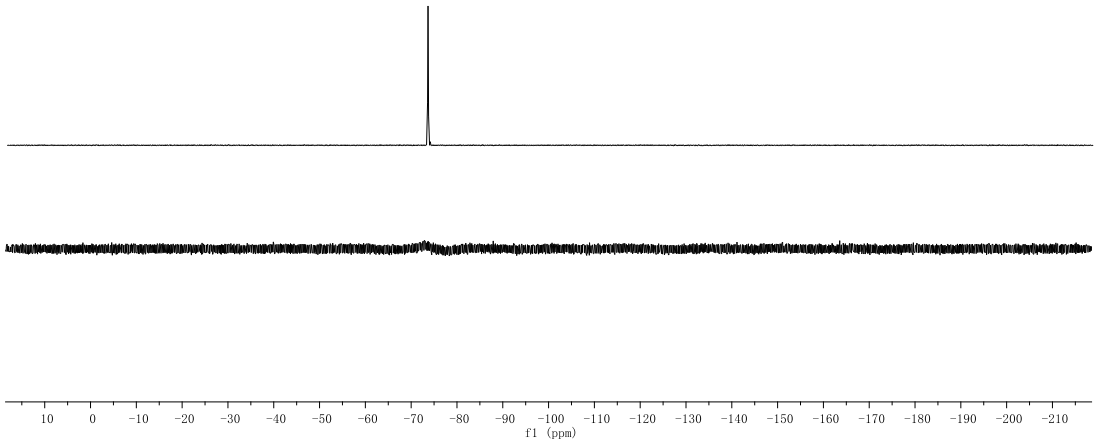

Figure 2.7 ^{19}F NMR spectrum of mPEG-b-PTFEMA in $CDCl_3$ (above) and D_2O (below) respectively

For all series of mPEG-b-PTFEMA (**10**), the GPC results showed high PDI and bimodality caused by the relatively low refractive index of the fluorinated block that exaggerated the RI signal of any remaining macro-initiator and underestimated the signal of diblock copolymers. [73,74](**Figure 2.8**)

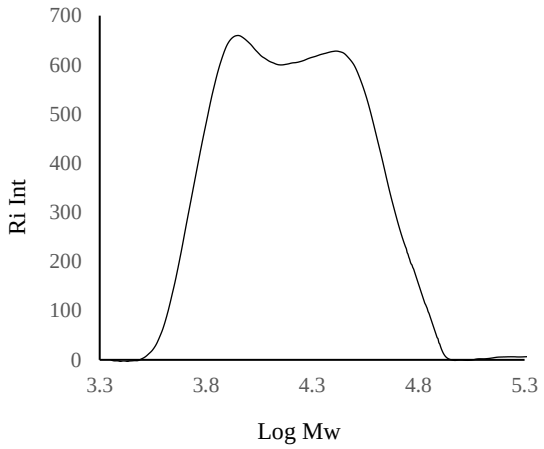

Figure 2.8 Representative GPC trace of mPEG-b-PTFEMA (**10b**) showing the bimodal peak

2.2.4 Self-assembly Study for mPEG-b-PTFEMA

As the fluorinated chain is hydrophobic and lipophobic, there was a possibility that mPEG-b-PTFEMA would not form proper micelles. Hence, aggregation and micellation were confirmed and quantified through critical micelle concentration (CMC) experiments. These were performed using a fixed concentration of pyrene and measuring changes in emission intensity with respect to increased polymer concentrations. From 350 nm to 450 nm wavelength, the pyrene vibronic fluorescence spectrum has five peaks. The ratio of the intensities (I1/I3) of the first to the third peaks depends on the polarity of the environment. From the outside to the inside of micelles, pyrene experienced different microenvironments indicated by the intensity ratio (I1/I3) of the fluorescence spectrum. Plots of polymer concentration vs. changes in pyrene emission were used to obtain the CMC values, which ranged from 0 .0024 to 0.0036 mg/mL and are typical of those reported for PEG-based polymeric micelles.

Specifically, copolymer mPEG-b-PTFEMA (**10d**) was difficult to dissolve, even when it was mixed with THF. The final solution of mPEG-b-PTFEMA (**10d**) was always distinctly turbid and it clearly precipitated overnight. Thus, it was not considered for further experiments.

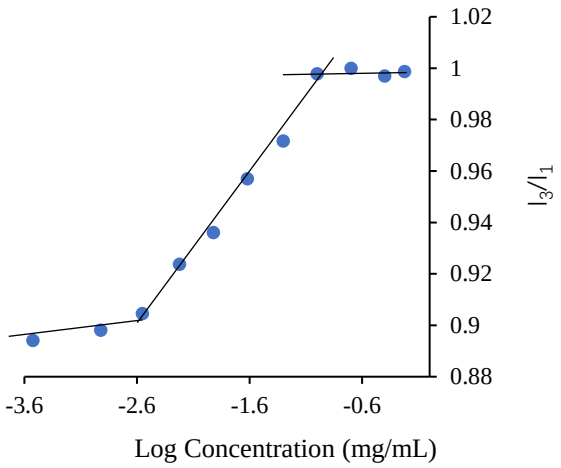

Figure 2.9 Representative CMC plot for mPEG-b-PTFEMA

Figure 2.9 shows the intensity ratio (I3/I1) vs logarithm of the various mPEG-b-PTFEMA diblock copolymer concentrations. A substantial increase of I3/I1 begins above a certain concentration, indicating the onset of the micelle formation. Therefore, the interception of two straight trend lines was used to determine the CMC. (**Table 3**)

Table 3 CMC of mPEG-b-PTFEMA with varies chain length

Copolymers[a]		Actual n^b	CMC/ mg ml^{-1}
mPEG-b-PTFEMA	**10a**	17	0.00355
	10b	25	0.00362
	10c	33	0.00239

Note: n in subscripts represents the number of repeat TFEMA monomer in copolymer chain. All the copolymers have contained fixed $mPEG_{45}$

a. A series composition of PTFEMA designed before the experiment

b. As determined by integration of ^1H NMR in $CDCl_3$

Furthermore, to verify the CMC, dynamic light scattering was carried out to determine the mean diameter of the aggregates formed at different concentrations. Theoretically, at a concentration lower than CMC, there would be no aggregates. Dynamic light scattering experiments were performed above and below the CMC. Whilst no significant peaks could be detected below the CMC, solvated particles with an average size of 80-100 nm were observed (**Table 4**) when the measurements were taken at a concentration above the CMC (0.006, 0.01,1 mg/mL).

Table 4 DLS results for a representative mPEG-b-PTFEMA

Copolymer	DLS
n^a=25 concentration/mg mL^{-1}	nm
0.001	xx
0.006	86.49
0.01	86.43
1	92.93

Note: n in subscripts represents the number of repeat TFEMA monomer in copolymer chain. The copolymers have contained fixed $mPEG_{45}$
a. A series composition of PTFEMA used for the DLS measurement.

The formation of micelles was confirmed by microscopy (TEM), which showed spherical particles with diameters around 30-50 nm. (**Figure 2.10**)

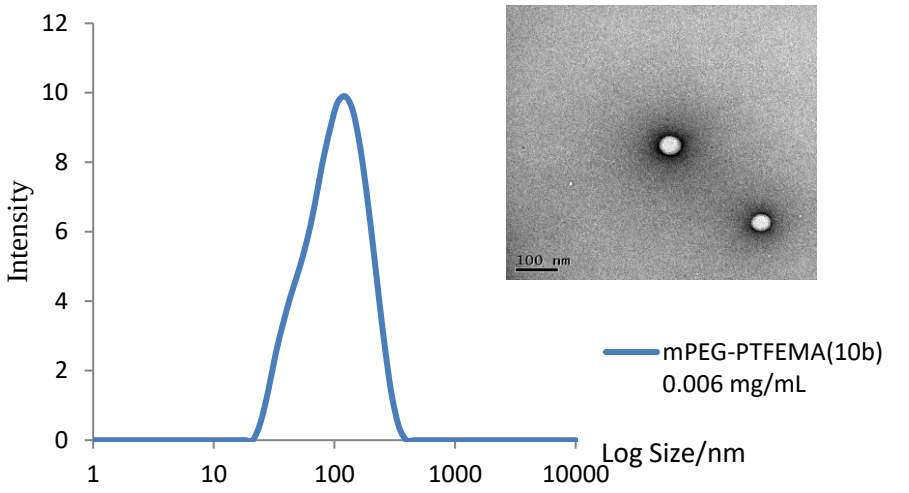
12
10
8
6
4
2
0
Intensity
1
10
100
1000
10000
Log Size/nm
100 nm
mPEG-PTFEMA(10b)
0.006 mg/mL

a)

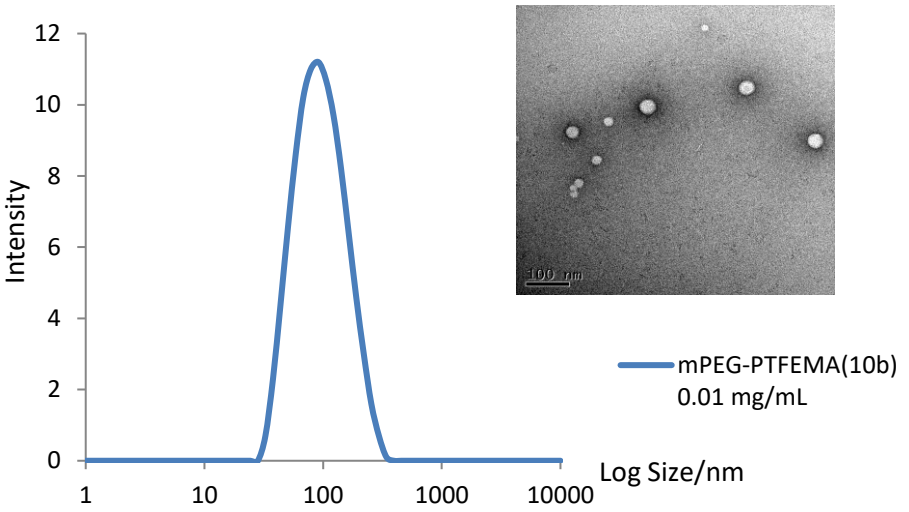
12
10
8
6
4
2
0
Intensity
1
10
100
1000
10000
Log Size/nm
100 nm
mPEG-PTFEMA(10b)
0.01 mg/mL

b)

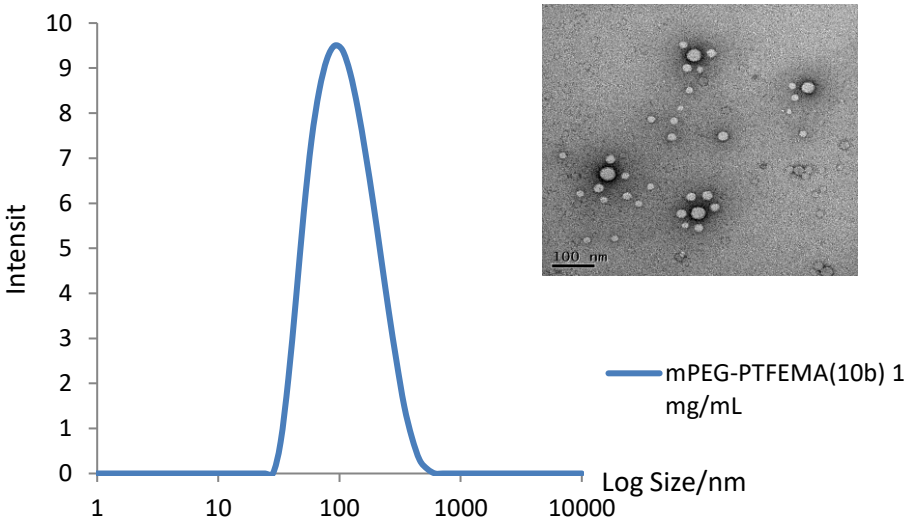
10
9
8
7
6
5
4
3
2
1
0
Intensit
1
10
100
1000
10000
Log Size/nm
100 nm
mPEG-PTFEMA(10b) 1
mg/mL

c)

Figure 2.10 DLS and TEM microscopies for mPEG-b-PTFEMA (**10b**) at different concentrations **a)** 0.006 mg/mL **b)** 0.01 mg/mL **c)** 1 mg/mL

According to DLS results for the same polymer, micelles started forming and the average size stayed consistent at lower concentrations. However, at a higher concentration, the average size increased, which was consistent with our TEM observation where particles tended to gather together to form bigger aggregations at high concentrations.

Although the DLS was not sensitive and accurate enough at a very low concentration, it still showed a big difference between concentrations below the CMC and those above the CMC. Combining the results with those obtained from fluorescence confirms the CMC (**Table 4**). Both fluorescence measurement and DLS provide clear evidence that the copolymer mPEG-b-PTFEMA was able to form stable micelles in an aqueous solution.

2.2.5 Dissolved Oxygen Study for mPEG-b-PTFEMA

Oxygen incorporation was initially studied using ^{19}F NMR, which can be used to probe where oxygen dissolves within the micelle. Specifically, as an example, ^{19}F NMR was used to investigate any effect on the chemical shift of the fluorine groups of mPEG-b-PTFEMA (**10b**) in the presence and absence of oxygen. To some extent, this was difficult, as the highly restricted mobility within the aggregated micelle results in strong dipolar coupling, leading to a significant attenuation of the ^{19}F NMR signal in D_2O (discussed above). [72] Nevertheless, it was still possible to observe a small peak at -73.1 ppm in the oxygen free sample. After bubbling oxygen through the same solution, a small but reproducible shift of

the fluorine peak, to -72.1 ppm, was observed (**Figure 2.11)**. This represents a shift of 1 ppm, which is consistent with the shifts observed for perfluoro emulsions under similar aqueous conditions.[75] Although this is a qualitative method and does not tell us how much oxygen has bound, it did provide some initial encouragement that the oxygen could be encapsulated/bound within the fluorine core/block of the polymeric micelle.

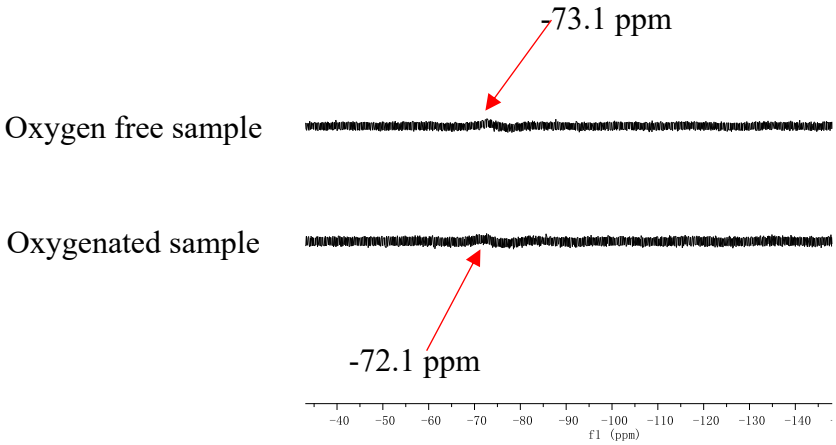

Figure 2.11 ^{19}F NMR spectrums for mPEG-b-PTFEMA (**10b**) in D_2O without oxygen (above) and with oxygen (below)

To obtain support that is more qualitative for oxygen dissolution, we used a commercial dissolved oxygen meter to determine the concentration of oxygen dissolved in an aqueous solution. This is a luminescent-based technique and can only measure the amount of oxygen dissolved within bulk water. The optical DO (dissolved oxygen) sensors could measure DO levels in-situ accurately and quickly by lifetime-based luminescent technology. To be more specific, when the oxygen-specific lumiphore is excited by a blue light, it will emit red light. In the presence of oxygen molecules, the excited lumiphore molecules will be quenched, which prevents the emission of red light. Due to the DO concentration and red-light emission being inversely proportional, the photodiode is able

to detect the red-light signal and the DO concentration can thus be calculated.

As we previous reported,[70] a dissolved oxygen probe/meter can only measure oxygen in bulk solution and it cannot directly measure or detect any oxygen dissolved within other species, such as a micelle, because the oxygen must touch the probe. However, if we saturate a bulk micellar solution with pure oxygen, we can measure the rate that oxygen in the solution equilibrates with the air, where the concentration of oxygen is much lower (around 20% in air), as shown in **Figure 2.12**.

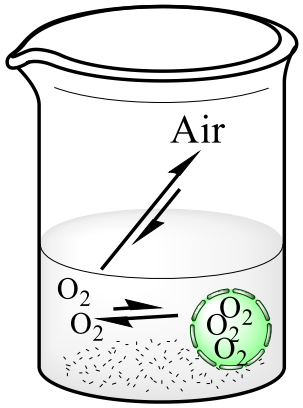

Figure 2.12 i, oxygen keeps equilibrating with oxygen in the air. **ii,** the oxygen released from the bulk solution to the air can be replaced by the oxygen released from the micelle. **iii,** overall, the release rate is slow.

This rate can then be compared with a control using a simple aqueous solution that does not contain a micelle. Any differences in rate will be related to the oxygen bound within the micelle, which can only be released when the oxygen dissolved in the saturated aqueous solution returns to the atmosphere. This is an established method and has previously been used to measure oxygen content and release from perfluoro systems [76] and fluoro-polymers.[42,77] All experiments were carried out using the same volume of

water and at the same temperature (20 °C). The levels of oxygen release from water are shown in **Figure 2.13.**

Initially, the release of oxygen from a saturated aqueous solution was studied as the control (no polymer). The rate of release and the half-life was calculated from a plot of oxygen concentration vs time, which could be matched with a first order decay. (**Figure 2.13**)

To ensure the oxygen solubility was mainly affected by the fluorine content, the second control was carried out using just the mPEG component in water. The release of oxygen from the mPEG solution was indistinguishable to the aqueous control, producing an identical plot and kinetic data. (**Figure 2.13**) This confirmed that at the concentration studied (5 mg/mL), the mPEG component had no positive effect on the solubilisation of oxygen, which is consistent with previous studies on the oxygen solubilisation within PEG solutions.[78] A third control was also carried out using mPEG-b-PMMA which forms micelles but does not have any fluorines. These experiments gave the same results as the mPEG or aqueous solutions. These results provide solid evidence that the oxygen solubility was dependent on the fluorine content.

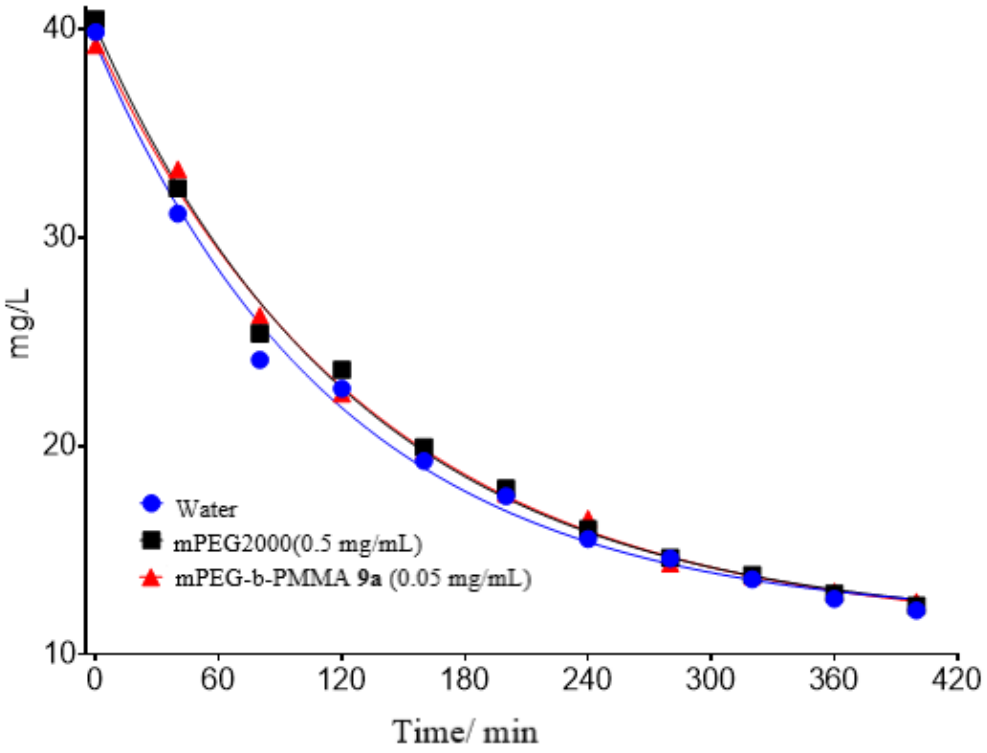

Figure 2.13 Oxygen release curve in water, mPEG2000 solution and mPEG-b-PMMA solution.

Having established the controls and baseline levels, the experiment was repeated using the mPEG-b-PTFEMA (**10**) diblock copolymers at various concentrations (**Table 5**). The solubility of the polymers was relatively poor and dependent on the length of the fluoro-block, which limited the amount of polymer that could be used. For example, although mPEG-b-PTFEMA (**10a**) was the most soluble, it was hard to solubilise at concentrations above 5.0 mg/mL.

Table 5: Oxygen release rates and half-lives for the mPEG-b-PTFEMA polymers.

Polymer		Concentration mg/mL	Fluorine content mmol/mL	Rate of O2 release 10^{-3} mg/mL/min	Half-life mins
Water		/	/	4.2	160
mPEG-b-PTFEMA	**10c**	0.5	0.007	2.9	240
	10b	0.5	0.006	3.9	180
	10a	0.5	0.005	4.2	165
	10b	2.0	0.024	3.6	195
	10a	2.0	0.021	3.8	182
	10a	5.0	0.053	2.1	325

The larger mPEG-b-PTFEMA (**10c**) sample was the least soluble and was only soluble at concentrations below 1.0 mg/mL. At higher concentrations, such as 2 mg/mL or 5 mg/mL, the solution started to become turbid, and after being left overnight, a thin layer of white film could be observed at the bottom. Clearly at higher concentration, small amounts of undissolved polymers were lost as a suspension. To make the measurements and data unified, efforts were made to measure the oxygen release rate at high concentrations of mPEG-b-PTFEMA (**10c**) despite the precipitation. Hence the actual concentrations of the polymer solutions were slightly lower than the designed concentrations. mPEG-b-PTFEMA (**10b**) solutions could be made to a maximum solubility of 5.0 mg/mL, but over

time, a colourless precipitation was also noticed. As a result, the solution became turbid during the oxygen release experiments, which limited the reliable data that could be collected (see **Figure 2.15**). Precipitation was also observed by others when studying similar polymers, where phase changes occurred in the presence of oxygen.[43,44] Nevertheless, despite the precipitation of mPEG-b-PTFEMA (**10b**) at the higher concentration (which limited the quality of data that could be collected), it does indicate good oxygen retention/solubility for these polymers at the high concentration.

For all solutions, the change in oxygen concentration was plotted with respect to time and the data matched with a first order decay. The rate of oxygen release, along with the half-lives for all soluble polymers, is shown in **Table 5**. The graphs and kinetic data from the polymer solutions clearly show that oxygen is released more slowly when compared to the rate of oxygen release from the simple aqueous solution (no polymer). This confirms that oxygen has been retained within the micelle and is only released into the aqueous phase when it can replace the dissolved oxygen as it returns to the atmosphere. The process continues until the equilibrium position is reached, which occurs at an oxygen concentration around 9 mg/L at 20 °C. At the higher concentrations, a common trend of longer half-lives and slower rates (of oxygen release) were observed.

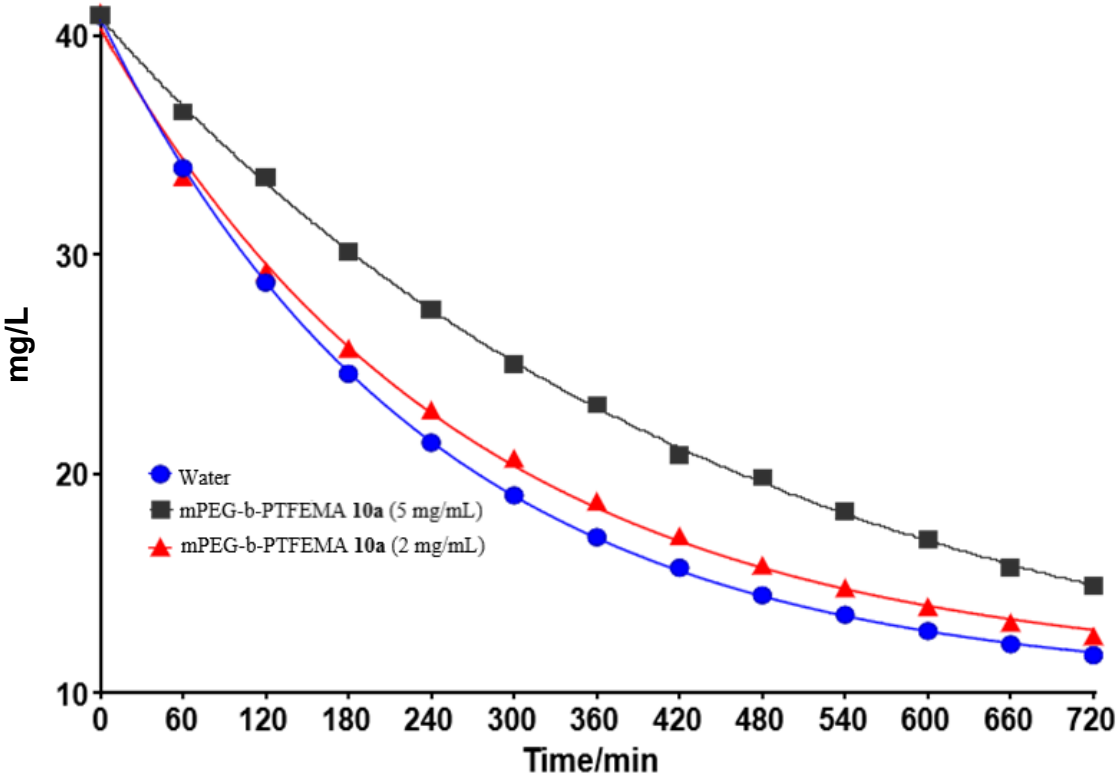

Figure 2.14 Oxygen release curve of mPEG-b-PTFEMA (**10a**) at various concentrations. (0.05 mg/ml was not shown in the graph since it effectively overlaps the water line)

For example, mPEG-b-PTFEMA **10a** at a concentration of 5.0 mg/mL had a half-life that was double the value recorded at 0.5 mg/mL. (**Figure 2.14**) Furthermore, even at 2 mg/mL concentration, it still displayed a 20-minute difference in half-life time compared with water. The results of mPEG-b-PTFEMA **10a** were most promising since the solution was transparent during the experiment and even after 48 hours. A similar result was observed when measuring the mPEG-b-PTFEMA **10b**. At a concentration of 2 mg/mL, the half-life was 15 minutes longer than that of 0.5 mg/mL. However, for the concentration 5 mg/mL, during the measurement, a precipitation formed, which led to irregular oxygen release. (**Figure 2.15**) Although the meter was designed to be used in polluted water in a small vial,

the sample that touched the probe was not a homogenous solution, which could have affected the signal. Even though the results fluctuated and could not be matched with a first order decay, the data still gave solid evidence that at 5 mg/mL the oxygen release rate was much slower.

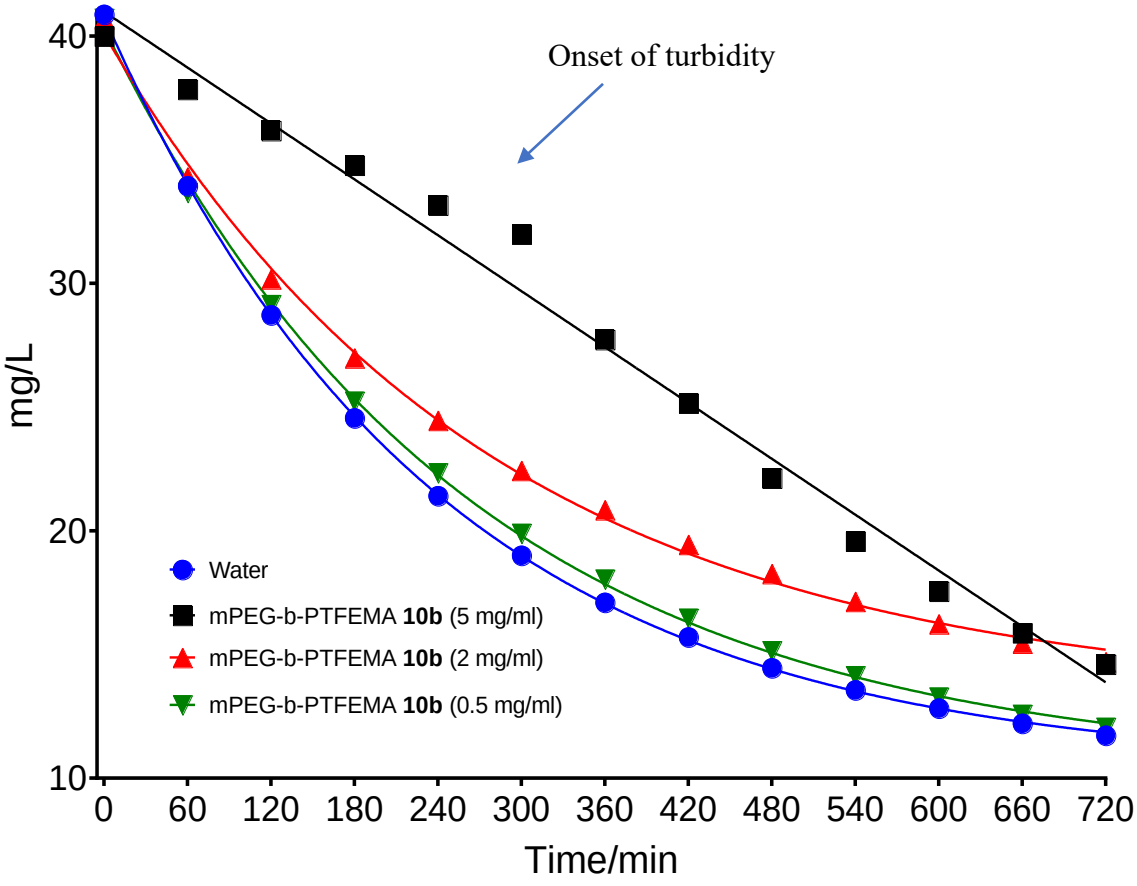

Figure 2.15 Oxygen release curve of mPEG-b-PTFEMA (**10b**) at various concentrations

Due to the low solubility of mPEG-b-PTFEMA (**10c**), all solutions were turbid. This explains why the results for all concentrations were similar. (**Figure 2.16**)

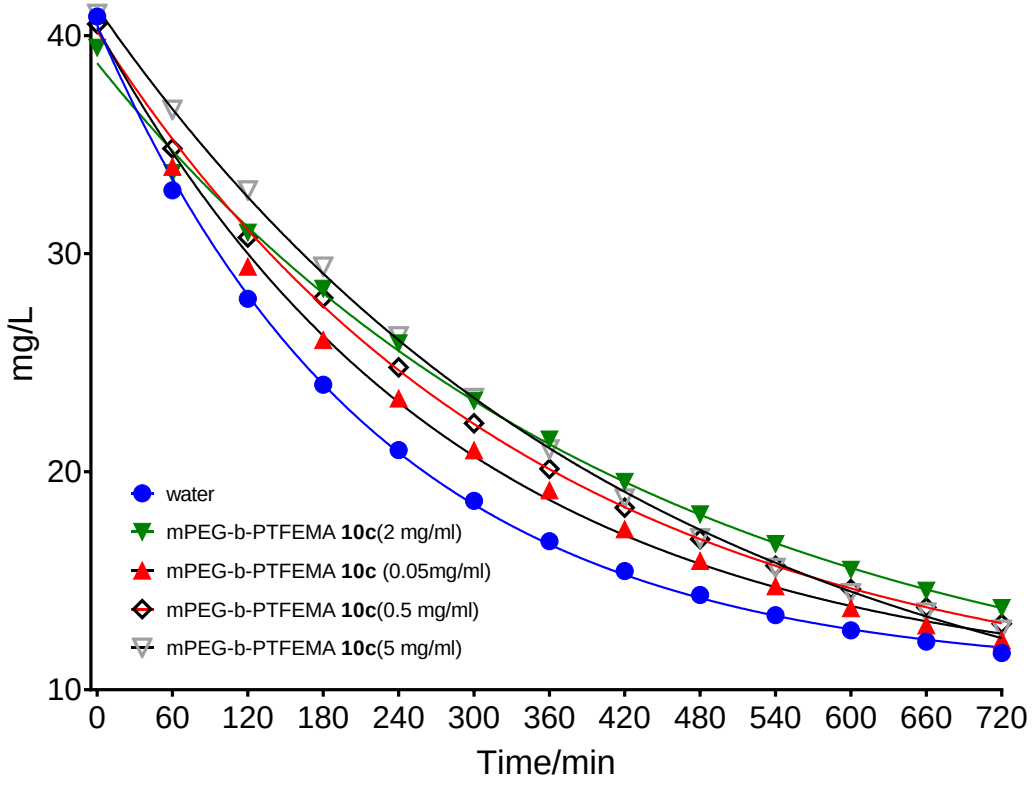

Figure 2.16 Oxygen release curve of mPEG-b-PTFEMA (**10c**) at various concentrations

From another perspective, if we consider all polymers at each concentration, we observe that half-lives and rates of release are also dependent on the length of the polyfluoro block. For example, at a concentration of 0.5 mg/mL, all copolymers have similar fluorine content, but mPEG-b-PTFEMA (**10c**) had the longest half-life and slowest rate of release. (**Table 5**). At a concentration of 2 mg/mL, mPEG-b-PTFEMA (**10b**) had the longest half-life and slowest rate of release. However, at 5 mg/mL, the mPEG-b-PTFEMA (**10a**) had the longest half-life, which was due to the best solubility. Overall, the ability to dissolve oxygen is directly related to the amount of fluorine in a solution.

In a further effort to establish and quantify oxygen dissolution, we attempted to measure the oxygen concentration using an enzyme-based method.[70] The method was originally developed by Ghosh[79] and subsequently refined for Marrucho.[80] This method is based on the oxidation of glucose by molecular oxygen and is catalysed by glucose oxidase.

Although this original aim of this method was to measure glucose concentration in the presence of excess oxygen, when glucose is the excess reactant, the method could be used to measure the concentration of molecular oxygen. The glucose and oxygen are reacted stoichiometrically for the measurement. The method is well established and the reagents are available in the form of a glucose assay kit (purchased from Sigma–Aldrich). As with the published procedures,[79,80] air was used instead of oxygen as there is no significant difference in solubility and it simplifies the experimental procedure.

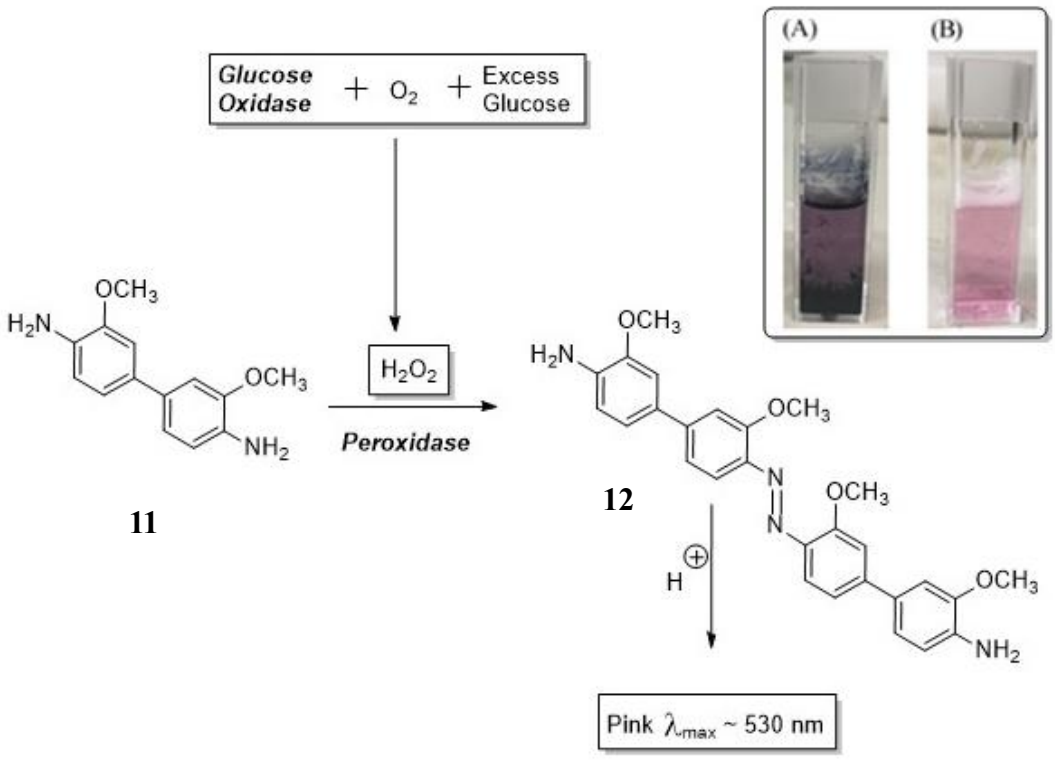

Scheme 2.5: Enzyme mediated reaction used to estimate oxygen concentrations in water. Reactions performed using excess glucose. Insert shows: (A) the dark precipitate that initially forms within the polymer solution after the oxidation reaction and (B) the same solution after 9 hours and filtration.

The assay was performed at 37 °C and the reactions are shown in **Scheme 2.5**. At this temperature, the solubility of oxygen in water is around 6.0 mg/L. As such, a glucose concentration of 55 μg/mL was used (equivalent to 10 mg/L of oxygen) as this was found to be optimal with respect to the experimental conditions. The reaction was initially performed in just water to give a reliable baseline/control reading. However, when the assay was repeated using a 5 mg/mL aqueous solution of mPEG-b-PTFEMA (**10b**), a coloured precipitate formed, which precluded an accurate determination of absorption and prevented us from making a comparison with the baseline/control reading. However, filtering or centrifuging the solution resulted in absorptions that were lower than those recorded for water. Alternatively, we left the so that the precipitate could settle and a UV measurement could be made by carefully removing the solution from the top of the sample, but the results were variable and dependant on the time (required for settlement). We assumed that some of the dye must be bound or trapped on the precipitate, reducing its concentration in the water. This assumption proved correct, as over time, the precipitate settled and the solution's colour became more intense as the dye was released. Solutions (baseline/control and polymer) were therefore left to settle for 12 hours. Afterwhich no change in colur could be detected. Solutions were then filtered to remove the percipitate (see insert, **Scheme 2.5**). The UV spectrum of the two solutions was recorded and the absorption intensity at 535 nm compared. The result indicates that the polymer solution has an absorption higher

than the similarly treated aqueous solution (without polymer). **(Figure 2.17.)** Comparing the intensities of the two peaks, we can estimate a minimum oxygen concentration that is 33% higher than that determined for water (6.0 mg/L at 37 °C) alone. This increase in absorption intensity corresponds to an oxygen concentration of around 8 mg/L at 37 °C. Although precipitation caused problems, the enzyme method qualitatively supports the results obtained from the NMR and dissolved oxygen experiments. Taking all of the results together, we can conclude that the polyfluoro micelles can increase the concentration of oxygen within water.

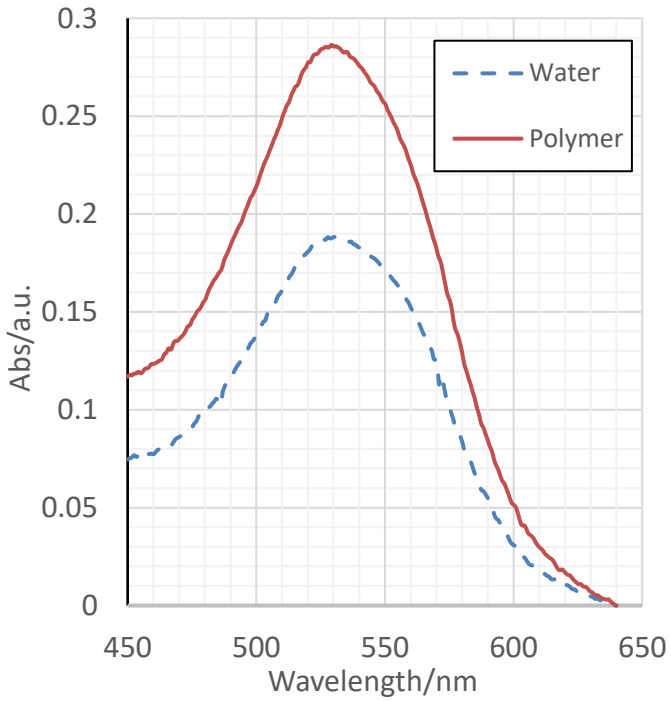

Figure 2.17 UV results from enzyme assay. The data shows a stronger absorption for the mPEG-b-PTFEMA (**10b**) solution, indicating a higher oxygen concentration

Based on the results from mPEG-b-PTFEMA, if more fluorine were introduced inside the

micelle, the oxygen capacity would increase. Moreover, the structural effect of the copolymer composed by other monomers with more fluorine on oxygen dissolution will be studied and compared with similar PTFEMA systems.

2.2.6 Synthesis of mPEG-b-PPFPMA (14)

In order to obtain polymers with more fluorine, whilst keeping the length of the polymer block short enough to maintain solubility, a monomer with more fluorine was used. Hence, PFPMA with five fluorines on the pendant chain was chosen for the second generation diblock copolymers.

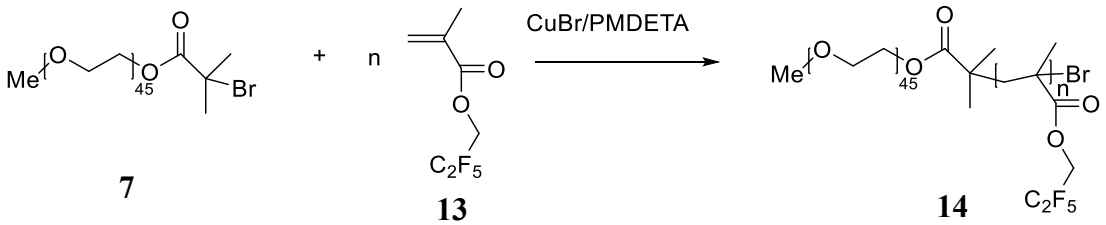

Scheme 2.6 Synthesis of mPEG-b-PPFPMA

The copolymer was also synthesised via ATRP with PMDETA as the ligand. (**Scheme 2.6**). As this fluorinated block also has low refractive index, the GPC produced the bimodal peak, which caused a slightly higher PDI than normal ATRP products. (**Table 6**)

Table 6 Synthesis results of mPEG-b-PPFPMA

Copolymers	target D_p	Obtained D_p	Mn(NMR)	Mn(GPC)	PDI(GPC)
14a	15	12	4616	4480	1.23
14b	25	23	7014	7300	1.30
14c	35	44	11592	12900	1.20

^{19}F and ^{1}H NMR were used to confirm the polymer's structure. (**Figure 2.18**).

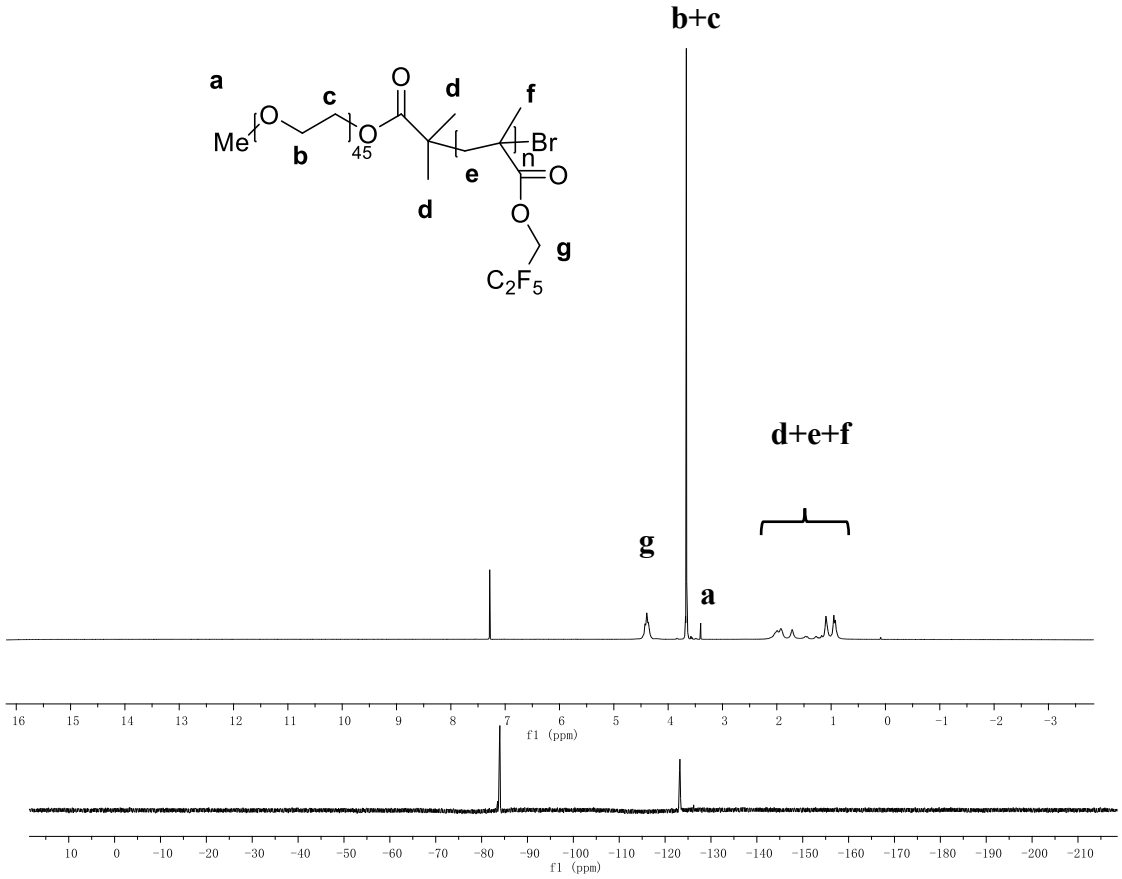

Figure 2.18 ^{1}H NMR spectrum (above) and ^{19}F NMR spectrum (below) for mPEG-b-PPFPMA (**14b**)

The mPEG-b-PTFEMA, backbone protons of the mPEG block were located at 3.66 ppm. The resonances at 3.40 ppm corresponded to the terminal methyl protons of the mPEG block. The peaks between 1.62 ppm and 2.24 ppm were due to the protons on the PPFPMA backbone. A further two peaks appeared between 0.77 and 1.22 ppm and were assigned to the methyl group along the backbone; the observed splitting was caused by the different tacticity. The D_p was calculated by comparing the integration value of the backbone protons of the mPEG block at 3.66 ppm with the CH_2 and CH_3 peaks at 4.40 ppm and 3.40 ppm respectively. The CF_3 and CF_2 peaks were found at -83.89 ppm and -123.10 ppm respectively with the integration ratio equal to 3:2.

2.2.7 Self-assembly Study of mPEG-b-PPFPMA

Due to the hydrophobicity and lipophobicity of the fluorinated block, the solubility of the copolymer in water was generally lower due to a higher number of fluorines on the block. For example, solutions of mPEG-PPFPMA with D_p higher than 25 started to show turbidity around 5 mg/mL. After standing overnight a precipitate was observed. This lack of solubility occurred at a much lower D_p than the 3F system and only became apparent at D_p over 33.

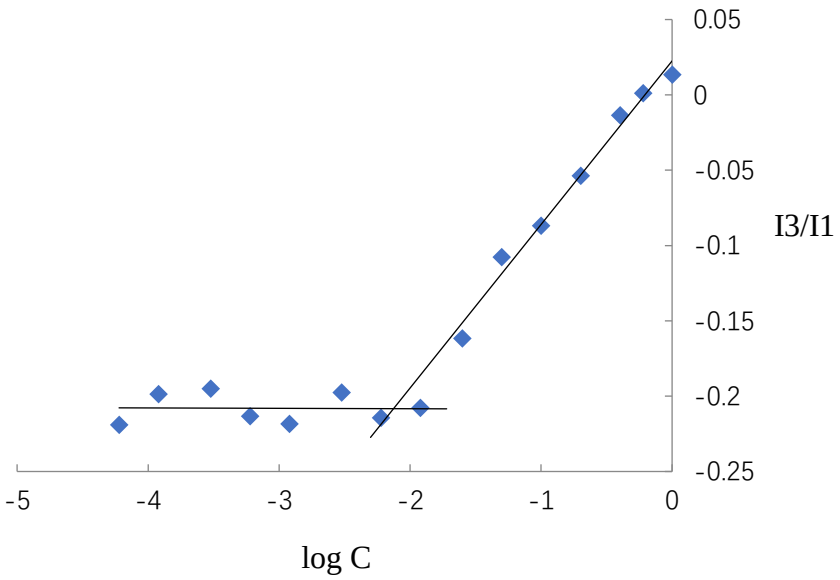

Figure 2.19 Representative CMC measurement for mPEG-b-PPFPMA (**14a**)

The CMC measurements were carried out as previously described and worked well for mPEG-PPFPMA. However, mPEG-b-PPFPMA (**14c**) was insoluble and the CMC could not be measured. A representative CMC plot for the other polymers is shown in **Figure 2.19.** Although the CMC values fell into a similar range to those measured for mPEG-b-PTFEMA (and shown in **Table 7),** they were slightly higher. As such, these micelles would be slightly less stable and would dissociate when diluted during blood circulation.

Table 7 CMC results for mPEG-b-PPFPMA

Copolymers		**CMC/ mg/mL**
mPEG-b-PPFPMA	**14a**	0.00927
	14b	0.03430
	14c	\

2.2.8 Dissolved Oxygen Study for mPEG-b-PPFPMA

Based on the oxygen measurements of mPEG-b-PTFEMA (**10**), the dissolved oxygen meter could provide a useful method for determining the oxygen content within the polymer micelle. However, for micellar solutions of the copolymer mPEG-b-PPFPMA (**14**), bubbling oxygen through the solution generated an abundance of foam. As such, the foam could carry material out of the vial, causing a reduction in the concentration of the polymer. Therefore, the flow rate of the oxygen was reduced. Additionally, time was required to allow any foam to settle before insertion of the probe. Overall, it was difficult to achieve full oxygen saturation, which limited any comparisons of oxygen release between mPEG-PPFPMA (**14**) and mPEG-b-PTFEMA (**10**). The release profiles are shown in **Figure 2.20** and the data for each polymer shown in **Table 8**. For polymer concentrations of 0.05 mg/mL and 2 mg/mL, the oxygen release rates of both mPEG-b-PPFPMA (**14a**) and (**14b**) were indistinguishable from the water, but at a concentration of 5 mg/mL, the oxygen was released more slowly. (**Figure 2.20**). This demonstrated that if the fluorine content was insufficient, differences of the fluorinated block's length would have insignificant effects on oxygen dissolution, which was consistent with the previous work. Increasing the fluorine content to a certain level, though, would result in solutions with oxygen capacity.

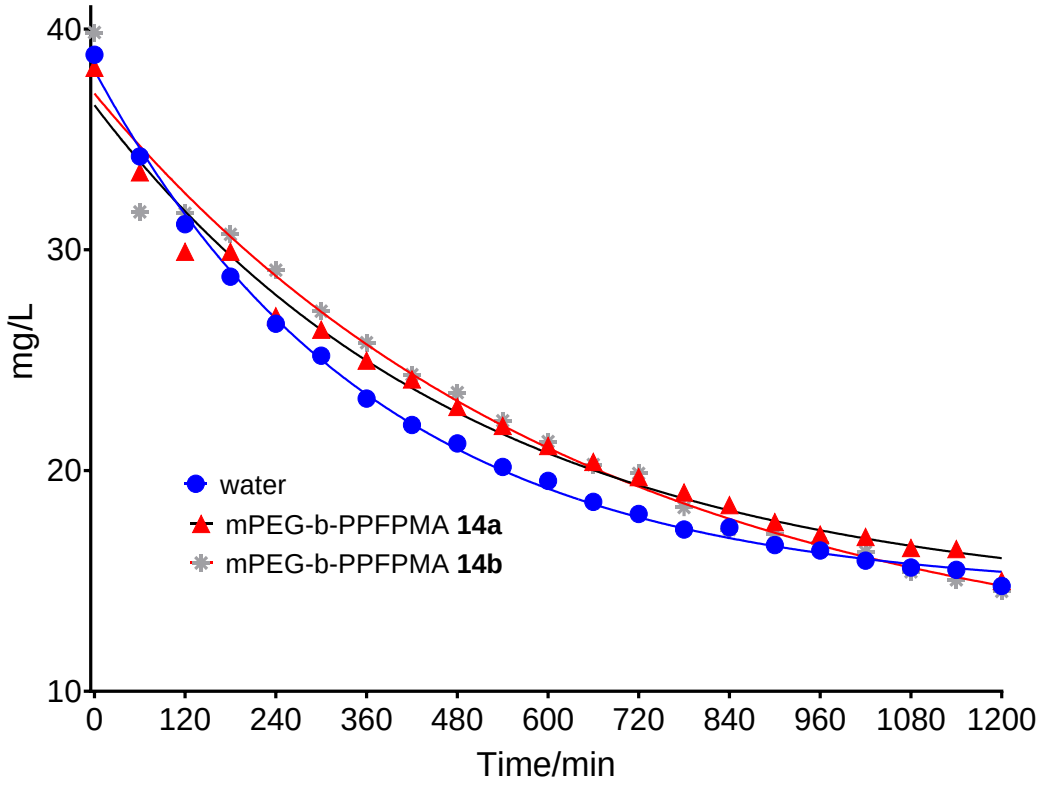

Figure 2.20 Oxygen release rate curve of mPEG-b-PPFPMA with different composition at 5 mg/mL

Statistically, the half-life of oxygen release for mPEG-b-PPFPMA was longer than water, and the longer fluorinated block (more fluorine) has a longer half-life than the shorter chain (less fluorine) (**Table 8**), which once again confirmed that the total fluorine amount affects oxygen dissolution.

Table 8 Oxygen release rates and half-lives for the mPEG-b-PPFPMA polymers.

Polymer System	Concentration- mg/mL	Fluorine content- mmol/mL	Rate of O_2 release – $\times 10^{-3}$ mg/mL/min	Half-life- mins
Water (no polymer)	/	/	2.7	257

mPEG-b-	**14a**	5	0.065	2.0	347
PPFPMA	**14b**	5	0.082	2.6	440

2.2.9 DLS Study for Oxygen Dissolution

As the oxygen meter could not provide us with information about oxygen release from low concentrations of mPEG-b-PPFPMA, we needed an alternative method to measure the oxygen dissolution. One thing we noticed during initial DLS measurements, was a difference in the size of the micelles, which was dependent on whether or not the micelles were degassed (oxygen free) or oxygenated. After oxygen was bubbled through the solutions, an increase in size was observed. Therefore, a series of DLS experiments were carried out to measure the sizes of all diblock copolymers at 25 °C. The first experiments measured the micelle sizes after degassing (i.e. an oxygen free solution), which were used as a reference. Before each measurement, the polymer solutions should be heated to 40 °C under a vacuum and then cooled down to room temperature under nitrogen. This was repeated three times and then DLS measurements were recorded in a sealed vial. Oxygen was then bubbled through the cuvette for 5 minutes before it was resealed and a second DLS measurement was carried out. The results are shown in **Table 9**. In all cases the results show that the particle sizes increased when loaded with oxygen. The obvious conclusion from these experiments is that oxygen encapsulation swells the micelles. These results are similar to those obtained by Q. Zhang, who used this property as a method to detect oxygen and other gases.[44] The process was reversible, and the original micelle size returned after

the same sample was again degassed.

Table 9 DLS results for particle sizes of the diblock copolymers between oxygen-free stage and oxygen-loaded stage

Copolymers		0.05 mg/ml		0.5 mg/ml		1.0 mg/ml	
		Oxygen Free (nm)	Oxygen Loaded (nm)	Oxygen Free (nm)	Oxygen Loaded (nm)	Oxygen Free (nm)	Oxygen Loaded (nm)
mPEG-b-PTFEMA	**10a**	37.4	92.5	22.3	399.9	21.0	91.9
	10b	81.0	100.3	67.3	99.1	44.8	87.6
	10c	49.1	57.5	41.4	89.4	36.0	166.3
mPEG-b-PPFPMA	**14a**	43.6	119.1	28.1	44.1	26.4	52.8
	14b	40.6	46.4	37.8	79.4	34.4	47.8

The size increases for the oxygenated diblock micelles were not consistent with each other. Although it is not wholly apparent why this is, there are several possible reasons. Firstly, each experiment took approximately 10 minutes to complete. During the transfer and measurement, oxygen could leak out of the solution, resulting in a smaller size being recorded. Furthermore, in order to use the same solution, for the degassed and oxygen-loaded experiments, the oxygen was bubbled into a small cuvette, which occasional generated foam, which could escape from the vial (for some of the micellar systems). In an

effort to try and prevent the solution foaming and splashing out, the oxygen flow rate was slowed, so as to control the foaming and minimise any loss of material. Although we tried to maintain a constant set of experimental conditions for all micellar solutions, this was difficult and it is possible that different solutions received different amounts of oxygen, leading to smaller-sized micelles (than was expected if full saturation had occurred). However, the results do provide us with qualitative data/evidence that the micelles are indeed dissolve oxygen and are bigger when doing so.

2.3 Conclusion

Our aim with this work was to synthesise and test the oxygen dissolution potential of a polyfluoro, self-assembled Nanomaterials. In this respect, the project was successful and the aims were achieved. The synthesis of the building blocks involved an ATRP process and was relatively straightforward. Using this method, we were able to obtain a series of diblock polymers, each possessing a hydrophilic mPEG-2000 block and various fluorinated blocks.

In the first phase of the work, polymers consisting of 2,2,2-trifluoroethyl methacrylate (**4**) (TFEMA, a monomer with 3 fluorines per monomer unit), were synthesised with degrees of polymerisation equal to 17, 25, 33, and 50. At a given concentration, the polymer's solubility was inversely proportional to the length of the fluoro-block. Nevertheless, with the exception of the polymer with the longer fluoro-block, all polymers were soluble in water. All of the soluble polymers could self-assemble to be micelle in water with CMC

values of around 0.003 mg/mL. DLS indicated that the aggregates for polymers containing PTFEMA block had a solvated diameter of 90-100 nm. TEM confirmed the micellar structures and indicated that the spherical structures had a diameter of 30-50 nm. The micellar aggregates were able to carry oxygen, as demonstrated indirectly through the use of oxygen release kinetics (from oxygen-saturated aqueous solutions). The rate of oxygen release was indirectly related to the amount of bound oxygen and was dependent on the amount of fluorine present. That is, oxygen was released more slowly for solutions containing higher concentrations and/or, polymers possessing more fluorine. This was supported by qualitative ^{19}F NMR data in D_2O, which showed an upfield shift of the fluorine resonance in the presence of oxygen. As well as supporting oxygen dissolution, this experiment also confirmed that the oxygen bound within the polyfluoro core of the micelle. In addition, the use of an enzyme assay, which can measure the amount of oxygen directly, indicated that the polymer could dissolve 33% more oxygen than water alone. However, this was a colourimetric based assay and due to significant loss of dye, caused by precipitation, the concentration of dissolved oxygen was probably higher than the value recorded. Taking these results together, we can conclude that micellar aggregates of a simple fluorine containing amphiphilic diblock polymer could increase the concentration of oxygen within an aqueous solution. As such, these polymers (or related systems) have the potential to be applied as a simple artificial blood product: Particularly in the area of first response or emergency situations, were replacing blood loss with an oxygen rich solution (a volume expander) is a significant improvement over current methods.

The second phase of the work was a simple expansion of the previous work, were a

monomer with more fluorine atoms 2,2,3,3,3-pentafluoropropyl methacrylate (PFPMA) (**13)** replaced previous monomer. This generated diblock copolymers containing more fluorine than the previous polymers with similar degrees of polymerization. Specifically, the degrees of polymerisation were 12, 23 and 45. As before, the polymer with the largest fluoro-block demonstrated poor aqueous solubility and was not studied further. The CMC values for the new mPEG-PPFPMA (**14**) diblocks were around 0.01 mg/mL, which was slightly larger than the previous mPEG-b-PTFEMA (**10**) diblocks. The oxygen release kinetics of the new polymer aggregates were also able to increase the concentration of oxygen within an aqueous solution. However, these polymers formed a large amount of foam during the oxygen bubbling process, which almost certainly affected the oxygen measurements. As such, the dissolution data for mPEG-PPFPMA (**14**) may not fully represent the full potential of the oxygen dissolving ability. For this reason, it was not possible to compare the 3F sytem with the 5F system. Furthermore, DLS measurements for oxygen loaded polymers and oxygen free polymers confirmed that the polymer micelles could dissolve oxygen within the core, which resulted is an obvious swelling of the micelle. This swelling was reversible, and smaller micelles were observed when the amount of oxygen was reduced.

To improve circulation times and in an effort to generate more stable and larger systems, this work was extended towards the development of much larger and irreversible self-assembled nano structures. In next chapter, we discuss a modified polymer design, that can assemble into a water soluble polyion complex, along with details about its ability to dissolve oxygen.

Chapter 3
Fluorinated Polyion Complex as Oxygen Carriers

3.1 Introduction

3.1.1 Polyion Complex Formation

For the self-assembly of amphiphilic diblock copolymers, the driving forces are mainly entropically driven hydrophobic interactions. These can be enhanced and supported by hydrogen bonding and Van der Waals interactions. During blood circulation, the integrity of micelles can be easily breached. The stability of the micelle can be enhanced significantly through electrostatic ionic interactions[81,82] Specifically, through the creation of a polyion complex micelle (PIC). A PIC is constructed of polyelectrolytes and can be applied to a number of applications, including drug delivery system. A soluble and stoichiometric mix of polyelectrolytes usually induces the formation of insoluble precipitates.[83,84] Therefore, one way to obtain a water soluble colloidal polyion complex, is to establish a non-stoichiometric mixture of oppositely charged polyelectrolytes. Due to the unbalanced charges in such a mixture, the core is formed of a 1:1 mixture of oppositely charged polymers and is surrounded by a shell of excess polyion chains, which repels other PIC particles in solution to prevent flocculating[85] (**Figure 3.1**).

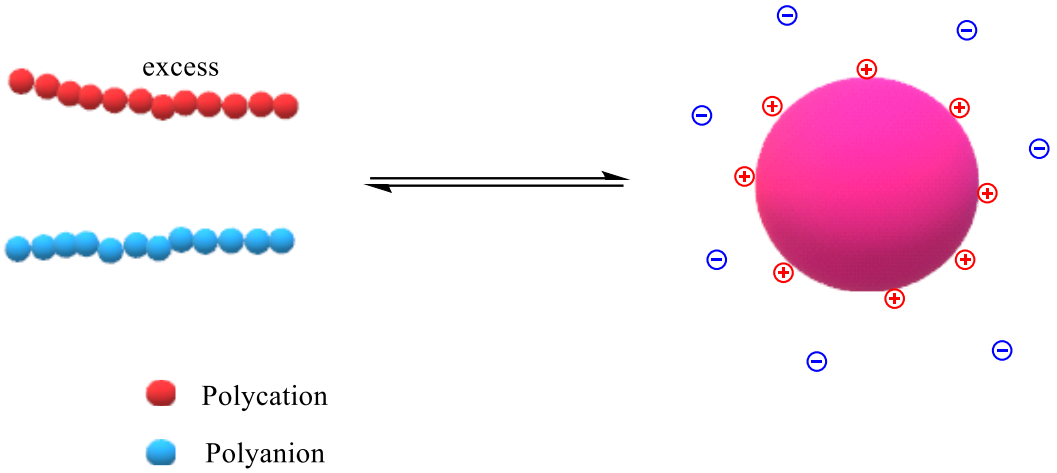

Figure 3.1 Demonstration of polyion self-assembly into PIC nanoparticles using a polyanion and an excess of polycation, forming a neutral core surrounded by an excess of cationic material

Another method is to mix a pair of oppositely charged amphiphilic block copolymers, which results in the spontaneous formation of PIC micelles with a good stability in aqueous solutions.[82] There are various choices for the neutral hydrophilic block, such as PEG, poly(glyceryl methacrylate)(PGMA),[86] poly(N-(2-hydroxypropyl) methacrylamide) (PHPMA).[87] As mentioned in previous chapters, PEG is a non-toxic, biocompatible and widely used in drug delivery systems, and it is thus commonly used in the preparation of PIC as the hydrophilic corona shell.[88,89] The oppositely charged blocks, such as poly(aspartic acid)(anion)/poly(L-lysine)(cation)[90] or poly(styrene-*alter*-maleic anhydride)(anion)/poly(N,N-dimethylaminoethyl methacrylate)(cation)[91], form the hydrophobic core through electrostatic ionic interactions.(**Figure 3.2**)

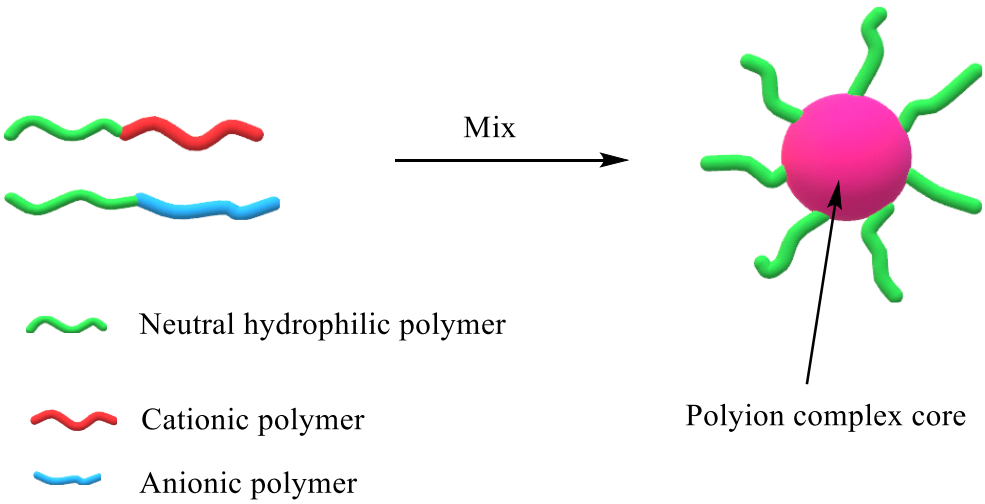

Figure 3.2 Formation of polyion micelles from diblock copolymers

3.1.2 Acid-Base Equilibrium

The formation of PIC is based on the binding of anionic/cationic polymers, and thus the binding properties are strongly dependent on the charge density and number of charged groups in the polyelectrolytes' structure, and this is dependent on pH. Normally, a higher charge density gives more stable complexes.[92, 93] For polyelectrolytes which are deprotonated/protonated in water, however, the pKa is an important parameter in terms of determining the proportion of ionized groups available to the copolymer.

An acid (HA) in water, according to Brønsted-Lowry acid/base theory, should protonate the water to form hydronium and the conjugate base (A^-) **(Scheme 3.1)**.[94]

$$HA + H_2O \rightleftharpoons H_3O^+ + A^-$$

Scheme 3.1 Acid equilibrium in water

Like all equilibria, acid dissociation has a constant (K_a) that determines the extent of the dissociation. K_a can be calculated based on the concentrations of each component, as shown in **Equation 3**

$$K_a = \frac{[H+][A-]}{[HA]}$$ **Equation 3**

By converting **Equation 3** to the logarithmic scale, pKa can be linked with pH, as shown in **Equation 4**

$$pK_a = pH + \log\frac{[HA]}{[A-]}$$ **Equation 4**

A similar equilibrium exists when a weak base is dissolved in water. The base is protonated by the water and generates a conjugate acid (HB^+) (**Scheme 3.2**).

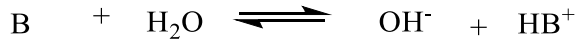

Scheme 3.2 Base equilibrium in water

The HB^+ is a conjugate acid of the base; thus, the K_a of a base can be interpreted as the dissociation constant of its conjugate acid. This equilibrium can be rearranged as in **Scheme 3.3**.

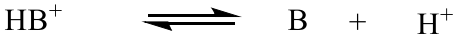

Scheme 3.3 Dissociation equilibrium of the conjugate acid of a base

In this case, the K_a can be expressed as **Equation 5.** Similarly, the pH can also be deduced as **Equation 6**

$$K_a = \frac{[H+][B]}{[HB+]}$$ **Equation 5**

$$pK_a = pH + \log\frac{[HB+]}{[B]}$$ **Equation 6**

3.2 Aim and hypothesis

The aim of this work was to develop a water soluble polyion complex that can carry oxygen efficiently and had a suitable particle size that was closer in size to a blood cell and big enough to stay longer in the blood circulation. To achieve this, two amphiphilic fluoro containing block copolymers, each with positive or negative ions, would be synthesised. When mixing these two polymers at appropriate stoichiometry, a polyion complex should form, as a result of favourable electrostatic interactions. This PIC should be designed to have a fluorine rich core that could dissolve oxygen, increasing the oxygen concentration in water (**Figure 3.3**).

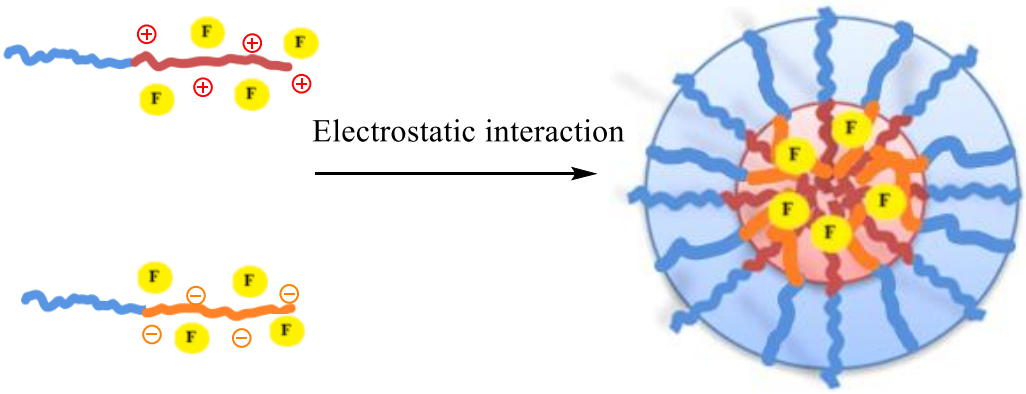

Figure 3.3 Amphiphilic diblock copolymers with positive or negative ions and fluorine forming PIC micelles by electrostatic interaction (the blue chain is the hydrophilic block; the red chain is the positive charged hydrophobic block, which covalently bonds with fluorine atoms; the brown chain is the negatively charged hydrophobic block, which covalently bonds with fluorine atoms)

In this study, the negative charge provider would be an acidic carboxylic acid group and a basic amine group chosen as the positive charge provider, as shown in **Figure 3.3**. When these two diblock copolymers are mixed, they will self-assemble into a PIC, involving a direct neutralisation between the acidic and basic components.

In addition, the size of any PIC should disperse in a range between 10 nm and 1 μm according to other reports.[95] This will allow it to stay longer in the blood circulation and prevent capillary blockage and embolism. The preparation of PIC can be affected by pH, hence a suitable ratio for the acidic and basic polymers must be calculated by investigating PIC formation at different mixing concentrations. To determine whether or not the PICs can improve the solubility of oxygen in water, oxygen concentrations will be measured indirectly using a DO meter and DLS.

3.3 Results and Discussion

To ensure the safety and efficacy of the micelles for use in a bio delivery system, a stable structure is required. Lengthy blood circulation durations are needed for both oxygen and nanomedicines, thus particles larger than 5 μm are unsuitable as they can cause capillary blockage and embolism. Meanwhile particles that are too small will be eliminated from the body very quickly. The optimal size of a drug carrier to deliver an antitumor agent efficiently to a tumour is around 100-200 nm. The polyion complex formed by the electrostatic interaction between oppositely charged species, which are more stable than micelles, was widely studied for use as a drug delivery system for photodynamic therapy (PDT).[96,97,98] One of the requirements of PDT is oxygen, which is lacking inside the tumour. Hence, the PIC, which could bind/carry the oxygen, was studied.

The DMAEMA and MAA are typical monomers for use in the delivery system[99,100,101] and they could be protonated/deprotonated by changing the pH. In addition, at neutral pH, these

two repeat units could react together to form a salt. Therefore, to provide the electrostatic interaction, they were introduced into the fluorinated block, to give a random fluoro/DMAEMA and fluoro/MAA block. These two random diblocks can then be combined to generate a PIC with a fluorine-enriched core. As such, the PIC should be able to dissolve oxygen as the previous research demonstrated. The following section will initially describe the synthesis of the various randomly functionalised diblock polymers.

3.3.1 Synthesis of mPEG-P(TFEMA-*ran*-DMAEMA) (15)

The PDMAEMA was used as the basic component, allowing incorporation of a positive charge-within the fluoro block. (**Scheme 3.4**).

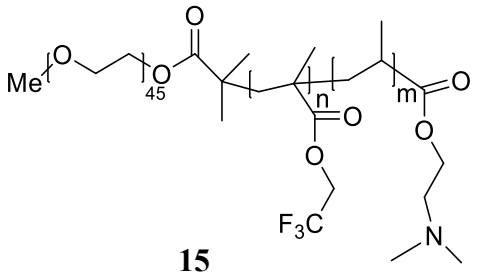

15

Scheme 3.4 mPEG-P(TFEMA-*ran*-DMAEMA) can be protonated in aqueous solution to be a polycation.

As the aim was to make the polymer self-assemble into a polyion complex with a fluorine-enriched core, the fluorinated block needed to be long enough to have an effect upon oxygen dissolution, yet not so long that it made the polymer insoluble. Based on our previous research, a D_p, for PTFEMA, ranging between 20 and 30 could achieve a good solubility with a good oxygen dissolution ability. A series of block copolymers with different D_p of DMAEMA were synthesised. At room temperature, a PDMAEMA block

would be water soluble; the block would become hydrophobic when forming random copolymers with PTFEMA. As such, this random block would be able to form the core of the micelle.

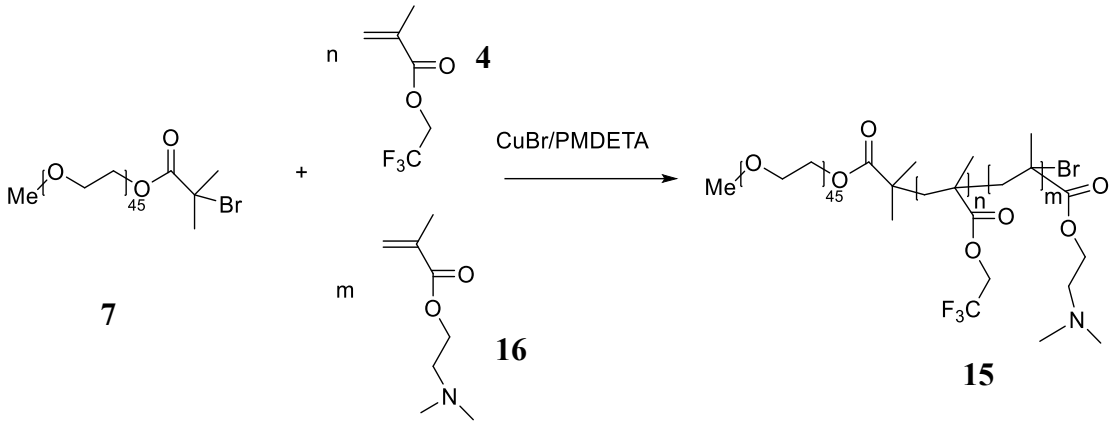

Scheme 3.5 Synthesis of mPEG-P(TFEMA-*ran*-DMAEMA) (**15**)

A series of mPEG-P(TFEMA-*ran*-DMAEMA) with different fluoro:amine ratios were synthesised. The fluoro content was kept constant, while the amount of DMAEMA was changed, in order to adjust the charge density of the block. The synthesis of mPEG-P(TFEMA-*ran*-DMAEMA) (**15**) was carried out using ATRP (**Scheme 3.5**). The initial design was to synthesise a triblock copolymer, which would have a fluorinated layer and a positively charged layer. However, this is a more complex synthesis and due to the sensitivity of ATRP to oxygen, adding another monomer would risk oxygen leaking into the system. Thus, the two monomers, TFEMA and DMAEMA were mixed together to form a random copolymer, having a fluorinated and positive core in water.

The ^{19}F NMR spectrum showed a singlet at -73.11 ppm, which confirmed that fluorine had been incorporated into the copolymers. ^{1}H NMR was used to confirm the synthesis of mPEG-P(TFEMA-*ran*-DMAEMA). The backbone protons of the mPEG block were

observed at 3.66 ppm. Meanwhile, two broad peaks occurring between 2.16 and 1.60 ppm were also observed, due to the protons on the backbone of the P(TFEMA-*ran*-DMAEMA) blocks. The protons of the CH_3 groups on the backbones of both blocks appeared as four broad peaks between 1.21 and 0.757 ppm, which were caused by the ununified tacticity. Two singlet peaks located at 4.08 ppm and 2.57 ppm, correspond to the -OCH_2 and the -CH_2N on the PDMAEMA block respectively. The degree of polymerisation was calculated by comparing the integration value of the peaks at 3.66 ppm with the CH_2 and $N(CH_3)_2$ peaks at 4.36 ppm and 2.29 ppm respectively (**Figure 3.4**). GPC showed a unimodal trace with a narrow molecular weight distribution, which confirmed the monomers were copolymerised rather than forming a polymer blends. The synthesis and characterisation results are shown in **Table 10**.

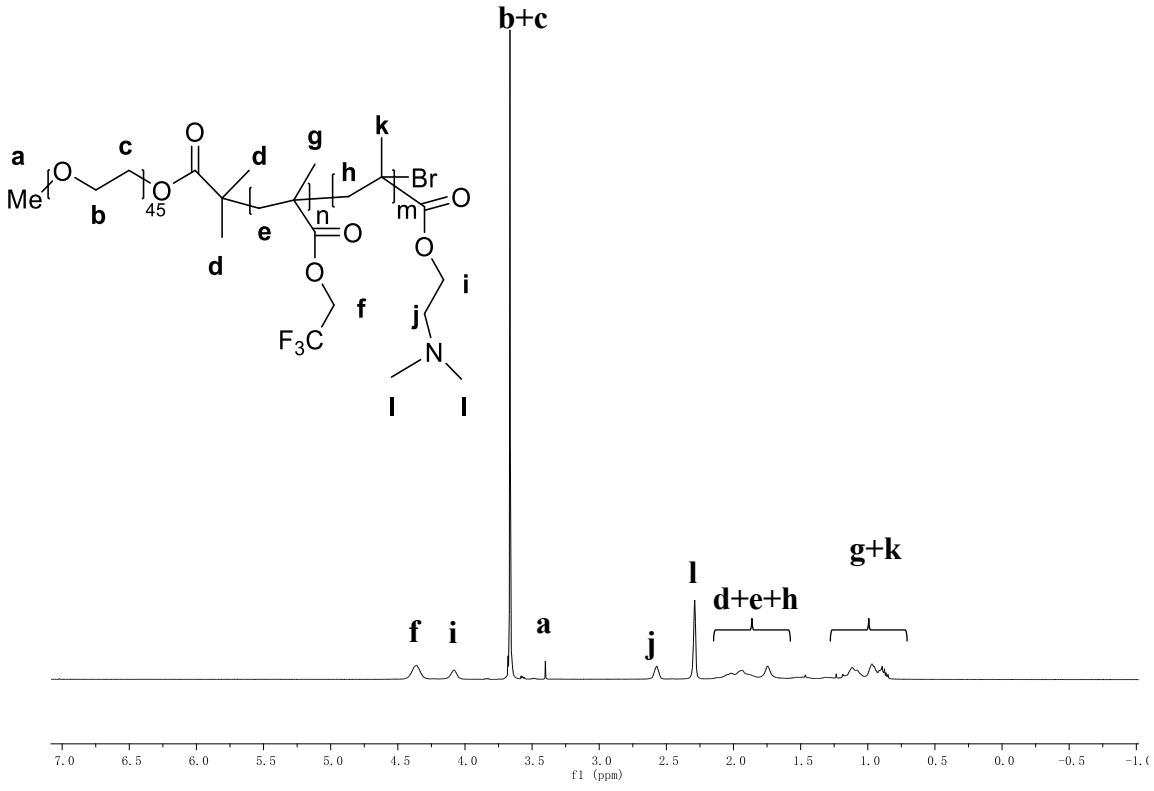

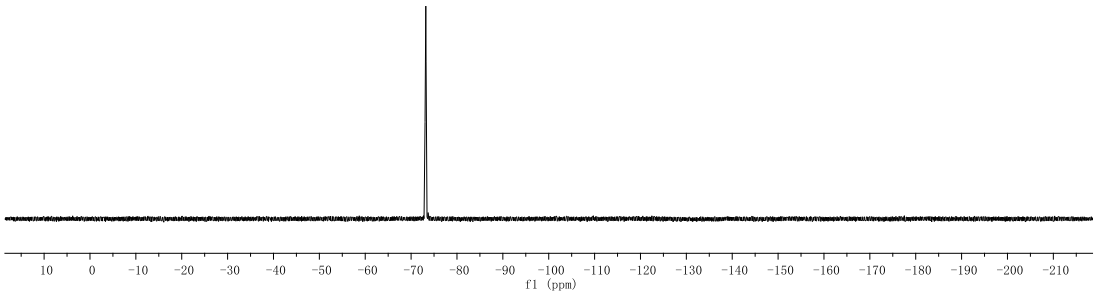

Figure 3.4 ^{1}H NMR spectrum (above) and ^{19} F NMR spectrum (below) for mPEG-P(TFEMA-*ran*-DMAEMA) (**15b**)

Table 10 Synthesis results for mPEG-P(TFEMA-*ran*-DMAEMA), degree of polymerisation (D_P) represented by TFEMA contents (n) and DMAEMA (m)

Copolymers		Designed D_p/ n:m	Actual D_p/ n:m	Mn（NMR）	Mn(GPC)	PDI
mPEG-	**15a**	20:5	18:3	5495	6200	1.12
P(TFEMA-*ran*-	**15b**	20:10	15:9	5933	8000	1.10
DMAEMA)	**15c**	20:15	23:17	8533	10040	1.21

3.3.2 Synthesis of mPEG-P(TFEMA-*ran*-MAA) (17)

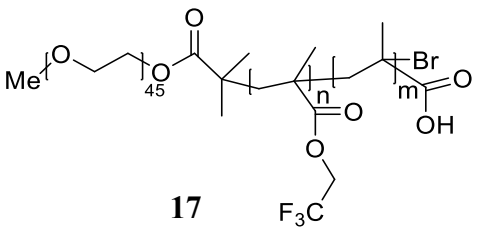

17

Scheme 3.6 mPEG-P(TFEMA-*ran*-MAA) deprotonates in aqueous solutions to be a polyanion

The mPEG-P(TFEMA-*ran*-MAA) (**17**) was chosen as the acidic component, allowing formation of a negative charge within the fluoro block. As with mPEG-P(TFEMA-*ran*-

DMAEMA) (**15**), to ensure there were enough fluorines on the block and the polymer was soluble, the fluorinated block needed to be of a suitable length; that is with a D_p between 20 and 30.

According to the literature[102], acrylic and methacrylic acid can react rapidly with metal complexes, forming metal carboxylates which cannot be reduced to active ATRP catalysts. Since the direct radical polymerisation of mPEG-P(TFEMA-*ran*-MAA) (**17**) was unachievable, due to the presence of the methacrylic acid, the initial design was changed and the synthesise mPEG-b-PTFEMA (**10**) was proposed. This polymer would have a much higher D_p and we would hydrolyse, or remove a part of the PTFEMA block to provide mPEG-P(TFEMA-*ran*-MAA) (**17**), as shown in **Scheme 3.7**.

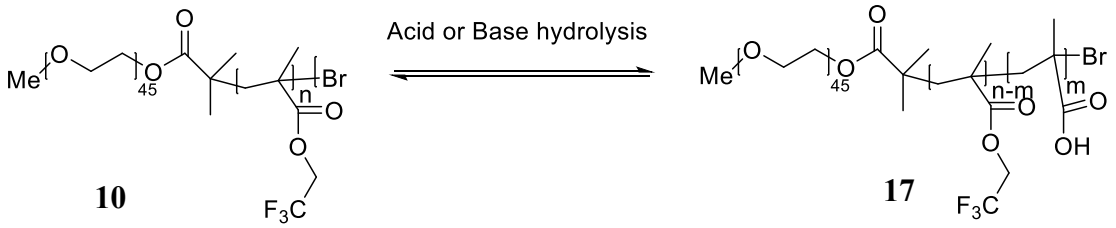

Scheme 3.7 mPEG-P(TFEMA-*ran*-MAA) synthesised by directly hydrolysis of PTFEMA block

However, hydrolysis is a reversible reaction, which is not easy to control as it could be affected by various elements like temperature, acid/basic concentration and reaction time. Furthermore, there are two types of ester bond on the polymer; one is the joint ester between mPEG and the PTFEMA block, the other is the pendant ester on PTFEMA. It was a great concern that conventional hydrolysis methods could cleave both esters and degrade the diblock polymer directly. Therefore, to maintain polymer integrity, it was necessary to investigate a different method that would enable the ester cleavage to be selective. It has

been widely reported that the poly(*tert*-butyl methacrylate) (PtBMA) segment could be transformed easily into a PMAA segment by a non-hydrolytic cleavage.[103,104] By using CF_3COOH with DCM as the solvent, the polymer could be selectively cleaved at the butyl ester (leaving the fluoroester and the PEG-Polymer ester linkage intact), making the synthesis more predictable and allowing the final product to be purified much more easily.

a) Synthesis of mPEG-P(TFEMA-*ran*-tBMA) (19)

The first step was to synthesise mPEG-P(TFEMA-*ran*-tBMA). (**Scheme 3.8**)

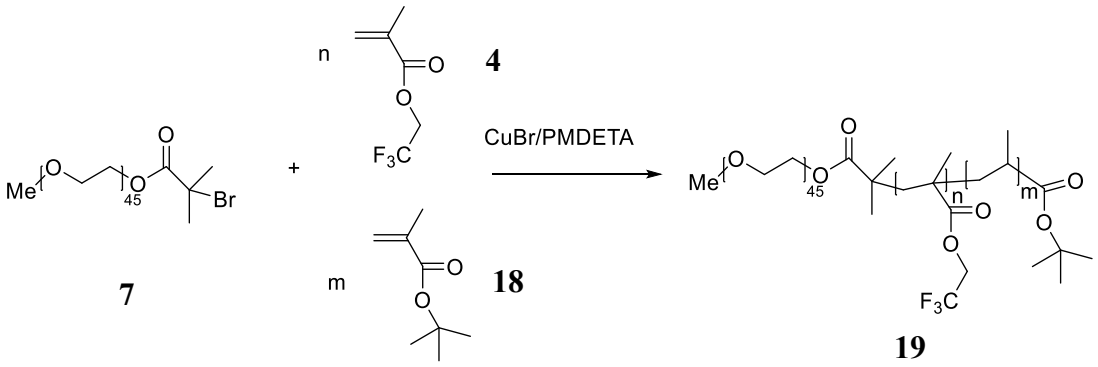

Scheme 3.8 Synthesis of mPEG-P(TFEMA-*ran*-tBMA)

As with the previous synthesis, TFEMA and tBMA were mixed with a molar ratio of 20:10 to give one final copolymer with a D_p equals 20:10 (fluoro:tBMA). The further experiments were all established on this copolymer. The synthesis was achieved using ATRP. Although ^{13}C NMR and ^{1}H NMR gave useful information about the structure, the ^{13}C NMR was sensitive to stereochemical sequences, which made it hard to assign the signals in regards to both tactic and comonomer sequences.[105] Due to the poor resolution of the spectra, ^{19}F NMR and GPC was also used to support and confirm the structure of the product.(**Figure**

3.5)

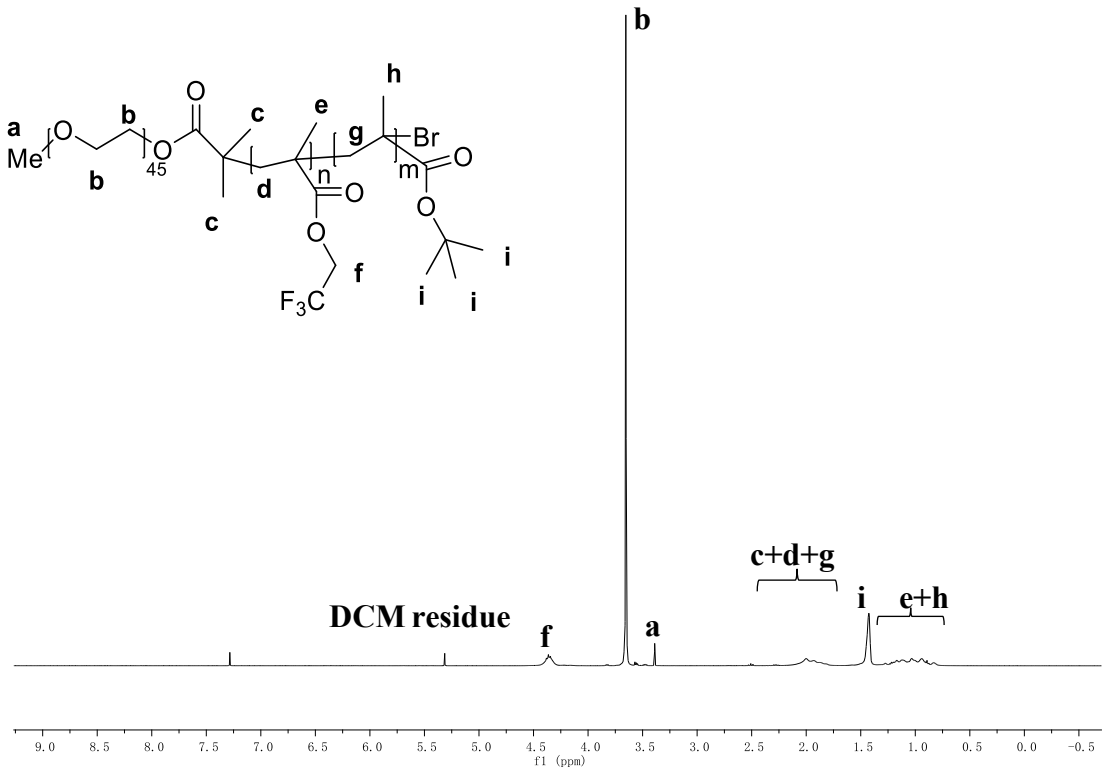

Figure 3.5 ^{1}H NMR spectrum for mPEG-P(TFEMA-*ran*-tBMA) (1-20-10)

The backbone protons of the mPEG block were located at 3.66 ppm; broad peaks corresponding to the CH_2 on the backbone of P(TFEMA-*ran*-tBMA) are located at similar ranges, between 1.70 ppm and 2.16 ppm, as well as the backbone methyl groups, between 0.76 ppm and 1.24 ppm. The CH_2 on the pendant chain of PTFEMA could be observed at 4.35 ppm as a single broad peak. The peak at 1.43 ppm represents the $C(CH_3)_3$ of the PtBMA block. The NMR data, together with a narrow unimodal peak from GPC, confirmed the copolymer had been successfully synthesised. The D_p was calculated by comparing the integration value of the peaks at 3.66 ppm, 4.35 ppm and 1.43 ppm.

b) Cleavage of mPEG-P(TFEMA-*ran*-tBMA)

Having synthesised the ester, the next reaction involved the selective cleavage of the t-butyl ester groups. The reaction was carried out overnight in the presence of CF_3COOH in DCM as shown in **Scheme 3.9**.

19 **20**

Scheme 3.9 Synthesis of mPEG-P(TFEMA-*ran*-tBMA-*ran*-MAA)

This reaction is not a hydrolysis and the conditions are not strong enough to cleave the ester group of PTFEMA. However, they are good enough to cleave the PtBMA group, as the process generates a stable leaving group. The mechanism is shown in Scheme 5 and involves an initial protonation of the carbonyl oxygen, which has a delocalised structure where the charge is on the carbon between the two oxygens. The t-butyl carbocation is a very good leaving group, and is generated by breaking the ester bond to form a new carbonyl. The t-butyl cation can then rearrange to the more stable isobutylene (regenerating the proton). This reaction pathway is much more stable (i.e. lower in energy) than the corresponding reaction via a trifluoroethyl carbocation.[106] This mechanism is catalysed by the organic acid CH_3COOH.

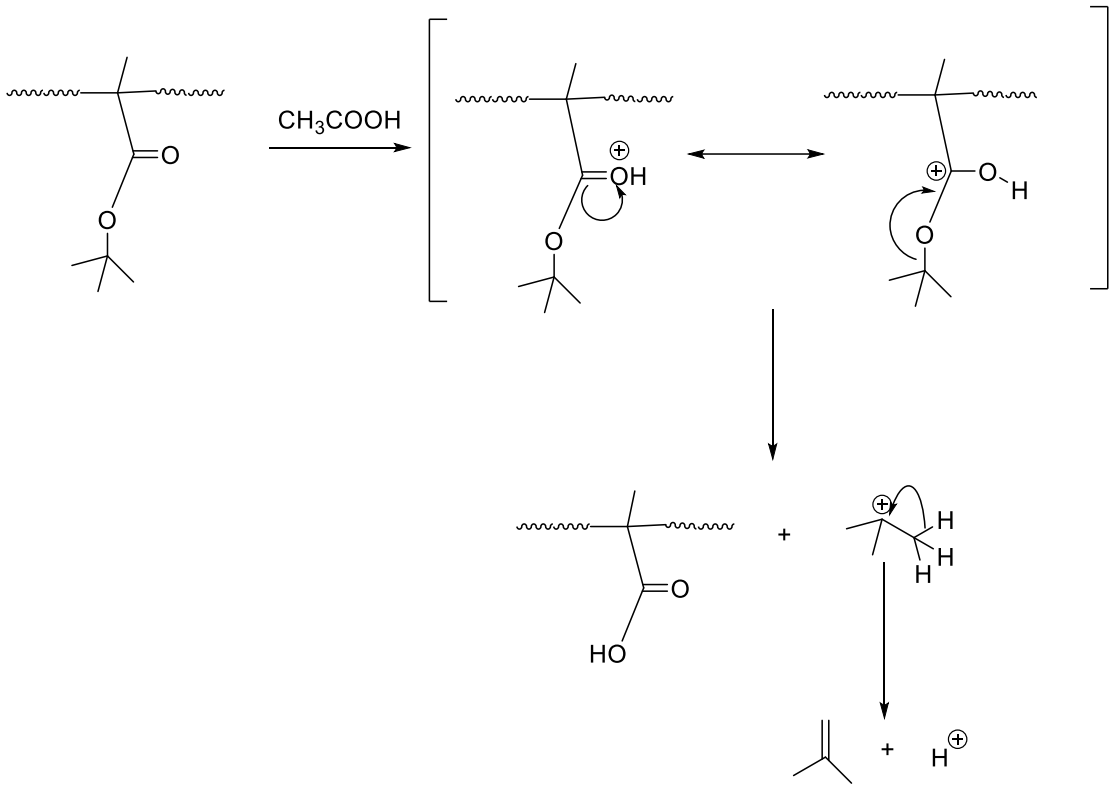

Scheme 3.10 Mechanism of the t-butyl ester cleavage. [106]

Although the reaction is well known, there was no evidence that the ester group on mPEG, or the ester group on the PTFEMA block would be inert to the conditions. Hence, the reaction was monitored and the duration of the reaction was shortened to prevent the other esters from being cleaved. As such, a certain amount of tBMA remained intact to maintain the integrity of the backbone.

The successful synthesis was confirmed using ^{1}H NMR, ^{19}F NMR (**Figure 3.6**) and GPC. When compared with the ^{1}H NMR spectrum of mPEG-P(TFEMA-*ran*-tBMA) (**19**) before the hydrolysis, only the peak corresponding to the $C(CH_3)_3$ proton at 1.43 ppm had been altered, giving a much smaller peak compared to the other signals. The peak for the CH_2CF_3 remained the same. The ^{19}F NMR spectrum showed a singlet peak at -73.33 ppm. This together with the unchanged peak at 4.35 ppm (of CH_2CF_3), confirmed that the esters on

the PTFEMA block did not break. The GPC trace was unimodal with a narrow molecular weight distribution, which confirmed the mPEG was not cleaved from the diblock polymer. The molecular weight from GPC was slightly decreased, compared with the starting polymer, which also provided evidence that the tBMA groups had been cleaved.

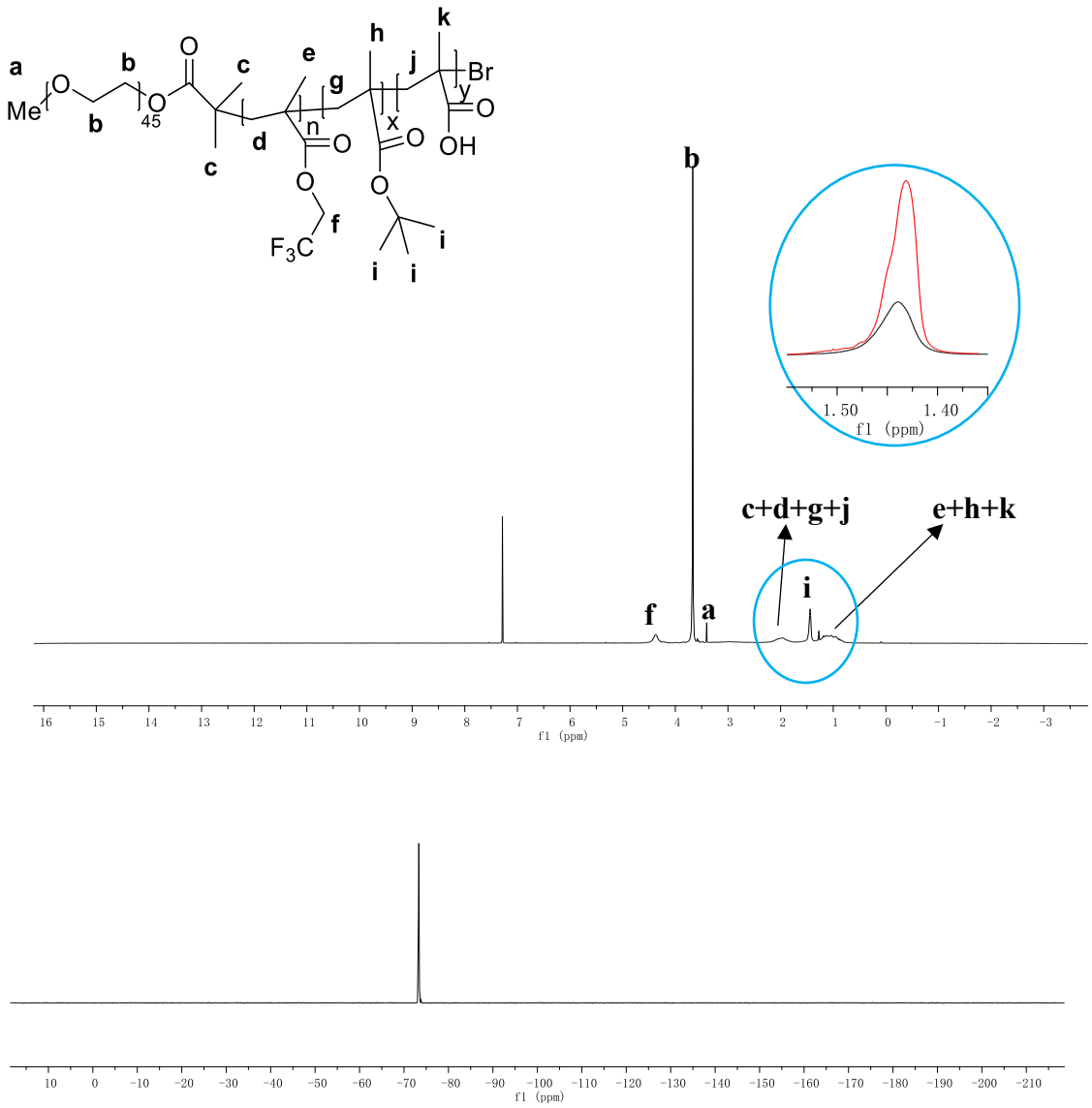

Figure 3.6 ^{1}H NMR spectrum of mPEG-P(TFEMA-*ran*-tBMA-*ran*-MAA) (**20**)(above) shows the peak (black) at 1.43 ppm was smaller than the spectrum of original mPEG-P(TFEMA-*ran*-tBMA)(**19**) (red). ^{19}F NMR confirmed the fluoro block was maintained.

The amount of cleaved PtBMA could be calculated by comparing the integration values of

the peaks at 3.66 ppm, 4.35 ppm and 1.43 ppm, with the ratio of the mPEG-P(TFEMA-*ran*-tBMA),. (**Table 11**).

Table 11 Synthesis results of mPEG-P(TFEMA-*ran*-tBMA) and the cleavage results calculation. (D_P) represented by TFEMA contents (n), DMAEMA (m) and MAA(x)

Note: Actual D_p was calculated based on ^1H NMR

Copolymers		Designed D_p/ n:m:x	Actual D_p/ n:m:x	Mn (NMR）	Mn(GPC)	PDI
mPEG-P(TFEMA-*ran*-tBMA)	**19**	20:10:0	23:12:0	7568	8010	1.27
mPEG-P(TFEMA-*ran*-tBMA-*ran*-MAA)	**20a**	20:0:10	23:9:3	7400	7550	1.35
	20b	20:0:10	23:6:6	7232	7820	1.29

3.3.3 Self-assembly Studies

a) Self-assembly of mPEG-P(TFEMA-*ran*-DMAEMA)

According to the literature, PDMAEMA is soluble in aqueous solution, because some of the tertiary amines are protonated, resulting in a change in pH.[107] Therefore, to ensure the pH of the experiments were consistent, all measurements were carried out using a pH 7 buffer solution. For the mPEG-P(TFEMA-*ran*-DMAEMA) (**15a**) with a D_p of 18:3 (fluoro:amine), the charge density would be too low for a stable polyion complex.[83]

Furthermore, with a D_p of 23:17 (**15c**), there is a much longer hydrophobic block, which would limit solubility at pH 7.0. This was tested and a turbid solution was observed at a concentration of 2 mg/mL. However, a polymer with a D_p equal to 15:9 (**15b**) was soluble at high concentrations and perfect for further study.

From the literature, the average pK_a of a PDMAEMA block is around 7.5,[108,109] hence in a pH 7 environment, the PDMAEMA components would be partly protonated, leading to an increased solubility of the whole hydrophobic block. Although the block was insoluble, it was necessary to establish whether or not mPEG-P(TFEMA-*ran*-DMAEMA) could form a stable micelle. Therefore, a CMC was determined using a pyrene probe and following changes in its fluorescence intensity as the concentration of polymer increased. In addition, dynamic light scattering would be used to see if large particles formed above the CMC.

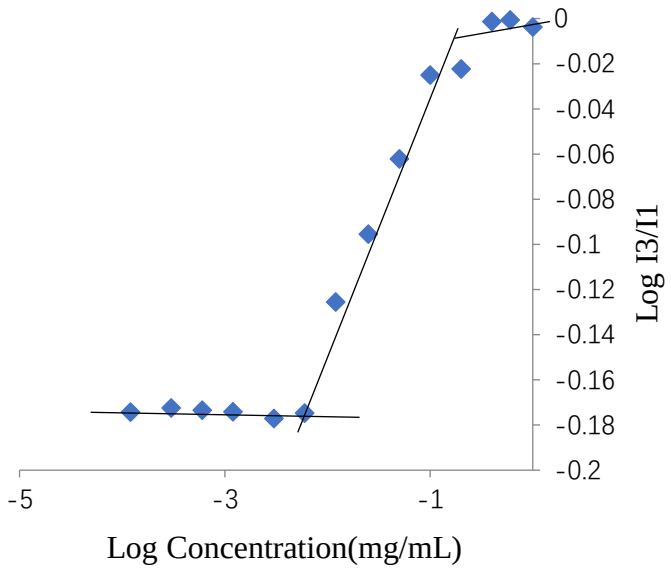

Figure 3.7 CMC plot for copolymer (**15b**)

The methods used were the same as those mentioned in the previous chapter. mPEG-P(TFEMA-*ran*-DMAEMA) (**15b**) was used for the measurement. **Figure 3.7** shows the

logarithm of the intensity ratio (I3/I1) vs the logarithm of the various mPEG-F_{15}-N_9 concentrations; I3/I1 begins to increase at 0.0063 mg/mL, which was therefore determined as the CMC. This was confirmed by DLS measurement of the polymer in pH 7.0 buffer and concentrations above and below the CMC. The results are shown in **Table 12**. The data shows that their particles are not observed at a concentration of 0.001 mg/mL and only become evident at a concentration of 0.01 mg/mL. The size of the hydrated particles is around 50 nm and remain constant up to a concentration of 0.1 mg/mL. Compared with the CMC of mPEG-b-PTFEMA, the CMC of copolymer (**15b**) are in the same range of the diblock copolymer micelles, which has also been demonstrated in other research.[110] However, the size of the micelles are smaller than those measured for the homo-diblock mPEG-PTFEMA. This may be due to the insertion of DMAEMA, which enhances the hydrophobic interaction of the core.

The proportion of protonated amines can be estimated using **Equation 6**

$$pK_a = pH + \log\frac{[HB+]}{[B]} \qquad \textbf{Equation 6}$$

HB^+ represents the protonated DMAEMA part in water and B represents unprotonated DMEAMA in water. Hence, $\frac{[HB+]}{[B]}$ is the ratio between protonated DMAEMA and unprotonated DMEAMA. As the pK_a of a PDMAEMA polymer is around 7.5, at pH 7, the $\frac{[HB+]}{[B]}$ was calculated to be 3.16. The proportion of protonated DMAEMA was $\frac{[HB+]}{[B]+[HB+]}$, which equals 76%. So, for the polymer (**15b**) in aqueous solution, there would be about 24% DMAEMA that was not protonated. This would behave like the alkyl hydrophobic fragments, decreasing the lipophobicity of the block and increasing the Van der Waals force between hydrophobic blocks. Although our polymer is only partially

DMAEMA and we do not know the pKa precisely, this calculation is a reasonable estimate of the level of protonation. As such, it does provide an explanation as to why the average size of copolymer (**15b**) was smaller than the size of mPEG-PTFEMA.

Table 12 DLS measurement for the mPEG-P(TFEMA-*ran*-DMAEMA) (**15b**) with a CMC of 0.00631 mg/mL.

Concentration mg mL^{-1}	Average size by DLS/nm
0.001	xx
0.01	49.43
0.1	47.01
1	48.21

b) Self-assembly of mPEG-P(TFEMA-*ran*-tBMA-*ran*-MAA)

mPEG-P(TFEMA-*ran*-tBMA-*ran*-MAA) (**20b**) has a similar amount of ionisable groups compared to copolymer (**15b**). As such, this was selected for further measurement. Using a solution with pH 7, the CMC was measured using the methods previously described. The CMC was determined as 0.0025 mg/mL, as shown in **Figure 3.8.** DLS analysis confirmed micelle formation, as particles were only observed at concentrations above the CMC. The particle size was around 100 nm and remained constant up to a concentration of 1 mg/mL. The DLS data is shown in **Table 13**.

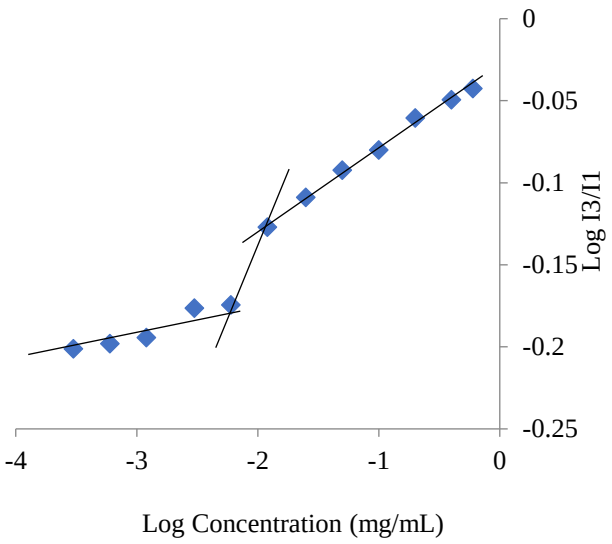

Figure 3.8 Representative CMC plot for mPEG-P(TFEMA-*ran*-tBMA-*ran*-MAA) (**20b**)

Table 13 DLS measurements for mPEG-P(TFEMA-*ran*-tBMA-*ran*-MAA) (**20b**) above and below the CMC (above and below the CMC (0.00252 mg/mL).

Concentration mg mL^{-1}	Average diameter by DLS/nm
0.001	xx
0.01	98.90
0.1	101.71
1	103.45

From the experimental observation, solutions of copolymer (**20b**) at concentrations higher than 2 mg/mL started showing turbidity, which was caused by the amount of fluorine within the block. However, it was still possible to measure the self-assembly behaviour and the particle size at a lower concentration. For this polymer, the particles were much larger than

those observed for mPEG-P(TFEMA-*ran*-DMAEMA) (**15**) and this is probably due to the level of charge. According to the literature, the pK_a of PMAA is usually around 5 to 6.[111] Based on **Equation 4**, pK_a 6 and pH 7 were substituted.

$$pK_a = pH + \log\frac{[HA]}{[A-]} \qquad \textbf{Equation 4}$$

where HA represents the acid and the A^- represents the deprotonated acid. So $\frac{[HA]}{[A-]}$ could be calculated as 0.1. Therefore, the deprotonated MAA accounts for 91%, which means most of the MAA is dissociated. The calculation is only an estimate, but it does suggest that most of the block is negatively charged, resulting in significant repulsion and making micelle bigger. This effect on the size of micelles has also been reported in other research. [112]

3.4 Polyion Complex Formation

The polyion complex was formed by mixing two polymers (with counter ions) at a certain concentration ratio. (**Scheme 3.11**) The mixing was done by "thin film hydration" as discussed in the literature.[113] When the negatively charged polymer (**20b**) was dissolved in water, the pH of the solution became more acidic, which was due to the dissociation of the carboxyl acid groups. Increasing the pH would increase the charge density on the chain, because there would be more dissociated carboxyl acid. A similar principle could also be applied to the positively charged polymer (15b), but the charge density would increase when the pH decreases.

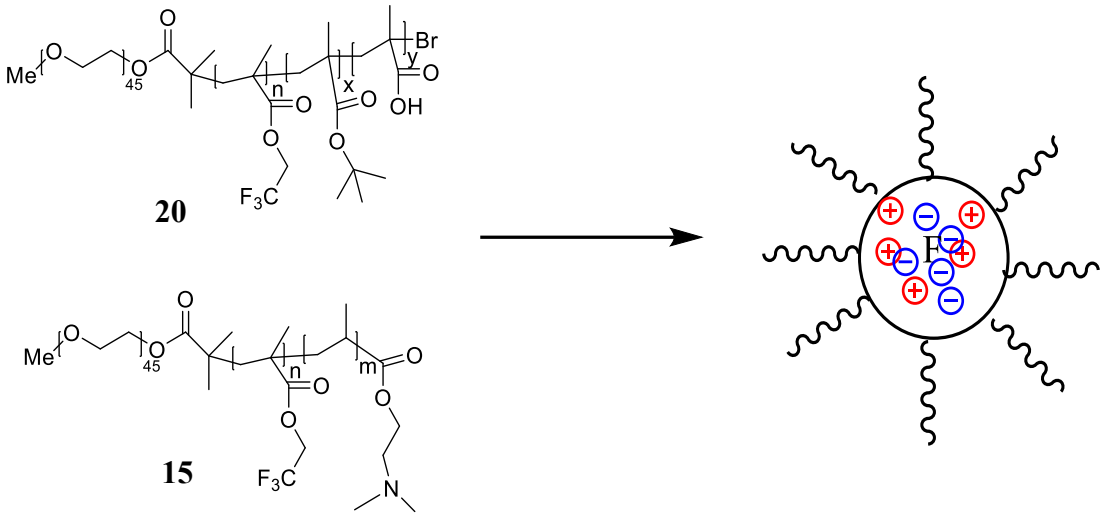

Scheme 3.11 The PIC formation model

Since all calculations regarding the level of charge in the previous sections were just estimates, it was important to find a suitable pH for stable PIC formation. Therefore, the two polymers were mixed in different ratios giving solutions with different pH. The pH is an indication regarding the presence of PIC and the optimum polymer ratios. When all the positive and negative charges are paired (with a counter ion), the solution should be neutral and the pH be 7.0 (or very close to 7.0). This is a characteristic property of PIC and has been reported before. [90]

Table 14 The DLS and pH measurement results.

Concentration Ratio (**15b**)/(**20b**) (mg/mL)	DLS/mm Main peak	pH
0.3:1	81	6.72
0.4:1	43	6.76
0.5:1	44	6.87
0.7:1	38	6.93
0.8:1	288	6.99
0.9:1	308	7.08
1:1	307	7.22

Note: the concentration ratio was the weight concentration ratio between negatively charged polymer, (**20b**) and positively charged polymer (**15b**). In all cases there were some additional peaks in the DLS, which were much less intense. This has been observed for other PIC systems and is due to each polymer forming a separate homo aggregates. The data in the table reports the strongest/most intense peaks, which were assumed to be from the PIC. There is a clear increase in size when the ratio is above 0.8:1. At this point the pH is effectively neutral. Together, the size and pH data is clear evidence for PIC formation.

Initially the polymers were hard to dissolve in water hence a "thin film hydration" method was used to prepare the PIC solutions.[113] First of all, various amounts of acid copolymer (**20b**) and basic copolymer (**15b**) were dissolved separately in methanol (to achieve the desired concentrations). The solutions were mixed together and slowly evaporated to leave a thin film on the wall of the vial. Deionised water was added to the vial, which then dissolved the film. However, for copolymer (**15b**)/copolymer (**20b**) with weight ratios higher than 0.4:1, the material floated on the surface of the water and could not be dissolved:

even after stirring for a few days. Thus, at higher concentrations, the solutions of anionic polymer (**20b**) and cationic polymer (**15b**) were made separately and then mixed together and then stirred overnight to allow the PIC to form and stabilise. This modifications was reported before for the preparation of the PIC.[114] The results are shown in **Table 14.**

As previously reported in the literature, PIC particles are often polydisperse systems and this was observed in our results. For all ratios, particles with a diameter of 40 nm were present and this is consistent with the size of the homo micelles, which are formed independently from each polymer. For polymer mixes with weight ratios between 0.3:1 and 0.7:1, 40 nm particles generated the most intense peak, suggesting that homo micelles were the dominant species in solution. When the polymer weight ratio equalled 0.3:1, the predominant particles were slightly larger and had an average size around 80 nm. This is probably due to the excess charge causing repulsions, making the homo micelle larger. At weight ratios of 0.8:1 and higher, larger particles were formed. In these cases, the most intense DLS peaks were generated by particles with a diameter around 300 nm, which was much bigger than the size of the homo micelles formed by either diblock copolymer. For the polymer mix with equal amounts of positive and negative groups (charge ratio of 1:1), the DLS showed only one peak at 300 nm. This is good evidence for formation of the required polyion complex and is consistent with the range of PIC sizes in the literature. The TEM graph (**Figure 3.9**) confirmed the coexistence of 200 nm and smaller spherical particles. Although the TEM images were not perfect, due to the undried staining, it did prove some support for the PIC structure and size. The size from TEM was smaller than that from DLS, because the particles were measured in a dry state, while the DLS measured

the hydrodynamic volume.

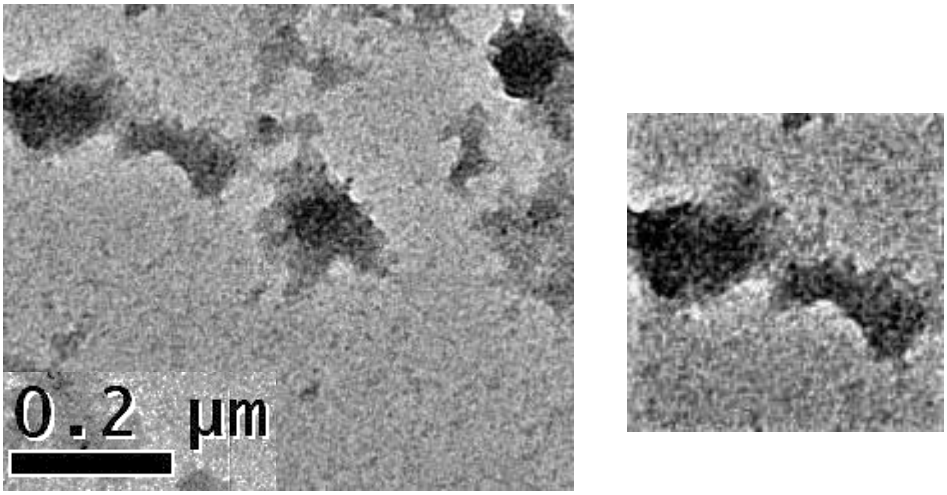

Figure 3.9 TEM microscopies for (**15b**)/(**20b**) PIC system at 0.5 mg/mL and pH 7. (Smaller image is an expansion of the top left quadrant.)

3.5 Dissolved Oxygen Study

The dissolved oxygen levels were measured using a dissolved oxygen meter (DO meter) and the methods described in the previous chapter. The solution of (**15b**)/ (**20b**) with a weight concentration ratio of 0.8:1 (mg/mL) was chosen for the measurement, since the pH was neutral under this concentration and earlier DLS analysis indicated large 300 nm particles had formed. The results are shown in **Table 15** and **Figure 3.10**. These show an obvious increase in the half-life for oxygen release and therefore an increased ability of the (**15b**)/ (**20b**) PIC solution to solubilize oxygen.

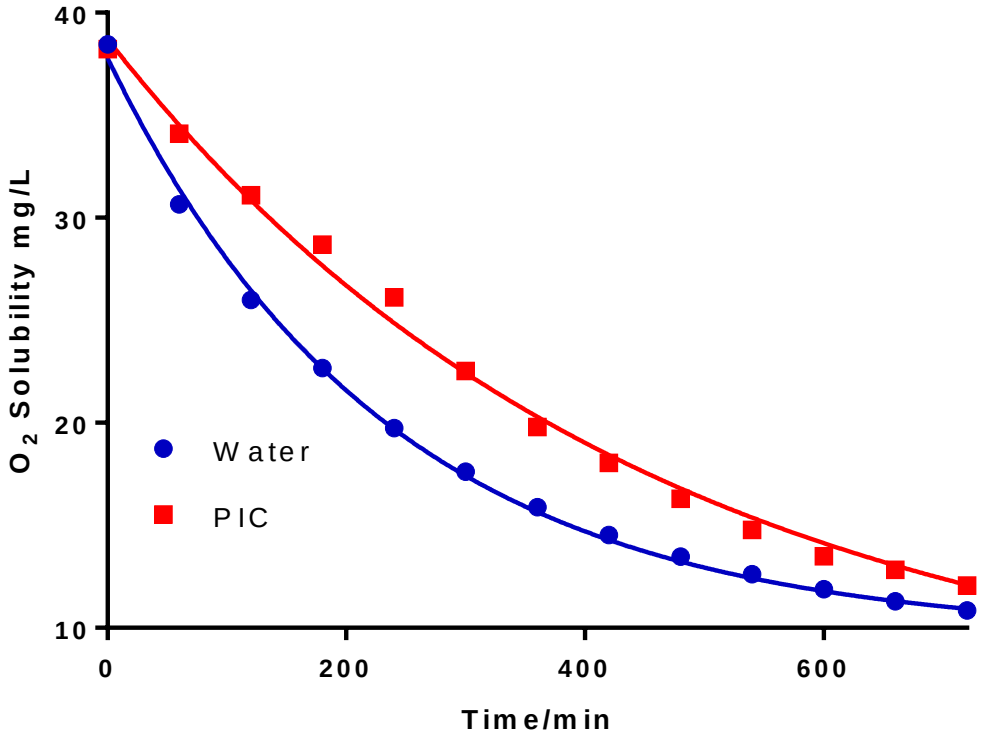

Figure 3.10 Oxygen release rate curve of (**15b**)/ (**20b**) PIC with a weight concentration ratio of 0.8 mg/l:1 mg/mL (pH 7)

The (**15b**)/ (**20b**) PIC has an ionically cross-linked core with a high fluorine content. Previously we had used ^{19}F NMR to measure shifts in the micelles fluorine peaks, in the presence and absence of oxygen. However, due to the complex conformation of the PIC and its low solubility, it cannot dissolve in D_2O for ^{19}F NMR with or without oxygen. Therefore, DLS measurement were used to compare the PIC size under this different condition to confirm that oxygen had be inserted inside the PIC. This method has been used previously to detect and measure various gases in solution[44] and in the earlier chapter to measure oxygen dissolution. The PIC solution was heated to 40°C under vacuum to degas the sample, as previously described. Cooling was carried out overnight to ensure there were no temperature dependant changes in PIC morphology.[115] After measuring the size of

the oxygen-free PIC, oxygen was bubbled through the system for 5 minutes and the DLS measurement retaken. To determine any reversibility of dissolution, a PIC loaded with 100% pure oxygen was exposed to air, allowing any bound oxygen to achieve gaseous equilibrium with the oxygen in air. As oxygen only makes up around 20% of air, the size of the PIC should change. After exposing the vial to air for a few hours, the DLS measurements were taken for a third time and the results for all measurements are shown in **Table 15**. After bubbling oxygen through the PIC solution, the particles were observed to swell, increasing in size from 270 nm to nearly 400 nm. When exposed to air, the particles did not return to the degassed size, but did get smaller. This was expected and is due to some oxygen remaining inside the PIC. This analysis confirms that oxygen has a definite effect on the size of the particles, with bigger particles observed for PIC solutions in air (compared to a degassed sample) and even bigger sizes recorded for PIC solutions saturated with pure oxygen. Overall, we can conclude that oxygen has been loaded inside the PIC particles, and these have potential applications as oxygen carriers.

Table 15 Dissolved oxygen measurement results by DO metre and DLS for (**15b**)/ (**20b**) PIC solution

System	Half-life mg/l/min	Diameter by DLS/nm
Water	160	xx
Polyion Complex	310	Oxygen Free (nm) Oxygen Loaded (nm)
		271 → 386 305

3.6 Conclusion and Future work

a) Conclusion

The aim of this work was to develop a polyion complex micelle that could dissolve oxygen for use as potential artificial blood materials or oxygen carriers for PDT. The synthesis was based on ATRP and tBMA cleavage. Two types of polymers were synthesized, they were both mPEG based diblock copolymers with fluorine segments, with each one containing a different counter ion. Polymers with a positive charged block were obtained using DMAEMA monomers that was randomly copolymerization with TFEMA. The negative charged block was synthesized in two steps. First, tBMA was randomly copolymerized with TFEMA. Then the t-butyl ester was cleaved, giving the acid after reaction with trifluoroacetic acid. Both copolymers could form micelles in water, with CMCs of 0.002 mg/mL to 0.006 mg/mL recorded for the anionic and cationic polymers respectively. The DLS and pH measurements confirmed that PICs could form when the weight ratios were greater than 0.8:1, giving a neutral solution and a PIC with a diameter around 300 nm. The TEM provided some additional support for PIC formation, as these were observed in a mixture containing some smaller homo micelles. The oxygen release kinetics indicated that solutions could dissolve more oxygen than water. It was hypothesized that the extra oxygen was trapped inside the PIC and released when the oxygen in solution re-equilibrated with oxygen in air. This was confirmed by DLS measurements, which showed that PIC solutions saturated with oxygen and air were much bigger than degassed solutions of the same PIC. This increase in size was a direct consequence of oxygen dissolution, which

resulted in a swollen or larger PIC. This was due to oxygen swelling the fluorine rich components of the PIC. We are currently extending these studies and attempting to directly measure the amount of oxygen in solution (using an enzyme assay). In the long run experiments to test the potential of these and/or related systems, for use as volume expanders of artificial blood will be carried out.

b) Future work

Photodynamic Therapy

Photodynamic therapy (PDT) was developed as an effective clinical treatment for superficial tumours. It involves a photosensitiser that can be excited using non-thermal light with a certain wavelength. The excited photosensitizer then produces a singlet oxygen or superoxide from molecular oxygen to destroy cancer cells[116] (**Figure 3.11**).

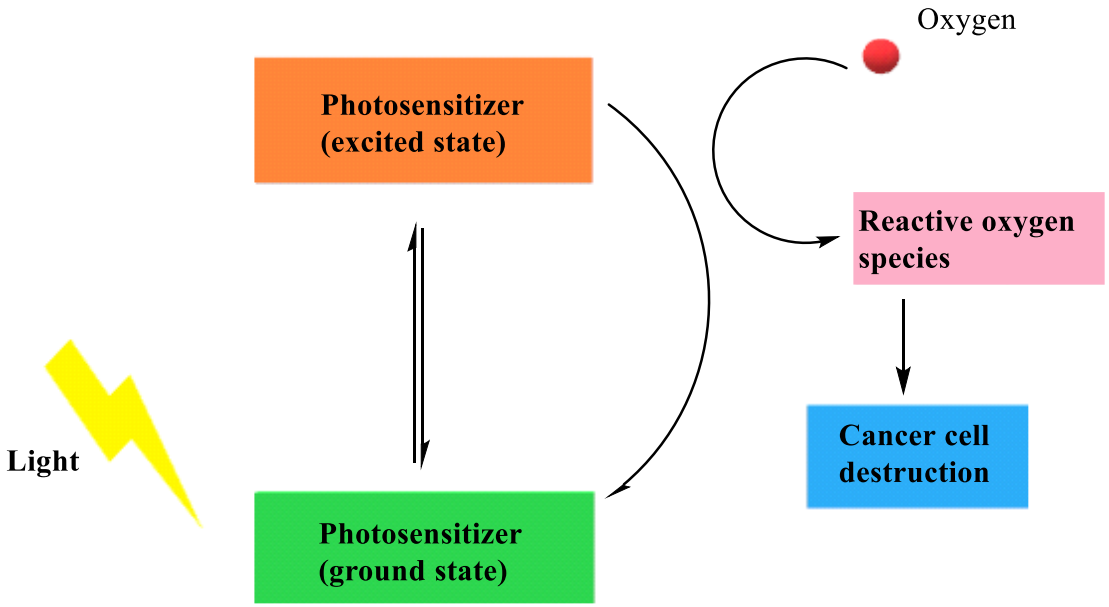

Figure 3.11 Simplified photodynamic therapy mechanism

As most photosensitizers utilised in PDT are hydrophobic, they resist intravenous injection,

and the oxygen singlet generated by the photosensitizer has a very short half-life; though it cannot spread widely, it still needs to be delivered to the targeted tumour sites selectively to prevent side effects.

The use of a polyion complex micelle as a delivery system for photodynamic therapy has been studied. These studies demonstrated that PIC micelles with a PEG shell can accumulate in solid tumour tissue effectively and specifically due to the size of the delivery systems and the hyperpermeability of tumour capillaries.[117] In addition, as a PIC is formed from electrostatic interactions between two block copolymers, its morphologies can be changed depending on the extent of protonation-deprotonation of the ionic blocks, such as those within the acidic microenvironment of a tumour,[118] which can result in selective release of their cargos.[97]

However, one inherent problem of PDT, is the hypoxic microenvironment of the tumour limits the efficacy of the PDT.[119] To solve this problem, oxygen (and a photosensitiser) also needs to be delivered to the tumor. There have been several attempts to provide sufficient oxygen sources for successful PDT. Luo et al. developed biomimetic artificial red cells by loading complexes of haemoglobin and photosensitizer to boost a photodynamic strategy.[120] A similar application of haemoglobin was achieved by Wang et al., who chemically conjugated the haemoglobin to polymeric micelles formed from poly(ethylene glycol)-block-poly(acrylic acid)-block-polystyrene. The authors found that an increased amount of reactive oxygen species was generated using this complex. As mentioned in Chapter 1, perfluorocarbon systems can also be applied as oxygen carriers to enhanced PDT. For example, Cheng et al. utilised perfluorohexane nanodroplets covering

a photosensitizer to create oxygen rich nanoparticle. When these were used for PDT, the photodynamic effect of the loaded photosensitizer was significantly enhanced.[121] However, all of these methods have some problems. For example, oxidative degradation of haemoglobin generated toxic subunits making the perfluorocarbon components extremely insoluble. This resulted in very rapid elimination, resulting in a loss of therapeutic activity. Since the fluorinated PIC developed in our work has the ability to carry oxygen within the core, and the formation of the PIC could be affected by pH. The system has a potential to be used in PDT to deliver oxygen and photosensitizers together. As this thesis only focused on the oxygen solubility, to extend this research, the photosensitizers encapsulation and release kinetic by the same PIC can be explored. In addition, to enhance the solubility and oxygen capacity, more acidic/basic polymers with different ionised group can be investigated.

Chapter 4
Experimental

4.1 General information of Chemicals and Instrumentations

Materials/Reagents

Unless stated otherwise, all reagents were purchased from Sigma-Aldrich, Inc. (Poole, UK) and used without further purification. 2,2,3,3,3-pentafluoropropyl methacrylate was purchased from Fluorochem Limited and was passed through basic aluminum column before use.

Instruments

Nuclear magnetic resonance (NMR) spectroscopy

NMR spectra were recorded using a Bruker BioSpin ADVANCED 400 MHz spectrometer (from Bruker BioSpin Billerica, MA, USA) at room temperature. Characterisation by ^{1}H, ^{13}C and ^{19}F were recorded at 400 MHz, 100 MHz and 376 MHz respectively. Chemical shifts are quoted in parts per million (ppm). MestReNova version 6.0.2-5475 was used to analyse the NMR data generated.

Gel permeation chromatography (GPC)

Samples were loaded onto two PL gel 3 μm MIXED-E columns which were 30 cm in length, with an inner diameter of 7.5 mm. Molecular weights are reported relative to calibrations

made using polystyrene standards (Mn 220-1, 1,000,000 Da). GPC grade tetrahydrofuran (THF) was used as both the solvent and the eluent. Samples were injected into the GPC circuit at a temperature of 25 °C at a flow rate of 1.0 mL/min with toluene as an internal standard. The characterisation was done using software released by Polymer Laboratories, Varian, Inc. (Amherst, MA, USA); PL DataStream Monitor version 1.2 and Cirrus GPC Online GPC/SEC Software version 3.0 were used to monitor the sample travelling through the columns and the data was analysed using Cirrus GPC Offline GPC/SEC Software version 3.0.

Mass spectroscopy

Mass-to-charge ratio of the products was determined by electrospray spectrometry (ES) using Waters LCT Premier XE (Milford, MA, U.S.A).

Fluorescence spectroscopy

FluoroMax®-4 was set as the excitation wavelength of 334 nm and the emission spectrum was recorded from 350 to 450 nm; the excitation/emission slits were set as 3/3 mm.

Transmission Electron Microscopy

The specimens are mounted on carbon-coated grids for negative staining by uranyl acetate. They were screened on a Philips CM100 100 kV electron microscope. This is equipped with a LaB6 gun and Gatan 1Kx1K digital camera. High-resolution images (15 Å to near-atomic) are recorded on a 200kV Tecnai Arctica, FEI Cryo-EM microscope.

Dynamic light scattering (DLS)

The Brookhaven instrument 90Plus Particle Size Analyzer (Holtsville, NY, USA) 35mW solid state standard laser was used to determine hydrodynamic diameter of nanoparticles. Light was scattered at an angle of 90° and samples were analysed using 10 runs, each lasting 1 minutes at 25 °C. Samples were filtered using Whatman® GD/X syringe filters (Kent, UK) with a pore size of 0.45 μm prior to analysis. Results reported are based upon volume distribution.

pH Measurements

pH measurement was carried out by Jenway 210 pH Meter. Calibration was based on pH = 4, pH = 7 and pH = 10 standard buffer solution.

4.2 Synthesis of 2, 2, 2-trifluoroethyl methacrylate (4)

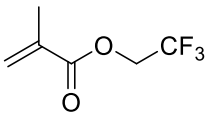

Figure 4.1 2, 2, 2-trifluoroethyl methacrylate **4**

2, 2, 2-trifluoroethanol (25.5 mL, 0.35 mol) and triethylamine (56.1 ml, 0.4 mol) were mixed with DCM in a double-neck flask and was cooled under an ice bath for 30 mins. methacryloyl chloride (31 mL, 0.38 mol) was added dropwise in 1 hour, generating white

smoke. Afterwards, the reaction was carried out under room temperature for overnight. The mixture was than washed by distilled cold water, 5% HCl and saturated $NaHCO_3$ solution. The solvent was removed by rotary evaporator at 30 °C under vacuum to yield liquid molecule **1**. (21.4 g, 40%) ^{1}H NMR (400MHz; $CDCl_3$; ppm) δ 4.53 (q, 2H, J=8.5 Hz, -C$\underline{H_2}$-CF_3), 5.68 (s, 1H, C$\underline{H_2}$=C-trans), 6.21 (s, 1H, C$\underline{H_2}$=C-cis), 1.96 (s, 3H, C(C$\underline{H_3}$)-). MH^+ = 168 g/mol

4.3 Synthesis of macro-initiator mPEG-Br (7)

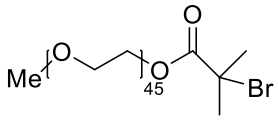

Figure 4.2 Poly (ethylene glycol) methyl ether 2-bromoisobutyrate **7**

mPEG (20 g, 10 mmol) was dried by azeotropic distillation with toluene, and then was added to 500 ml double-neck flask with 250 ml dry toluene. The solution was cooled to 0 °C in ice bath followed by addition of triethylamine (2 ml, 14.3 mmol). α-Bromoisobutyl bromide (1.5 ml, 12.1 mmol) was added via syringe over 1 hour. The mixture was stirred at ambient temperature for 24 h and then was filtered under vacuum to remove salt by-product. The filtrated solution was concentrated under reduced pressure and precipitated in diethyl ether. The cream colour solid product was yielded by vacuum filtration, followed by recrystallization in absolute ethanol for the further purification to give methyl poly (ethylene glycol) bromide (16.5 g, 77%) as white solid. ^{1}H NMR (400 MHz; $CDCl_3$; ppm) δ 1.95 (s, 6H, -CO_2Br(C$\underline{H_3}$)$_2$), 3.40 (s, 3H, C$\underline{H_3}$O-), 3.66 (s, 181H, -OC$\underline{H_2}$C$\underline{H_2}$O-), 4.34 (m,

2H, -C$\underline{H_2}$OOCMe$_2$Br); ^{13}C NMR (100MHz; $CDCl_3$; ppm): 174, 70.6. GPC (LMW; THF) Mn = 2890, Mw/Mn = 1.03.

4.4 General Method for CuBr and Monomer Purification

CuBr was purified by washing with acetate acid for three times and then with ethanol, diethyl ether for three times respectively, followed by drying in vacuum oven for 24 hours to yield white powder. Inhibitor of monomer was removed by passing through the basic aluminium oxide column.

CuBr and monomers were purified by this method prior to all polymerisation.

4.5 General Synthesis of mPEG-b-PMMA (9) by 2, 2'-Bipyridyl As the Ligand

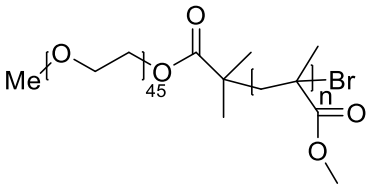

Figure 4.3 mPEG-b-PMMA **9**

mPEG-Br, methyl methacrylate and CuBr in 30% m/v toluene was prepared in a Schlenk tube. The mixture was degassed by freeze-pump-thaw for three times. 2, 2'-Bipyridyl was added quickly at the final freeze stage, and then the freeze-pump-thaw was carried out for another three times. The reaction was carried out under positive N_2 pressure at 70 °C overnight. The solution was opened to the air to kill the reaction and was dissolved in excess

toluene. The resulting blue solid was removed by vacuum filtration. The filtrate was reduced under vacuum to yield green oil which was then flushed through a small basic aluminium column in dichloroform to remove the catalyst. The solution was concentrated by rotary evaporator and precipitated from petroleum ether. The sticky product was dried in vacuum oven for 24 hours to yield white solid as crude mPEG-PMMA. The crude product was washed twice with distilled water at room temperature in order to remove possible unreacted PEG macroinitiator.

Synthesis of mPEG-b-PMMA ***9a***

According to the general method, mPEG (2.15 g, 1 mmol) was reacted with methyl methacrylate (2.1 ml, 20 mmol), catalysed by CuBr (0.144 g, 1 mmol)/ 2, 2'-Bipyridyl (0.328 g, 2.1 mmol), to give mPEG-*b*-$PMMA_{45}$ (1.41 g, 34%); ^{1}H NMR (400 MHz; $CDCl_3$; ppm) δ 0.80 – 1.09 (m, 135H, -CO($C\underline{H}_3$)), 1.09 – 2.0 (m, 91H, -$C\underline{H}_2$-$CO(CH_3)$), 3.40 (s, 3H, $C\underline{H}_3O$-), 3.66 (s, 178H, -$OC\underline{H}_2C\underline{H}_2O$-), 3.62 (s, 132H, -$COOC\underline{H}_3$) GPC (LMW; THF) Mn = 8800, Mw/Mn = 1.18.

Synthesis of mPEG-b-PMMA ***9b***

According to the general method, mPEG (2.15 g, 1 mmol) was reacted with methyl methacrylate (2.1 ml, 20 mmol) to give mPEG-*b*-$PMMA_{21}$ (3.14 g, 77%). The ligand was changed from 2, 2'-Bipyridyl to PMDETA (0.251 ml, 1.2 mmol); ^{1}H NMR (400 MHz; $CDCl_3$; ppm) δ 0.80 – 1.09 (m, 63H, -CO($C\underline{H}_3$)), 1.09 – 2.0 (m, 43H, -$C\underline{H}_2$-$CO(CH_3)$), 3.40 (s, 3H, $C\underline{H}_3O$-), 3.66 (s, 180H, -$OC\underline{H}_2C\underline{H}_2O$-), 3.62 (s, 64H, -$COOC\underline{H}_3$); GPC (LMW; THF)

Mn = 5100, Mw/Mn = 1.15

Synthesis of mPEG-b-PMMA ***9c***

According to the general method, mPEG (2.15 g, 1 mmol) was reacted with methyl methacrylate (1.1 ml, 10 mmol) to give mPEG-*b*-$PMMA_9$ (2.16 g, 69%). The ligand was changed from 2, 2'-Bipyridyl to PMDETA (0.251 ml, 1.2 mmol); ^1H NMR (400 MHz; $CDCl_3$; ppm) δ 0.80 – 1.09 (m, 27H, -CO($C\underline{H}_3$)), 1.09 – 2.0 (m, 19H, -$C\underline{H}_2$-$CO(CH_3)$), 3.40 (s, 3H, $C\underline{H}_3O$-), 3.66 (s, 178H, -$OC\underline{H}_2C\underline{H}_2O$-), 3.62 (s, 27H, -$COOC\underline{H}_3$); GPC (LMW; THF) Mn = 4200, Mw/Mn = 1.16

4.6 General Synthesis of mPEG-Poly (2, 2, 2-trifluoroethyl methacrylate) (mPEG-b-PTFEMA) (10)

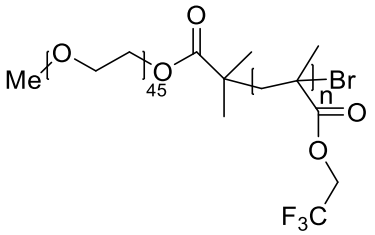

Figure 4.4 mPEG-b-PTFEMA **10**

mPEG-Br, 2, 2, 2- trifluoroethyl methacrylate and CuBr in 30% m/v toluene was prepared in a Schlenk tube. The mixture was degassed by freeze-pump-thaw for three times. PMDETA was degassed by bubbling nitrogen for 30 min and was added into the Schlenk tube. The reaction was carried out under positive N_2 pressure at 80 °C overnight. The

solution was opened to the air to kill the reaction and was dissolved in excess toluene. The resulting blue solid was removed by vacuum filtration. The filtrate was reduced under vacuum to yield a green oil which was then flushed through a small basic aluminium column in dichloroform to remove the catalyst. The solution was concentrated by rotary evaporator and precipitated from petroleum ether. The sticky product was dried in vacuum oven for 24 hours to yield white solid as mPEG-b-PTFEMA. The precipitated polymer was washed twice with distilled water at room temperature in order to remove possible unreacted mPEG macroinitiator.

Synthesis of mPEG-b-PTFEMA ***10a***

The general method for the synthesis of mPEG-Poly (2, 2, 2-trifluoroethyl methacrylate) was followed, with the following amounts, mPEG (2.15 g, 1 mmol) was reacted with 2, 2, 2-trifluoroethyl methacrylate (2.15 mL, 15 mmol), catalysed by CuBr (0.144 g, 1 mmol)/PMDETA (0.251 ml, 1.2 mmol), to give mPEG-*b*-PTFEMA$_{17}$ (2.53 g, 54%); ^{1}H NMR (400 MHz; $CDCl_3$; ppm) δ 0.80 – 1.19 (m, 51H, -CO(C$\underline{H}_3$)), 1.86 – 2.22 (m, 36H, -C$\underline{H}_2$-CO(CH_3)), 3.40 (s, 3H, C$\underline{H}_3$O-), 3.65 (s, 182H,-OC$\underline{H}_2$C$\underline{H}_2$O-), 4.36 (s, 34H, -C$\underline{H}_2$$CF_3$); ^{19}F NMR (100 MHz; $CDCl_3$; ppm); δ -73.29; GPC (LMW; THF) Mn = 5200, Mw/Mn = 1.42.

Synthesis of mPEG-b-PTFEMA ***10b***

Following the general method, mPEG (2.15 g, 1 mmol) was reacted with 2, 2, 2-trifluoroethyl methacrylate (3.58 mL, 25 mmol), catalysed by CuBr (0.144 g, 1

mmol)/PMDETA (0.251 ml, 1.2 mmol), to give mPEG-*b*-PTFEMA$_{25}$ (5.15 g, 43%); ^{1}H NMR (400 MHz; $CDCl_3$; ppm) δ 0.80 – 1.19 (m, 78H, -CO(C$\underline{H}_3$)), 1.86 – 2.22 (m, 51H, -C$\underline{H}_2$-CO(CH_3)), 3.40 (s, 3H, C$\underline{H}_3$O-), 3.65 (s, 178H, -OC$\underline{H}_2$C$\underline{H}_2$O-), 4.36 (s, 50H, -C$\underline{H}_2CF_3$); ^{19}F NMR (100 MHz; $CDCl_3$; ppm); δ -73.29; GPC (LMW; THF) Mn = 6630, Mw/Mn = 1.55.

Synthesis of mPEG-b-PTFEMA ***10c***

Following the general method, mPEG (2.15 g, 1 mmol) was reacted with 2, 2, 2-trifluoroethyl methacrylate (5.02 mL, 35 mmol), catalysed by CuBr (0.144 g, 1 mmol)/PMDETA (0.251 ml, 1.2 mmol), to give mPEG-*b*-PTFEMA$_{33}$ (2.42 g, 30%); ^{1}H NMR (400 MHz; $CDCl_3$; ppm) δ 0.80 – 1.19 (m, 100H, -CO(C$\underline{H}_3$)), 1.86 – 2.21 (m, 65H, -C$\underline{H}_2$-CO(CH_3)), 3.40 (s, 3H, C$\underline{H}_3$O-), 3.65 (s, 180H, -OC$\underline{H}_2$C$\underline{H}_2$O-), 4.36 (s, 66H, -C$\underline{H}_2CF_3$); ^{19}F NMR (100 MHz; $CDCl_3$; ppm); δ -73.29; GPC (LMW; THF) Mn = 8540, Mw/Mn = 1.53.

Synthesis of mPEG-b-PTFEMA ***10d***

mPEG (2.15 g, 1 mmol) was reacted with 2, 2, 2-trifluoroethyl methacrylate (6.45 mL, 45 mmol), catalysed by CuBr (0.144 g, 1 mmol)/PMDETA (0.251 ml, 1.2 mmol), to give mPEG-*b*-PTFEMA$_{50}$ (2.34 g, 24%); ^{1}H NMR (400 MHz; $CDCl_3$; ppm) δ 0.80 – 1.19 (m, 153H, -CO(C$\underline{H}_3$)), 1.86 – 2.22 (m, 101H, -C$\underline{H}_2$-CO(CH_3)), 3.40 (s, 3H, C$\underline{H}_3$O-), 3.65 (s, 180H, -OC$\underline{H}_2$C$\underline{H}_2$O-), 4.36 (s, 100H, -C$\underline{H}_2CF_3$); ^{19}F NMR (100 MHz; $CDCl_3$; ppm); δ -73.29; GPC (LMW; THF) Mn = 11400, Mw/Mn = 1.60.

4.7 General Synthesis of mPEG-Poly(2,2,3,3,3-pentafluoropropyl methacrylate) (mPEG-PPFPMA)(14)

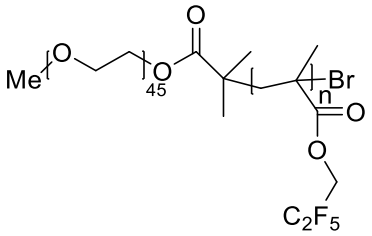

Figure 4.5 mPEG-b-PPFPMA **14**

mPEG-Br, 2,2,3,3,3-pentafluoropropyl methacrylate and CuBr in 20% m/v toluene was prepared in a Schlenk tube. The mixture was degassed by freeze-pump-thaw for three times. PMDETA was degassed by bubbling nitrogen for 30 min and was added into the Schlenk tube. The reaction was carried out under positive N_2 pressure at 90 °C overnight. The solution was opened to the air to kill the reaction and was dissolved in excess toluene. The resulting blue solid was removed by vacuum filtration. The filtrate was reduced under vacuum to yield a green oil which was then flushed through a small basic aluminium column in dichloroform to remove the catalyst. The solution was concentrated by rotary evaporator and precipitated from petroleum ether. The sticky product was dried in vacuum oven for 24 hours to yield white solid as mPEG-PPFPMA. The precipitated polymer was washed twice with distilled water at room temperature in order to remove possible unreacted mPEG macroinitiator.

Synthesis of mPEG-b-PPFPMA ***14a***

mPEG (2.15 g, 1 mmol) was reacted with 2,2,3,3,3-pentafluoropropyl methacrylate (2.56 mL, 15 mmol), catalysed by CuBr (0.144 g, 1 mmol)/PMDETA (0.251 ml, 1.2 mmol), to give mPEG-*b*-PPFPMA$_{12}$ (2.33 g, 43%); ^{1}H NMR (400 MHz; $CDCl_3$; ppm) δ 0.77 – 1.22 (m, 36H, -CO(C$\underline{H_3}$)), 1.62 – 2.24 (m, 25H, -C$\underline{H_2}$-CO(CH_3)), 3.40 (s, 3H, C$\underline{H_3}$O-), 3.66 (s, 178H, -OC$\underline{H_2}$C$\underline{H_2}$O-), 4.40 (t, 24H, J=12 Hz, -C$\underline{H_2}C_2F_5$); ^{19}F NMR (100 MHz; $CDCl_3$; ppm); δ -83.89, -123.10; GPC (LMW; THF) Mn = 4480, Mw/Mn = 1.23

Synthesis of mPEG-b-PPFPMA ***14b***

mPEG (2.15 g, 1 mmol) was reacted with 2,2,3,3,3-pentafluoropropyl methacrylate (4.27 mL, 25 mmol), catalysed by CuBr (0.144 g, 1 mmol)/PMDETA (0.251 ml, 1.2 mmol), to give mPEG-*b*-PPFPMA$_{23}$ (3.88 g, 51%); ^{1}H NMR (400 MHz; $CDCl_3$; ppm) δ 0.77 – 1.22 (m, 69H, -CO(C$\underline{H_3}$)), 1.62 – 2.24 (m, 46H, -C$\underline{H_2}$-CO(CH_3)), 3.40 (s, 3H, C$\underline{H_3}$O-), 3.66 (s, 180H, -OC$\underline{H_2}$C$\underline{H_2}$O-), 4.41 (t, 46H, J=12 Hz, -C$\underline{H_2}C_2F_5$); ^{19}F NMR (100 MHz; $CDCl_3$; ppm); δ -83.89, -123.10; GPC (LMW; THF) Mn = 7300, Mw/Mn = 1.30

Synthesis of mPEG-b-PPFPMA ***14c***

mPEG (2.15 g, 1 mmol) was reacted with 2,2,3,3,3-pentafluoropropyl methacrylate (5.978 mL, 35 mmol), catalysed by CuBr (0.144 g, 1 mmol)/PMDETA (0.251 ml, 1.2 mmol), to give mPEG-*b*-PPFPMA$_{44}$ (3.04 g, 31%); ^{1}H NMR (400 MHz; $CDCl_3$; ppm) δ 0.77 – 1.22 (m, 132H, -CO(C$\underline{H_3}$)), 1.62 – 2.24 (m, 87H, -C$\underline{H_2}$-CO(CH_3)), 3.40 (s, 3H, C$\underline{H_3}$O-), 3.66 (s, 178H, -OC$\underline{H_2}$C$\underline{H_2}$O-), 4.41 (t, 88H, J=12 Hz, -C$\underline{H_2}C_2F_5$); ^{19}F NMR (100 MHz; $CDCl_3$;

ppm); δ -83.89, -123.10; GPC (LMW; THF) Mn = 12900, Mw/Mn = 1.20

4.8 General Procedure for Measurement of Critical Micelle Concentrations.

0.01 mg/ml pyrene acetone solution was made as a probe of CMC measurement.

A series of volumetric flasks were prepared, and 0.5 ml of pyrene solution was added to each one. All flasks were left for 24 hours to evaporate acetone. Meanwhile, 100 mg of polymer was dissolved in 10 ml THF, followed by mixing with 100 ml distilled water. The mixture was heated to 40 °C under vacuum with stirring for 5 hours and transferred to 100 ml volumetric flask to make 1 mg/mL batch solution.

A series of solutions with different concentrations from 1 mg/ml to 0.0003 mg/ml was made by diluting the batch solution to the volumetric flasks which contain pyrene. Each solution was stirred for 30 mins and left overnight, and then was ready to measure.

The fluorescence measurements were carried out on FluoroMax-4 Spectrometer with excitation wavelength of 334 nm and the emission spectrum was recorded from 350 to 450 nm; the excitation/emission slits were set as 2.5/2.5 mm. The fluorescence intensities of the peaks at 372 nm (I_1) and 383 nm (I_3) were extracted from the spectra, and the logarithm of the I_3/I_1 value vs. polymer concentration was plotted to determine the CMC.

4.9 Oxygen Solubility Measurements

4.9.1 General Procedure for the Indirect Measurement of Dissolved Oxygen using a Dissolved Oxygen Meter.

5 mg/mL polymer batch solution was prepared by dissolving 100mg of solid polymer in 2 mL of THF followed by addition of 20ml of deionised water. The mixture was heated to 40 °C under vacuum with stirring for 5 hours and made up to 20 mL by deionised water again.

The dissolved oxygen was measured by Seven2Go pro DO Meter S9 overnight. The meter was calibrated before the test. The solution was moved into a vial and the probe of the meter was inserted into the solution. The measurement was set as 5 minutes interval which meant it could record the oxygen concentration every 5 minutes.

The solutions of 0.05 mg/mL and 2 mg/mL were diluted from 5 mg/mL batch solution directly. The same oxygen measurement was carried out with these solutions.

4.9.2 General Procedure for the Direct Measurement of Dissolved Oxygen Measurement using a Glucose(GO) Assay

The dissolved oxygen was also measured by a commercial glucose(GO) kit which was available form Sigma-Aldrich. The kit came with the enzymes glucose oxidase, peroxidase,

the o-dianisidine reagent and a glucose standard solution. The procedure was provided with the kit, with the exception that an excess amount of glucose was used.

The assay reagent was made up according to the instruction provided (within the kit) and a sample containing 2 mL of the assay reagent and 39.2 mL of glucose oxidase/peroxidase reagent was made up. Air was then bubbled through the solution for 2 minutes. 3 mL of this solution was transferred to a 4 mL tube and sealed with a rubber suba seal, that ensured no dead volume above the liquid. A small volume of concentrated glucose was added such that the concentration in the tube was 55 μg/mL. The mixture was stirred for 30 mins, after which the reaction was stopped and the process quenched by adding 2 mL of sulfuric acid (12 N). The mixture was left to stand for 12 hours before filtering. The intensity of the peak at 540 nm was measured using UV. The reaction was repeated, but in presence of the polymer with a concentration of 5 mg/mL

4.9.3 General Procedure for the indirect Measurement of Dissolved Oxygen using DLS

40 mg of polymer was added into a sample vial, followed by the addition of 1 mL THF and 20 mL deionized water. The mixture was heated to 40 °C under vacuum with stirring for 5 hours, then was made up to 20 mL again at ambient temperature. The solution was gently shaken overnight for further use.

After the solution was prepared, it was heated to 40 °C under the vacuum and then cooled down to room temperature under nitrogen, which was repeated for 3 times. Then the solution was quickly transferred to a cuvette with a seal lid by the syringe equipped with a

0.45 μm filter for the DLS measurement at 25 °C. Then the lid was taken off and oxygen was bubbled through the cuvette for 5 minutes before it was resealed and a second DLS measurement was carried out. The cuvette was then left open to the air for 1 hour to get the air equilibrated and was measured under DLS again.

4.10 General Synthesis of mPEG-P(TFEMA-*ran*-DMAEMA) (15)

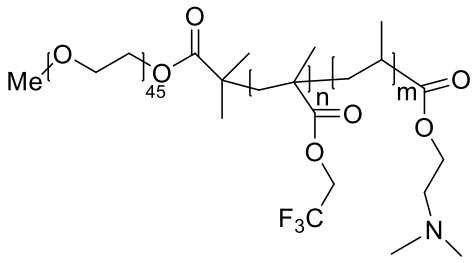

Figure 4.6 mPEG-P(TFEMA-*ran*-DMAEMA) **15**

mPEG-Br, TFEMA, DMAEMA and CuBr in 30% m/v toluene was prepared in a Schlenk tube. The mixture was degassed by freeze-pump-thaw for three times. PMDETA was degassed by bubbling nitrogen for 30 min and was added into the Schlenk tube. The reaction was carried out under positive N_2 pressure at 80 °C overnight. The solution was opened to the air to kill the reaction and was dissolved in excess toluene. The resulting blue solid was removed by vacuum filtration. The filtrate was reduced under vacuum to yield a green oil-like mixture which was then flushed through a small basic aluminium column in toluene to remove the catalyst. The solution was concentrated by rotary evaporator and precipitated in petroleum ether. The sticky product was dried in vacuum oven for 24 hours to yield white solid as mPEG-P(TFEMA-*ran*-DMAEMA). The precipitated polymer was

extracted twice with distilled water at room temperature in order to remove possible unreacted mPEG macroinitiator.

Synthesis of mPEG-P(TFEMA-ran-DMAEMA) ***15a***

mPEG (2.15 g, 1 mmol) was reacted with 2,2,2-trifluoroethyl methacrylate (2.87 mL, 20 mmol) and 2-(dimethylamino)ethyl methacrylate(0.84 mL, 5 mmol), catalysed by CuBr (0.144 g, 1 mmol)/PMDETA (0.251 ml, 1.2 mmol) as the procedure to give mPEG-*b*-P($TFEMA_{18}$-*ran*-$DMAEMA_3$)(4.17 g, 66 %); ^{1}H NMR (400 MHz; $CDCl_3$; ppm) δ 0.757 – 1.21 (m, 63H, -CO(C$\underline{H}_3$)), 1.60 – 2.16 (m, 44H, -C$\underline{H}_2$-CO(CH_3)), 2.29(s, 18H, -N(C$\underline{H}_3$)$_2$), 2.57 (s, 6H, -C$\underline{H}_2$N-), 3.40 (s, 3H, C$\underline{H}_3$O-), 3.66 (s, 180H, -OC$\underline{H}_2$C$\underline{H}_2$O-), 4.08 (s, 6H, -COC$\underline{H}_2$-CH_2N-) 4.36 (s, 36H-C$\underline{H}_2$$CF_3$); ^{19}F NMR (100 MHz; $CDCl_3$; ppm); δ -73.11; GPC (LMW; THF) Mn = 6200, Mw/Mn = 1.12.

Synthesis of mPEG-P(TFEMA-ran-DMAEMA) ***15b***

mPEG (2.15 g, 1 mmol) was reacted with 2,2,2-trifluoroethyl methacrylate (2.87 mL, 20 mmol) and 2-(dimethylamino)ethyl methacrylate(1.68 mL, 10 mmol), catalysed by CuBr (0.144 g, 1 mmol)/PMDETA (0.251 ml, 1.2 mmol) as the procedure to give mPEG-*b*-P($TFEMA_{15}$-*ran*-$DMAEMA_9$)(4.34 g, 61%); ^{1}H NMR (400 MHz; $CDCl_3$; ppm) δ 0.757 – 1.21 (m, 72H, -CO(C$\underline{H}_3$)), 1.60 – 2.16 (m, 49H, -C$\underline{H}_2$-CO(CH_3)), 2.29(s, 54H, -N(C$\underline{H}_3$)$_2$), 2.57 (s, 18H, -C$\underline{H}_2$N-), 3.40 (s, 3H, C$\underline{H}_3$O-), 3.66 (s, 178H, -OC$\underline{H}_2$C$\underline{H}_2$O-), 4.08 (s, 18H, -COC$\underline{H}_2$-CH_2N-) 4.36 (s, 30H, -C$\underline{H}_2$$CF_3$); ^{19}F NMR (100 MHz; $CDCl_3$; ppm); δ -73.11; GPC (LMW; THF) Mn = 8000, Mw/Mn = 1.10.

Synthesis of mPEG-P(TFEMA-ran-DMAEMA) ***15c***

mPEG (2.15 g, 1 mmol) was reacted with 2,2,2-trifluoroethyl methacrylate (2.87 mL, 20 mmol) and 2-(dimethylamino)ethyl methacrylate(2.52 mL, 15 mmol), catalysed by CuBr (0.144 g, 1 mmol)/PMDETA (0.251 ml, 1.2 mmol) as the procedure to give mPEG-*b*-P(TFEMA$_{23}$-*ran*-DMAEMA$_{17}$)(4.30 g, 55%); ^{1}H NMR (400 MHz; $CDCl_3$; ppm) δ 0.757 – 1.21 (m, 121H, -CO(C$\underline{H}_3$)), 1.60 – 2.16 (m, 80H, -C$\underline{H}_2$-CO(CH$_3$)), 2.29(s, 102H, -N(C$\underline{H}_3$)$_2$), 2.57 (s, 34H, -C$\underline{H}_2$N-), 3.40 (s, 3H, C$\underline{H}_3$O-), 3.66 (s, 180H, -OC$\underline{H}_2$C$\underline{H}_2$O-), 4.08 (s, 34H, -COC$\underline{H}_2$-CH$_2$N-) 4.36 (s, 46H, -C$\underline{H}_2$CF$_3$); ^{19}F NMR (100 MHz; $CDCl_3$; ppm); δ -73.11; GPC (LMW; THF) Mn = 10040, Mw/Mn = 1.21

4.11 Synthesis of mPEG-P(TFEMA-*ran*-tBMA) (19)

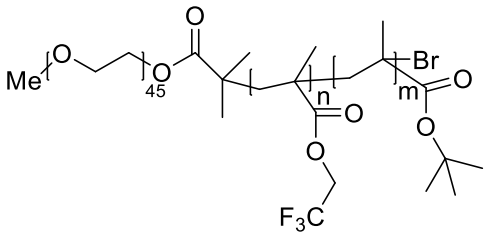

Figure 4.7 mPEG-P(TFEMA-*ran*-tBMA) **19**

mPEG-Br (2.15 g, 1 mmol), TFEMA (2.87 mL, 20 mmol), DMAEMA (1.62 mL, 10 mmol) and CuBr (0.144 g, 1 mmol) in 30% m/v toluene was prepared in a Schlenk tube. The mixture was degassed by freeze-pump-thaw for three times. PMDETA (0.251 ml, 1.2 mmol) was degassed by bubbling nitrogen for 30 min and was added into the Schlenk tube. The

reaction was carried out under positive N_2 pressure at 80 °C overnight. The solution was opened to the air to kill the reaction and was dissolved in excess toluene. The resulting blue solid was removed by vacuum filtration. The filtrate was reduced under vacuum to yield a green oil-like mixture which was then flushed through a small basic aluminium column in toluene to remove the catalyst. The solution was concentrated by rotary evaporator and precipitated in petroleum ether. The sticky product was dried in vacuum oven for 24 hours to yield white solid as mPEG-P(TFEMA$_{23}$-*ran*-tBMA$_{12}$). The precipitated polymer was extracted twice with distilled water at room temperature in order to remove possible unreacted mPEG macroinitiator. (3.16 g, 66%) ^{1}H NMR (400 MHz; $CDCl_3$; ppm) δ 0.76 – 1.24 (m, 105H, -CO(C$\underline{H}_3$)), 1.43 (s, 108H, C(C$\underline{H}_3$)$_3$) 1.70 – 2.16 (m, 70H, -C$\underline{H}_2$-CO(CH$_3$)), 3.40 (s, 3H, C$\underline{H}_3$O-), 3.66 (s, 180H, -OC$\underline{H}_2$C$\underline{H}_2$O-), 4.35 (s, 46H, -C$\underline{H}_2$CF$_3$); ^{19}F NMR (100 MHz; $CDCl_3$; ppm); δ -73.11; GPC (LMW; THF) Mn = 8010, Mw/Mn = 1.27

4.12 General Procedure for mPEG-P(TFEMA-*ran*-tBMA) Cleavage.

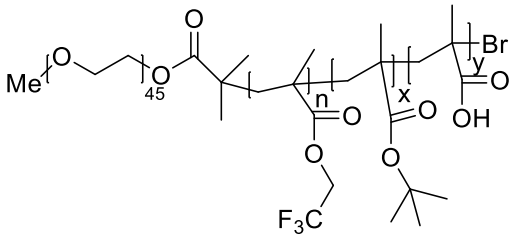

Figure 4.8 mPEG-P(TFEMA-*ran*-tBMA-*ran*-MAA) **20**

To a 100 mL two-neck round bottom flask equipped with stirrer bar and sealed with a rubber septum, 20 mL dry DCM and mPEG-P(TFEMA$_{23}$-*ran*-tBMA$_{12}$) were added. After the polymer dissolved, TFA was added by a syringe. The flask was sealed, and the mixture was

stirred at ambient temperature for 8 hours. Afterwards, the solution was concentrated by rotary evaporator and precipitated in hexane. The white precipitate was recovered and dissolved in DCM again, followed by evaporating the solvent under rotary evaporator to remove the TFA residue. The final product was dried in the vacuum oven to yield white solid as the final product.

Synthesis of mPEG-P(TFEMA-ran-tBMA-ran-MAA) ***20a***

mPEG-P($TFEMA_{23}$-*ran*-$tBMA_{12}$) (1 g, 0.13 mmol) was cleaved in DCM with TFA (1.5 mL, 19.6 mmol) as a catalyst. The procedure was followed as the one mentioned above to give mPEG-P($TFEMA_{23}$-*ran*-$tBMA_9$-MAA_3) (0.35 g, 37%); ^{1}H NMR (400 MHz; $CDCl_3$; ppm) δ 0.76 – 1.24 (m, 105H, -CO($C\underline{H}_3$)), 1.43 (s, 81H, C($C\underline{H}_3$)$_3$) 1.70 – 2.16 (m, 70H, -$C\underline{H}_2$-CO(CH_3)), 3.40 (s, 3H, $C\underline{H}_3$O-), 3.66 (s, 180H, -O$C\underline{H}_2C\underline{H}_2$O-), 4.35 (s, 46H, -$C\underline{H}_2CF_3$); ^{19}F NMR (100 MHz; $CDCl_3$; ppm); δ -73.11; GPC (LMW; THF) Mn = 7550, Mw/Mn = 1.35

Synthesis of mPEG-P(TFEMA-ran-tBMA-ran-MAA) ***20b***

mPEG-P($TFEMA_{23}$-*ran*-$tBMA_{12}$) (1 g, 0.13 mmol) was cleaved in DCM with TFA (1.5 mL, 19.6 mmol) as a catalyst. The main procedure was followed as the one mentioned above, but the reaction time was extended from 8 hours to 12 hours to give mPEG-P($TFEMA_{23}$-*ran*-$tBMA_6$-MAA_6) (0.32 g, 33%); ^{1}H NMR (400 MHz; $CDCl_3$; ppm) δ 0.76 – 1.24 (m, 105H, -CO($C\underline{H}_3$)), 1.43 (s, 54H, C($C\underline{H}_3$)$_3$) 1.70 – 2.16 (m, 70H, -$C\underline{H}_2$-CO(CH_3)), 3.40 (s, 3H, $C\underline{H}_3$O-), 3.66 (s, 180H, -O$C\underline{H}_2C\underline{H}_2$O-), 4.35 (s, 46H, -$C\underline{H}_2CF_3$); ^{19}F NMR (100

MHz; $CDCl_3$; ppm); δ -73.11; GPC (LMW; THF) Mn =7820, Mw/Mn = 1.29

4.13 Polyion Complex Preparation

A batch methanol solution of polymer mPEG-P(TFEMA$_{23}$-*ran*-tBMA$_6$-*ran*-MAA$_6$) (**20b)** with a concentration of 1 mg/ml was prepared by dissolving directly. A series of mPEG-P(TFEMA$_{15}$-*ran*-DMAEMA$_9$) (**15b**) solutions with the concentrations from 0.3 mg/ml to 1 mg/ml were made by using methanol as the solvent as well. Each copolymer（**15b**) solution with a certain concentration was mixed with copolymer (**20b**) solution by same volume separately. The final solutions were put on the rotary evaporators to eliminate the solvent, generating a layer of thin film on the wall of the vials. Deionized water (20 mL) was added to the vials to dissolve the mixture, then the pH was tested for all mixed solutions. The mixing ratio was recorded when the pH reached to 7, the further tests for polyion complex was based on the same ratio.

Chapter 5

References

1 G. E. Morgan, M. S. Mikhail, M. J. Murray, W. Kleinman, G. J. Nitti, J. T. Nitti, J. Raya, R. F. Bedford, J. F. Bion, J. Butterworth and N. H. Cohen, *Clinical Anesthesiology*, McGraw-hill, New York, 2002.

2 Ch. P. Mangum, *Blood and Tissue Oxygen Carriers*, Springer-Verlag, Berlin Heidelberg, 1992.

3 T. J. Greenwalt, *Transfusion*, 1997, **37**, 550-563.

4 R. M. Winslow, K. D. Vandegriff and M. Intaglietta, *Blood Substitutes: Physiological Efficacy*, Birkhäuser, Boston, 1995.

5 M. L. Nucci and A. Abuchowski, *Sci. Am.*, 1998, **278**, 72–-77.

6 RM. Oswalt, *Transfusion*, 1977, **17**, 123-135.

7 T. Hovav, S. Yedgar, N. Manny and G. Barshtein, *Transfusion*, 1999, **39**, 277-281.

8 J. G. Riess and J. G. Riess, *Chem. Rev.*, 2001, **101**, 2797-2919.

9 M. Paoli, R. Liddington, J. Tame, A. Wilkinson and G. Dodson, *J. Mol. Biol.*, 1996, **256**, 775- 792.

10 M. F. Perutz, *Annu. Rev. Biochem.*, 1979, **48**, 327-386.

11 S. E. Phillips, *J. Mol. Biol.*, 1980, **142**, 531-554.

12 R. C. Hardison, *Cold Spring Harb Perspect Med.*, 2012, **2**, a011627-a011627.

13 W. A. Eaton, E. R. Henry, J. Hofrichter and A. Mozzarelli, *Rend. Lincei*, 2006, **17**, 147-162.

14 D. H. Chin, J. Del Gaudio, G. N. La Mar and A. L. Balch, *J. Am. Chem. Soc.*, 1977, **99**, 5486-5488.

15 L. Latos-Grazynski, R. J. Cheng, G. N. La Mar and A. L. Balch, *J. Am. Chem. Soc.*, 1982, **104**, 5992-6000.

16 L. Kresie, *Proc. (Bayl. Univ. Med. Cent).*, 2001, **14**, 158-161.

17 E. M. Ketcham and C. B. Cairns, *Ann. Emerg. Med.*, 1999, **33**, 326-337.

18 D. Looker, D. Abbott-Brown, P. Cozart, S. Durfee, S. Hoffman, A. J. Mathews, J. Miller- Roehrkh, S. Shoemaker, S. Trimble, G. Fermi, N. H. Komiyama, K. Nagai and G. L. Stetler, *Nature*, 1992, **356**, 258-60.

19 K. M. Bobofchak, T. Mito, S. J. Texel, A. Bellelli, M. Nemoto, R. J. Traystman, R. C. Koehler, W. S. Brinigar and C. Fronticelli, *Am. J. Physiol. Heart Circ. Physiol.*, 2003, **285**, H549-H561.

20 M. D. Bhadange, A. Y. Joshi, A. B. Darekar and R R. Saudagar, *World J. Pharm. Pharm. Sci.*, 2015, **4**, 518-532.

21 R. Benesch and R. E. Benesch, *Nature*, 1969, **221**, 618-622.

22 T. F. Zuck, J. G. Riess and G. P. Biro, *Crit. Rev. Clin. Lab. Sci.*, 1994, **31**, 295-324.

23 B. Chesebro and H. Metzger, 1968, **246**, 766-771.

24 G. Gregoriadis, *Liposome Technology*, Informa healthcare, USA, 2007.

25 L. Djordjevich and I.F. Miller, *Exp. Hematol.*, 1980, **8**, 584-592.

26 B.P. Gaber and M.C. Farmer, *Prog. Clin. Biol. Res.*, 1984, **165**, 179-190.

27 M. Marta, M. Patamia, A. Lupi, M. Antenucci, M. Di Iorio, S. Romeo, R. Petruzzelli, M. Pomponi and B. Giardina, *J. Biol. Chem.*, 1996, **271**, 7473-7478.

28 W. K. Bleeker, J. van der Plas, R. I. J. Feitsma, J. Agterberg, G. Rigter, A. De Vries-van Rossen, E. K. J. Pauwels, J. C. Bakker, Transl. Res., 1989, **113**, 145-150.

29 M. Nozue, I. Lee, J. M. Manning, L. R. Manning and R. K. Jain, *J. Surg. Oncol.*, 1996, **62**, 109-114.

30 D. J. Schaer, C. a Schaer, P. W. Buehler, R. a Boykins, G. Schoedon, A. I. Alayash, A. Schaffner and W. Dc, *Blood*, 2013, **107**, 373-380.

31 Z. Tao and P. P. Ghoroghchian, *Trends Biotechnol.*, 2014, **32**, 466-473.

32 G. A. Berbers, W. K. Bleeker, P. Stekkinger, J. Agterberg, G. Rigter and J. C. Bakker, *Transl. Res.*, 1991, **117**, 157-165.

33 R. O. Beauchamp, M. B. St Clair, T. R. Fennell, D. O. Clarke, K. T. Morgan and F. W. Kari, *Crit. Rev. Toxicol.*, 1992, **22**, 143-174.

34 A. Zingg, B. Felber, V. Gramlich, L. Fu, J. P. Collman and F. Diederich, *Helv. Chim. Acta*., 2002, **85**, 333-351.

35 L. J. Twyman and Y. Ge, *Chem. Commun. (Camb).*, 2006, **15**, 1658-1660.

36 L. Shen, R. Qu, H. Shi, F. Huang, Y. An and L. Shi, *Biomater. Sci.*, 2016, **4**, 857-862.

37 L. C. Jr. Clark and F. Gollan, *Sci.*, 1966, **152**, 1755-1756.

38 B. D. Spiess, *Diving Hyperb. Med.*, 2010, **40**, 23-28.

39 S. F. Flaim, *Artif. Cells. Blood Substit. Immobil. Biotechnol.*, 1994, **22**, 1043-1054.

40 M. J. Barthel, T. Rudolph, S. Crotty, F. H. Schacher and U. S. Schubert, *J. Polym. Sci., Part A: Polym. Chem.*, 2012, **50**, 4958-4965.

41 K. Knop, R. Hoogenboom, D. Fischer and U. S. Schubert, *Angew. Chemie - Int. Ed.*, 2010, **49**, 6288-6308.

42 G. Pitarresi, A. P. Piccionello, R. Calabrese, A. Pace, S. Buscemi and G. Giammona, *J. Fluor. Chem.*, 2008, **129**, 1096-1103.

43 X. Jiang, F. Chun, G. Lu and H. Xiaoyu, *Polym. Chem*. 2017, **8**, 1163-1176.

44 Q. Zhang and S. Zhu, *ACS Macro Lett*. 2014, **3**, 743-746.

45 G.Riess, *Prog. Polym. Sci.*, 2003, **28**, 1107-1170.

46 A. Blanazs, R. Verber, O. O. Mykhaylyk, A. J. Ryan, J. Z. Heath, C. W. I. Douglas and S. P. Armes, *J. Am. Chem. Soc.*, 2012, **134**, 9741-9748.

47 L. Zhang and A. Eisenberg, *Macromolecules*, 1996, **29**, 8805- 8815.

48 B. Karagoz, L. Esser, H. T. Duong, J. S. Basuki, C. Boyer and T. P. Davis, *Polym. Chem.*, 2014, **5**, 350-355.

49 I. Larue, M. Adam, M. da Silva, S. S. Sheiko and M. Rubinstein, *Macromolecules*, 2004, **37**, 5002-5005.

50 I. Larue, M. Adam, M. Pitsikalis, N. Hadjichristidis, M. Rubinstein and S. S. Sheiko, *Macromolecules*, 2006, **39**, 309-314.

51 H. Shen, A. Eisenberg, *J. Phys. Chem. B*, 1999, **103**, 9473-9487.

52 A. Ghosh, M. Haverick, K. Stump, X. Yang, M. F. Tweedle and J. E. Goldberger, *J. Am. Chem. Soc.*, 2012, **134**, 3647-3650.

53 G. G. Odian, *Principles of Polymerization, 4th Edition*, John Wiley & Sons, Inc., 2004.

54 G. Moad, E. Rizzardo and S. H. Thang, *Acc. Chem. Res.* ,2008, **41**, 1133-1142.

55 O. W. Webster, *Science*, 1991, **251**, 887-893.

56 J. Nicolas, Y. Guillaneuf, C. Lefay, D. Bertin, D. Gigmes and B. Charleux, *Prog. Polym. Sci.*, 2013, **38**, 63-235.

57 N. Chagneux, T. Trimaille, M. Rollet, E. Beaudoin, P. Gérard, D. Bertin and D. Gigmes, *Macromolecules*, 2009, **42**, 9435-9442.

58 Y. K. Chong, J. Krstina, T. P. T. Le, G. Moad, A. Postma, E. Rizzardo and S. H. Thang, *Macromolecules*, 2003, **36**, 2256-2272.

59 G. Moad, E. Rizzardo and S. H. Thang, *Aust. J. Chem.*, 2005, **58**, 379-410.

60 B.Y.K.Chong, T.p.t.Le, G.Moad, E. Rizzardo and S. H. Thang, *Macromolecules*, 1999, **32**, 2071-2074.

61 N. J. Warren, O. O. Mykhaylyk, D. Mahmood, A. J. Ryan and S. P. Armes, *J. Am. Chem. Soc.*, 2014, **136**, 1023-1033.

62 J. S. Wang and K. Matyjaszewski, *Macromolecules*, 1995, **28**, 7901-7910.

63 K. Matyjaszewski and J. H. Xia, *Chem. Rev.*, 2001, **101**, 2921-2990.

64 W.Jakubowski and K.Matyjaszewski, *Macromolecules*, 2005, **38**, 4139-4146.

65 C. Henrickson, *Chemistry*, Wiley, 2005.

66 T. M. Brand, M. E. Brand and G. D. Jay, *J. Clin. Monit. Comput.*, 2002, **17**, 93-96.

67 Y. Rabi, D. Kowal and N. Ambalavanan, in *Assisted Ventilation of the Neonate*, ed. J. Goldsmith, E. Karotkin, G. Suresh and M. Keszler, Elsevier, 2017, ch. 10, pp. 80-96.e3

68 C. McDonagh, C. Kolle, A.K. McEvoy, D.L. Dowling, A.A. Cafolla, S.J. Cullen and B.D. MacCraith, *Sensor Actuat. B-Chem.*, 2001, **74**, 124-130

69 C. Windsor, A. Steinbach and A. Lockwood, *In-Situ ® Optical RDO ® Methods for Dissolved Oxygen Measurements Outperform Traditional Methods(white paper)*, In-Situ Inc., 2012.

70 M. Fan, T. S. Alghassab and L. J. Twyman, *ACS Appl. Bio Mater.*, 2018, **1**, 708-713.

71 C. Fu, S. Herbst, C. Zhang and A. K. Whittaker, *Polym. Chem.*, 2017, **8**, 4585-4595.

72 L. Nurmi, H. Peng, J. Seppälä, D. M. Haddleton, I. Blakey and A. K. Whittaker, *Polym. Chem.*, 2010, **1**, 1039-1047.

73 M. Semsarilar, E. R. Jones and S. P. Armes, *Polym. Chem.*, 2014, **5**, 195-203.

74 N. Binboga, D. Kisakürek and B. M. Baysal, *J. Polym. Sci. pol. Phys.*, 1985, **23**, 925-931

75 J.Y. Choi, J.Y. Kim, H.J. Moon, M.H. Park and B. Jeong, *Macromol. Rapid. Comm.*,2014, **35**, 66-70.

76 T. Gotoh, G. Mochizuki and K. Kikuchi, *Biochem. Eng. J.*, 2001, **7**, 69-78

77 D. Mandracchia, A. P. Piccionello, G. Pitarresi, A. Pace, S. Buscemi and G. Giammona*Macromol. Biosic.*, 2007, **7**, 836-845.

78 J. Mexal, J. T. Fisher, J. Osteryoung, C. P. P. Reid, *Plant. Physiol.*, 1975, **55**, 20-24

79 A. Ghosh, V. Janic and H. A. Sloviter, *Anal. Biochem.*, 1970, **38**, 270-276

80 M. G. Freirea, A. M. A. Diasa, J. A. P. Coutinhoa, M. A. Z. Coelhob and I. M. Marrucho, *Fluid Phase Equilibria*. 2005, **231**, 109-113

81 H. S. Oberoi, F. C. Laquer, L. A. Marky, A. V. Kabanov and T. K. Bronich, *J. Control. Release*, 2011, **153**, 64-72.

82 A. Harada and K. Kataoka, *Macromolecules*, 1995, **28**, 5294-5299

83 H. Dautzenberg and W. Jaeger, *Macromol. Chem. Phys.*, 2002, **203**, 2095-2102

84 R.M. Fuoss and H. Sadek, *Science*, 1949, **110**, 552-554

85 X. Feng, R. Pelton, M. Leduc and S. Champ, Langmuir, 2007, **23**, 2970- 2976

86 I. K. Voets, A. de Keizer and M. A. C. Stuart, *Macromolecules*, 2006, **39**, 5952-5955.

87 C. W. Scales, F. Huang, N. Li, Y. A. Vasilieva, J. Ray, A. J. Convertine and C. L. McCormick, *Macromolecules*, 2006, **39**, 6871-6881.

88 S. Herlambang, M. Kumagai, T. Nomoto, S. Horie, S. Fukushima, M. Oba, K. Miyazaki, Y. Morimoto, N. Nishiyama and K. Kataoka, *J. Control. Release*, 2011, **155**, 449-457.

89 S. Katayose and K. Kataoka, *Bioconjug. Chem.*, 1997, **8**, 702-707.

90 S. Florinas, M. Liu, R. Fleming, L. V. Vlerken-Ysla, J. Ayriss, R. Gilbreth, N. Dimasi, C. Gao, H, Wu, Z. Xu, S. Chen, A. Dirisala, K. Kataoka, H. Cabral and R. J. Christie, *Biomacromolecules*, 2016, **17**, 1818-1833

91 Y. Luo, X. Yao, J. Yuan, T. Ding and Q. Gao, *Colloids Surf. B*, 2009, **68**, 218-224

92 N. Karibyants and H. Dautzenberg, *Langmuir*, 1998, **14**, 4427-4434

93 D. Fischer, H. Dautzenberg, K. Kunath and T. Kissel, *Int. J. Pharm.*, 2004, **280**, 253-269.

94 G. B. Kauffman, *J. Chem. Educ*., 1988, **65**, 28-31.

95 I. Insua, A. Wilkinson and F. Fernandez-Trillo, *Eur. Polym. J.*, 2016, **81**, 198-215.

96 G. Zhang, A. Harada, N. Nishiyama, D. Jiang, H. Koyama, T. Aida and K. Kataoka, *J. Control. Release*, 2003, **93**, 141-150

97 Y. Lee and K. Kataoka, Soft *Matter*, 2009, **5**, 3810-3817.

98 K. Miyata, R. J. Christie and K. Kataoka, *React. Funct. Polym.*, 2011, **71**, 227-234.

99 N. Bayó-Puxan, M.Dufresne, A. E.Felber, B.Castagner and J. Leroux, *J. Control. Release*, 2011, **156**, 118-127.

100 M. Dufresne, M. Elsabahy and J. Leroux, *Pharm. Res.*, 2008, **25**, 2083-2093.

101 J. Zhang, Y. Zhou, Z. Zhu, Z. Ge and S. Liu, *Macromolecules*, 2008,**41**,1444-1454.

102 T. E. Patten and K. Matyjaszewski, *Adv. Mater.*, 1999, **10**, 901-915.

103 B. F. Lundt, N. L. Johansen, A. Vølund and J. Markussen, *Int. J. Pept. Protein Res.*, 1978, **12**, 258-268

104 M. Mishra, *Concise Encyclopedia of Biomedical Polymers and Polymeric Biomaterials*, CRC Press, United States, 2017.

105 T. Kitayama, K. Ute, M. Yamamoto, N. Fujimoto and K. Hatada, *Polym. J.*, 1990, **22**, 386-396.

106 I. W. Ashworth, B. G. Cox and B. Meyrick, *J. Org. Chem.*, 2010, **75**, 8117-8125.

107 C. Zhang and M. Maric, *Polymers*, 2011, **3**, 1398-1422.

108 O. Samsonova, C. Pfeiffer, M. Hellmund, O. M. Merkel and T. Kissel, *Polymers*, 2011, **3**, 693-718

109 P. van de Wethering, N. J. Zuidam, M. J. V. Steenbergen, O. A. G. J. van der Houwen, W. J. M. Underberg and W. E. Hennink, *Macromolecules*, 1998, **31**, 8063-8068

110 M. M. Mok, R. Thiagarajan, M. Flores, D. C. Morse and T. P. Lodge, *Macromolecules*, 2012, **45**, 4818-4829.

111 M. Guo, Y. Yan, H. Zhang, H. Yan, Y. Cao, K. Liu, S. Wan, J. Huang and W. Yue, *J. Mater. Chem.*, 2008, **18**, 5104-5112

112 Y. Tao, R. Liu, X. Liu, M. Chen, C. Yang and Z. Ni, *Nanoscale Res. Lett.*, 2009, **4**, 341-343.

113 X. Ai, L. Zhong, H. Niu, Z. He, *Asian J. Pharm. Sci.*, 2014, **9**, 244-250

114 R. Nakahata and S. Yusa, *Polymers*, 2018, **10**, 205-218.

115 D. Xiong, Z. He, Y. An, Z. Li, H. Wang, X. Chen and L. Shi, *Polymer*, 2008, **49**, 2548-2552.

116 T. Dai, B. B. Fuchs, J. J. Coleman, R. A. Prates, C. Astrakas, T. G. St. Denis, M. S. Ribeiro, E. Mylonakis, M. R. Hamblin and G. P. Tegos, *Front. Microbiol.*, 2012, **3**, 120-135.

117 Y. Kakizawa and K. Kataoka, *Adv. Drug Deliv. Rev.*, 2002, **54**, 203-222.

118 K. Smallbone, D. J. Gavaghan, R. A. Gatenby, P. K. Maini, *J. Theo. Bio.*, 2005, **235**, 476-484

119 J. M. Brown and W. R. Wilson, *Nat. Rev. Cancer*, 2004, **4**, 437-447.

120 Z. Luo, M. Zheng, P. Zhao, Z. Chen, F. Siu, P. Gong, G. Gao, Z. Sheng, C. Zheng, Y. Ma and L. Cai, *Sci. Rep.*, 2016, **6**, 23393-23403.

121 Y. Cheng, H. Cheng, C. Jiang, X. Qiu, K. Wang, W. Huan, A. Yuan, J. Wu and Y. Hu, *Nat. Commun.*, 2015, **6**, 8785-8792.